

# Investigating the transcriptional control mechanisms mediated by Gb $\gamma$ subunits and the mSWI/SNF complex on the cardiac fibrotic response

# Jacob M. Blaney

Co-supervised by Dr. Terence Hébert and Dr. Jason Tanny

Degree of Master of Science

Department of Pharmacology & Therapeutics

McGill University, Montreal, QC, Canada

# August 2024

A thesis submitted to McGill University in partial fulfillment of the requirements of the degree of Master of Science

#### **ACKNOWLEDGEMENTS**

First, to my supervisors, Terry and Jason, thank you for your guidance, encouragement, and support throughout the challenges and successes of this degree. You brought me into your labs when I had no previous lab experience and believed in my abilities throughout. I am very grateful for all of the opportunities you provided me to learn and grow as a scientist and young professional. I could not have asked for better co-supervisors.

To all of the members of the Hébert and Tanny labs; Darlaine, Domo, Phan, Robert, Deanna, Étienne, Julianna, Karima, Kyla, Grace, Cara, Kim, Hanan, Leyla, Ashika, Mikhail, Giada, Aneesah, Jace, Jenn, Sarah, Calvin, Ali, Viviane, Peiran, Sicheng, thank you for all of your support in experiments, collaboration, troubleshooting, and encouragement throughout the progression of my degree. This work could not have come together without you all. To Giada and Yujin, supervising you was one of the highlights of this degree, thank you for your contributions and for teaching me just as much as I taught you. To Nico, thank you for all your help and teaching in many aspects of this work and for all the laughs and positivity. Tire-toi une bûche, j'ai une thèse à te faire lire.

À Darlaine, tu étais la première personne qui m'as montré ce qui signifie un scientifique. Merci pour toute ta formation quand j'ai commencé à travailler dans un laboratoire sans aucune expérience. Tes encouragements, ton soutien et tes conseils de carrière m'ont tellement aidé tout au long de ce diplôme et m'ont aidé à déterminer ce qui viendra prochainement.

To Viviane, Domo, and Phan, you have been incredible role models throughout this degree.

Thank you for answering all my many questions, for making such a positive learning environment where we felt safe to try new things, and for encouraging me at every stage of the process.

To Étienne, Emma, Ashika, and Darlaine, thank you for being an incredible team to work with in the primary cell work. Your collaboration made a difficult aspect of this work a success.

To the members of the Pharmacology Admin team, Hong, Nadee, Chantal, Cathy, Christiaan, and Tina, thank you for facilitating this degree and for all your hard work in making the student experience in the Pharmacology department so enriching and successful.

To my Thesis Advisory Committee, Dr. Bruce Allen and Dr. Jacquetta Trasler, thank you for your feedback and guidance as I progressed through this work. Thank you to the FRQS for contributing funding to my graduate research.

To my friends outside the lab who were a huge part of my life during these years, Justin, Luis, Alyson, Sabrina, Cara, and Deanna, you all stood by my side through thick and thin, through success and failure, and lifted me up no matter what. I owe much of this success to your friendship and support. The memories we have made will stay with me forever.

Finally, to my parents; Mom and Dad, you always believed in me no matter what. You have stood by my side through every day of my life. Thank you for supporting me through this journey, for your sacrifices, and for sharing in the joy and successes. I am here thanks to you, and I am forever grateful.

# TABLE OF CONTENTS

ABS	STRA	1CT	7
RÉS	SUM	$\acute{E}$	8
CONTRIBUTION OF AUTHORS			10
LIST OF ABBREVIATIONS			
LIS	T OI	FFIGURES	12
INT	ROL	DUCTION	15
<i>1. 1</i>	De	fining Cardiac fibrosis and its pathophysiological functions	15
1.2	Ca	rdiac Fibrosis in Heart Failure	17
1.3	Ca	rdiac fibroblast biology	18
1.4	GF	PCR Signalling pathways involved in cardiac fibrosis	21
1	.4.2	Renin-Angiotensin-Aldosterone-System (RAAS) in cardiac fibroblasts	24
1	.4.3	$Geta\gamma$ signalling	25
1.5	TG	F-β signalling	27
1.6	Tre	eatment options and pharmacological interventions in cardiac fibrosis	27
1	.6.1	ARBs, ACE-I, and Renin Inhibitors: Targetting the RAAS	28
1	.6.2	Statins: Inhibition of RhoGTPases	29
1	.6.3	Antagonizing TGF-β signalling	30
<i>1.7</i>	Th	e role of epigenetics and chromatin remodelling complexes on the transcriptional	
con	trol d	of cardiovascular diseases	30
1	.7.1	The role of Smarca4 in cardiovascular development and disease	33
1	.7.2	Epigenetic control of myofibroblasts	35
1.8	Lir	nking Gβγ signalling to transcriptional control of cardiac fibrosis	36

HYF	POTHESIS AND AIMS	38	
MA	TERIALS AND METHODS	39	
2.1	Isolation and culturing of Rat Neonatal Cardiac Fibroblasts	39	
2.2	Fixed Transfection of RNCFs on plastic plates with siRNA	40	
2.3	Suspended Transfection of RNCFs on plastic plates with siRNA	41	
2.4	Scratch assays	42	
2.5	Proliferation Assays	44	
2.6	Western blots for knockdown validation	45	
2.7	Western blots for collagen secretion	46	
2.8	RNA extraction and RT-qPCR	47	
2.9	qPCR mRNA primer design	48	
2.10	Morphology microscopy image acquisition	48	
2.11	Immunofluorescent microscopy image analysis	48	
2.12	RNA isolation for RNA sequencing	49	
2.13	RNA sequencing data processing and bioinformatics	50	
RES	RESULTS		
Resi	ults Section 1- Developing and optimizing a knockdown protocol to investigate the effec	<u>ts</u>	
of G	proteins and chromatin remodelers on the fibrotic response using	53	
3.1	Determining plating conditions for optimal knockdown of $G\beta$ and $Smarca4$ subunits	53	
3.	1.1 siRNA lipofection performed on fixed RNCFs grown on plastic yields low knockdov	vn	
effic	iency	53	
3.	1.2 siRNA lipofection performed on RNCFs in suspension yields more efficient target		
knoc	kdown	55	
3.2	siRNA knockdown optimization for phenotypic assays	<i>57</i>	
3.3	siRNA knockdown validation for RNA sequencing	58	
Resi	ults Section 2: Investigating the phenotypic effects of knocking down G\beta subunits and		
<u>Sma</u>	rca4 on the fibrotic response	62	
3.4	Ang II induces proliferation via division and not cell migration in scratch assays	62	
3.5	RNCF proliferation is potentially accelerated by G\beta1 knockdown in this RNCF		
mod	l'el	63	

3.6 Ang II treatment increases 24-hour collagen secretion but not collagen	mRNA	
transcription	66	
3.7 Our RNCF model shows attributes of an advanced myofibroblast state	69	
Results Section 3: Profiling the role of G protein and mSWI/SNF subunits or	<u>n the</u>	
transcriptional response to Ang II	70	
3.8 qPCR profiling of select pro-fibrotic and transcriptionally relevant gene	es 71	
3.9 Profiling the transcriptomic changes of G\beta and mSWI/SNF knockdow	n on Ang II-	
induced transcription via RNA sequencing	73	
3.9.1 Investigating the effects of G $\beta$ 1, G $\beta$ 2 and Smarca4 on the Ang II ind	'uced fibrotic gene	
expression	81	
3.9.2 Gene Ontology pathway analysis of Ang II-induced gene expression	83	
3.9.3 Effects of siRNA knockdown on basal gene expression in RNCF mode	el 88	
3.9.4 Evaluating the changes from siRNA knockdown on Ang II-induced my	vofibroblast	
differentiation	94	
DISCUSSION	97	
4.1 Comparing proliferation and migration phenotypes in the myofibroblast r	model 97	
4.2 Understanding the collagen response to Ang II stimulation in our myofi	broblast model 98	
4.3 Exploring targetted gene expression analysis by qPCR	99	
4.4 Exploring the gene expression changes via RNA sequencing	100	
4.4.1 Investigation of knocking down $G\beta$ subunits on other $G$ protein express	sion 100	
4.4.2 Exploring the transcriptomic potentiation of Ang II induction from siR	NA knockdown of	
$G\beta1$ , $G\beta2$ , and $Smarca4$	103	
4.4.3 Exploring the transcriptomic repression of basal fibrotic gene expressi	on from siRNA	
knockdown of Gβ1, Gβ2, and Smarca4	105	
4.5 Temporal control of fibrotic gene expression	107	
LIMITATIONS	108	
CONCLUSIONS AND FUTURE PERSPECTIVES		
REFERENCES		

#### **ABSTRACT**

Cardiac fibrosis is a necessary repair and maintenance process in the healthy heart that can become dysregulated during the development of heart failure. Cardiac fibroblasts can enter into an activated myofibroblast state in response to cardiac damage, depositing extracellular matrix proteins and secreting fibrosis-inducing signalling molecules. Angiotensin II (Ang II) signalling through the G protein-coupled angiotensin II type 1 receptor is a key mediator of cardiac fibroblast activation. We found a non-canonical, nuclear function for G protein by complexes that regulates the fibrotic transcriptional program and may involve binding to RNA polymerase II and the mSWI/SNF complex. We hypothesize that Gβy signalling acts as a transient brake to suppress the fibrotic response through interactions with mSWI/SNF. To assess changes in the fibrotic response following siRNA knockdown of mSWI/SNF subunit Smarca4, Gβ1, or Gβ2 in rat neonatal cardiac fibroblasts (RNCFs), this work aims to 1) assess fibrotic phenotypes including Ang II-induced proliferation, collagen secretion, and fibrotic gene expression between treatment conditions and 2) investigate the underlying transcriptional patterns impacted by knockdown of Gβ1/2 and Smarca4 on the fibrotic response. Knockdown of our targeted genes did not yield appreciable alterations to the phenotypic fibrotic response in the myofibroblast context. However, RNA sequencing analysis revealed rewiring of the fibrotic gene expression program in the knockdowns that was consistent with a modulatory role of  $G\beta$  subunits in response to fibrotic stimuli. Future work will aim to further characterize important genomic loci where G $\beta$ 1, G $\beta$ 2, and Smarca4 may regulate the fibrotic response to develop our understanding of the complex control of cardiac fibrosis in the development of heart failure.

## RÉSUMÉ

La formation de tissus fibrotiques par les fibroblastes cardiaques est un processus de réparation et d'entretien nécessaire dans un cœur sain, mais qui peut être déréglé au cours du développement de l'insuffisance cardiaque. Les fibroblastes cardiaques peuvent adopter un état myofibroblastique activé en réponse à des lésions cardiaques, en déposant des protéines de la matrice extracellulaire et en sécrétant des molécules de signalisation induisant la fibrose. La stimulation des fibroblastes par l'angiotensine II (Ang II) induit la réponse fibrotique en activant les récepteurs de type 1 de l'angiotensine II, un récepteur couplé à la protéine G. Nous avons découvert une fonction nucléaire non canonique pour les sous-unités Gβγ qui régule le programme transcriptionnel fibrotique et peut impliquer la liaison à l'ARN polymérase II et au complexe mSWI/SNF. Nous émettons l'hypothèse que la signalisation Gβy agit comme un frein temporaire pour diminuer la réponse fibrotique par des interactions avec le complexe mSWI/SNF. Afin d'évaluer les changements dans la réponse fibrotique suite au réduction par ARNi de la sous-unité mSWI/SNF SMARCA4, Gβ1, ou Gβ2 dans les fibroblastes cardiaques néonataux de rat (FCNR), ce travail vise à 1) évaluer les phénotypes fibrotiques, y compris la prolifération induite par l'Ang II, la sécrétion de collagène, et l'expression des gènes fibrotiques entre les conditions de traitement et 2) étudier les profils transcriptionnels sous-jacents impactés par le knockdown de Gβ1/2 et de Smarca4 sur la réponse fibrotique. Nous avons démontré que nos FCNR ont adopté le phénotype myofibroblaste qui produit certaines réponses fibrotiques attendues, comme la prolifération cellulaire, mais pas d'autres, comme l'expression de tous les gènes pro-fibrotiques. En outre, l'élimination des gènes ciblés par ARNi n'a pas entraîné de modifications appréciables de la réponse fibrotique phénotypique dans le contexte des myofibroblastes. Cependant, l'analyse du séquençage de l'ARN a révélé des changements uniques dans les gènes différentiellement exprimés associés au programme d'expression des gènes fibrotiques entre les différentes conditions de ARNi. En outre,

des caractéristiques uniques ont été observées entre les échantillons traités par véhicule ou par Ang II, en fonction du traitement par ARNi, ce qui suggère que ces sous-unités de protéines G et de remodelage de la chromatine affectent à la fois l'expression génique basale des myofibroblastes et les réponses ultérieures aux stimuli fibrotiques. Les travaux à venir viseront à caractériser davantage les lieux génomiques importants où  $G\beta1$ ,  $G\beta2$  et Smarca4 peuvent réguler la réponse fibrotique afin de mieux comprendre le contrôle complexe de la fibrose cardiaque dans le développement de l'insuffisance cardiaque.

#### **CONTRIBUTION OF AUTHORS**

Ms. Darlaine Pétrin, Dr. Kyla Bourque, Dr. Jace Jones Tabah, Dr. Shahriar Khan, and Dr. Ryan Martin developed the RNCF isolation protocol and the siRNA transfection protocol upon which the optimizations in this thesis are based. RNA sequencing was performed by Canada's Michael Smith Genome Sciences Centre (Vancouver, BC, Canada). RNA and DNA bioanalyzer quality control was performed by Dr. Nicolas Audet. Dr. Jennifer Chen and Dr. Ryan Martin generated the original scripts upon which the sequencing data processing and differential expression analysis in R were based. Ms. Giada Castagnola performed the qPCR experiments presented in section 3.8 as part of her undergraduate research project.

Unless specified above, all work in this thesis was completed by Jacob M. Blaney. This thesis was written by Jacob M. Blaney and co-edited by Dr. Terry Hébert and Dr. Jason Tanny. The translation of the French abstract was edited by Ms. Darlaine Pétrin and Ms. Viviane Pagé.

#### LIST OF ABBREVIATIONS

5mC = 5 methyl cytidine

**ACE** = Angiotensin-converting enzyme

**ACE-I** = Angiotensin-converting enzyme inhibitor

**Ang I** = Angiotensin 1

Ang II = Angiotensin II

 $\alpha 1AR = \alpha 1$  adrenergic receptor

 $\alpha$ **2AR** =  $\alpha$  2 adrenergic receptor

 $\alpha$ -SMA =  $\alpha$  smooth muscle actin

**ARB** = Angiotensin receptor blocker

**Ara-C** = Cytosine arabinoside

**AT1R** = Angiotensin II type 1 receptor

**AT2R** = Angiotensin II type 2 receptor

 $\beta 1AR = \beta 1$  adrenergic receptor

 $\beta 2AR = \beta 2$  adrenergic receptor

**cAMP** = Cyclic adenosine monophosphate

**Colla1** = Type 1 collagen

Col3a1 = Type 3 collagen

**DAG** = Diacylglycerol

**DCM** = Dilated Cardiomyopathy

**ECM** = Extracellular matrix

**ER** = Endoplasmic reticulum

**ETAR** = Endothelin A receptor

**ETBR** = Endothelin B receptor

FN = Fibronectin

**GPCR** = G protein-coupled receptor

**Gnb1** =  $G\beta1$ 

 $Gnb2 = G\beta2$ 

**HF** = Heart failure

**HFmrEF** = Heart Failure with moderately reduced Ejection Fraction

**HFpEF** = Heart Failure with preserved Eiection Fraction

**HFrEF** = Heart Failure with reduced Ejection Fraction

**hnRNP** = Heterologous ribonuclear

**II-1β** = Interleukin 1 β

**II-6** = Interleukin 6

**IP3** = Inositol 1, 4, 5-triphosphate

**MI** = Myocardial infarction

**MMP** = Matrix metalloprotease

**mSWI/SNF** = mammalian SWItch/Sucrose Non-Fermentable

**PIP2** = Phosphatidylinositol 4, 5 biphosphate

**PI3K** = Phosphoinositide 3 kinases

PKA = Protein kinase A

**PKC** = Protein kinase C

**PLC** $\beta$  = Phospholipase C  $\beta$ 

**RAAS** = Renin-Angiotensin-Aldosterone system

RNAPII = RNA polymerase II

**RNCF** = Rat neonatal cardiac fibroblast

**siRNA** = Small interfering RNA

**TGF-\beta** = Transforming growth factor –  $\beta$ 

- **Table 1**. Canonical G protein partners.
- Diagram 1. Schematic depicting mSWI/SNF functional outcomes
- **Table 2.** Settings for NCBI Primer BLAST
- **Table 3.** Summary of siRNA target knockdown percentage by qPCR and western blot on adherent RNCFs
- Figure 1. Quantification of mRNA and protein of suspended RNCFs.
- **Table 4.** Quantification of siRNA knockdown percentages for suspended transfection in 6-well plates to be used for phenotypic tests (not scratch assays) by qPCR.
- **Figure 2**. 6 and 24-hour quantification of RNA yield from lysis using Qiagen RNeasy Isolation columns
- **Table 5.** Quantification of siRNA knockdown percentages for RNCFs to be used in RNA sequencing experiment by qPCR.
- **Figure 3**. qPCR quantification of siRNA target gene knockdowns for RNA seq samples.
- Figure 4. Brightfield images of RNCFs under different agonist treatments
- **Figure 5.** Pearson correlation plot of RNCF nuclei versus confluency
- Figure 6. Assessment of mitotic divisions via Ki-67 immunofluorescence
- **Figure 7**. Quantification of RNCF proliferation, induced by Ang II and measured between siRNA treatments
- Figure 8. Ang II-mediated collagen secretion pilot
- Figure 9. Western blot and qPCR analysis of collagen type 1 secretion
- **Figure 10.** Quantification of  $\alpha$ -SMA fluorescence intensity.
- **Figure 11.** qPCR quantification of 6 and 24-hour Ang II-treated RNCFs, expression between siRNA knockdowns
- Figure 12. PCA analysis of sequencing conditions, before (A, B) and after batch effect removal
- **Figure 13.** Heatmaps comparing the relative levels of Gβ subunits and Smarca4 subunits to show knockdown fold changes between 6 and 24 hours
- **Figure 14.** Quantity of up and down-regulated differentially expressed genes induced by Ang II and antagonized by losartan between siRNA treatments
- **Figure 15.** Log2FC heatmaps comparing genes that were assessed in the qPCR assays at A) 6 hours of Ang II and B) 24 hours of Ang II treatment

- **Figure 16.** Log2FC heat maps comparing relative expression of G protein subunits between siRNA treatments
- Figure 17. Venn diagrams containing counts of differentially expressed genes induced by Ang II
- **Figure 18**. Log2FC heat maps depicting fold changes between the core set of upregulated Ang II genes
- **Figure 19.** Summary bar plots of GO terms enriched in Ang II-treated samples vs vehicle-treated samples, within the Ctrl siRNA conditions
- Figure 20. Summary bar plots of GO terms enriched in Ang II-treated samples vs vehicle treated samples, within the G $\beta$ 1 siRNA conditions
- Figure 21. Summary bar plots of GO terms enriched in Ang II-treated samples vs vehicle-treated samples, within the G $\beta$ 2 siRNA conditions
- **Figure 22.** Summary bar plots of GO terms enriched in Ang II-treated samples vs vehicle-treated samples, within the Smarca4 siRNA conditions
- **Figure 23**. Log2FC heat map and Venn diagrams depicting the genes upregulated in the Muscle Systems Processes GO term between treatments and siRNA conditions
- **Figure 24.** Venn diagrams containing counts of differentially expressed, up and downregulated genes caused by siRNA treatments at basal conditions
- **Figure 25.** Log2FC heat maps depicting all up and down regulated genes at basal conditions between siRNA conditions
- **Figure 26.** Volcano plots showing significantly up and downregulated genes between siRNA treatments at basal conditions
- **Figure 27.** Summary bar plots of GO terms downregulated in Gβ1 siRNA-treated conditions vs Ctrl siRNA-treated conditions under basal conditions
- **Figure 28.** Summary bar plots of GO terms downregulated in Gβ1 siRNA-treated conditions vs Ctrl siRNA-treated conditions under basal conditions
- **Figure 29.** Summary bar plots of GO terms downregulated in Smarca4 siRNA-treated conditions vs Ctrl siRNA-treated conditions under basal conditions
- Figure 30. Log2FC heat maps depicting changes in canonical myofibroblast genes
- **Table 5.** Summary table of changing G protein expression in differential gene expression results

# Included in supplementary materials

**Supplementary Table 1:** Primer sequences for qPCR

Supplementary Table 2: Upregulated GO Terms, 24 hours Ang II

Supplementary Table 3: Downregulated GO Terms, 24 hours Ang II

Supplementary Table 4: Basal gene expression changes, up and downregulated genes

Supplementary Table 5: upregulated GO terms, 6 hrs, Baseline with Knockdown

Supplementary Table 6: upregulated GO terms, 24 hrs, Baseline with Knockdown

Supplementary Figure 1. Co-immunoprecipitation of Smarca4 and Gβ1 in HEK293-F cells

Supplementary Figure 2. Summary of FBS and FN coating optimizations in scratch assays.

Supplementary Figure 3: Bar plots representing wound closure rate between siRNA knockdowns

Supplementary Figure 4. Wound closure in response to Ang II

Supplementary Figure 5. Transcription factor Gene expression by qPCR

## Included in Appendix A

**Appendix A-** Technical Notes and Considerations for Generating and Optimizing siRNA Knockdown Models in Primary Rat Neonatal Cardiac Fibroblasts

#### **INTRODUCTION**

# 1. 1 Defining Cardiac fibrosis and its pathophysiological functions

Fibrosis is a seemingly paradoxical pathophysiological response wherein the body forms fibrotic tissue in response to some insult or injury. This tissue remodelling is necessary to heal and maintain organ function in the short term, but in the medium to long term, unresolved scar tissue accumulation can interfere with organ function. In the heart, accumulation of fibrotic tissue impairs contractility, impedes signal transduction between cardiac cells, promotes inflammation, and ultimately contributes to reduced cardiac output and heart failure[1].

Heart failure contributes greatly to global disease burden and reductions in quality of life. Across the world, according to the Global Burden of Disease study of 2017, 64.3 million people are estimated to be living with heart failure[2, 3]. In Canada, this presents a significant disease burden as well. The Canadian Heart and Stroke Foundation estimates that in 2024, 750,000 Canadians are living with heart failure [4]. As global life expectancies increase with improved healthcare access, more people are surviving acute events such as heart attacks (myocardial infarction or MI) as well as living longer with other clinical diseases and manifestations that are the background upon which the syndrome of heart failure exists[5].

Fibrosis is described in many cardiac pathologies, many of which contribute to heart failure. Important pathologies for this thesis include ischemic fibrosis associated with MI, and non-ischemic fibrosis associated with dilated cardiomyopathy, hypertension, myocarditis-associated cardiomyopathy, and diabetic cardiomyopathy[6].

Ischemic fibrosis is also called replacement fibrosis since the infarcted area is replaced by fibrotic tissue [6, 7]. After the cardiomyocytes in the infarct zone die, the inflammatory phase of

remodelling begins[6]. Immune cells are recruited to the infarct site to clear away damaged tissue and matrix metalloproteases (MMPs) begin to digest the ECM in preparation for the fibrotic tissue deposition[8]. TGF-β release in the infarct zone occurs 3-4 days after initial insult and results in the early deposition of collagen fibres via activation of local fibroblasts into the myofibroblast state and enhancement of the recruitment of migratory fibroblasts[6]. These fibroblasts deposit an organized matrix of scar tissue in the infarct zone to restore the structural integrity of the myocardium. This process continues long after the resolution of the acute insult[6] leading to further stiffening of the myocardial tissue around the infarct zone, secretion of profibrotic signals, and spreading of fibrosis to other areas of the myocardium[6, 9].

Non-ischemic fibrosis is seen in many pathologies other than post-MI remodelling. In hypertensive heart disease, the myocardium becomes subjected to significant interstitial fibrosis[6]. Activated fibroblasts and myofibroblasts secrete large amounts of type 1 and 3 collagen in response to increased renin-angiotensin-aldosterone system (RAAS) signalling and this contributes to increased resistance to contraction in the ventricles, leading to diastolic failure, followed by systolic failure as progression worsens[6]. Myocarditis is another cardiac pathology that is associated with the development of cardiac fibrosis. In myocarditis, the initial inflammation causes the release of pro-fibrotic factors similar to post-MI recovery[10]. If the inflammation following the resolution of the initial infection does not resolve, persistent fibroblast activation deposits fibrotic tissue in the area, which in many cases progresses to dilated cardiomyopathy (DCM) [10, 11]. DCM is a cardiovascular disease characterized by dilation of the left ventricles, associated with cardiomyocyte hypertrophy. Replacement fibrosis, is common and irreversible once present in patients with DCM[11]. Replacement fibrosis is associated with reduced left ventricular ejection fraction in DCM and stratifies these patients as high-risk [11]. Diabetes

mellitus is associated with the activation of the RAAS and is also associated with the development of diabetes-induced DCM[12]. Initially, the remodelling associated with diabetes may drive hypertrophic cardiomyopathy, but as the disease progresses, this regresses into a dilated myopathy[12]. This is associated with high ROS production and myocyte death [12].

#### 1.2 Cardiac Fibrosis in Heart Failure

When the underlying cardiac co-morbidities result in certain clinical manifestations, the syndrome of heart failure (HF) can be diagnosed. According to the European Society of Cardiology, heart failure is defined as the presentation of symptoms and signs (i.e. fatigue, dyspnea, peripheral edema, elevated jugular venous pressure and/or pulmonary crackles) associated with reduced cardiac output or increased intracardiac pressure at rest or under stress[13]. To be considered heart failure, signs and symptoms must be present and there must be a structural and/or functional abnormality demonstrated [13]. Heart failure can be classified into 3 categories: heart failure with preserved ejection fraction (HFpEF), heart failure with low or reduced ejection fraction (HFrEF), and heart failure with mid-range ejection fraction (HFmrEF) depending on how the cardiac output changes[5, 13]. Fibrosis can be present in all forms of heart failure, but depending on the different pathophysiology can contribute differently. For example, both HFrEF and HFpEF are fibrosis-associated pathologies, with increased interstitial and perivascular fibrosis[14]. However, HFrEF is also associated with replacement fibrosis, whereas HFpEF is associated with relatively higher levels of perivascular fibrosis compared to HFrEF [14, 15]. Because HFrEF is associated with the loss of myocytes due to an ischemic event like an MI, the myocyte replacement by fibrotic tissue brings with it highly activated fibroblasts and myofibroblasts[14, 15]. Particularly, remodelling of the ECM reduces the amount of fibrillar type 1 and 3 collagen that is normally present to transduce cardiomyocyte contractile force throughout

the tissue[14]. Contrastingly, HFpEF retains the fibrillar collagen, however, there is a reduction in the proportion of the more elastic type 3 collagen, which results in a stiffening of the heart[14]. Finally, while perivascular fibrosis occurs in both types of HF, it occurs more frequently in HFpEF, resulting in a greater number of activated fibroblasts caused by pro-fibrotic signalling from immune cells infiltrating the vasculature[14, 16].

# 1.3 Cardiac fibroblast biology

Tissue-resident fibroblasts in the heart rapidly respond to cardiac insult and injury. These tissue-resident fibroblasts differentiate with the heart and their lineage can be traced via activation of the Tcf21 transcription factor. Tcf21-positive cardiac fibroblasts (CFs) are not the only subpopulation, however, since fibroblasts may also be introduced via the endothelial-tomesenchymal transition of endothelial cells to respond to pro-fibrotic stimuli [17, 18]. A clear illustration of the spectrum of fibroblast activation can be understood by discussing the fibroblast response to myocardial infarction. The stages of MI healing can broadly be stratified into 3 phases: inflammation, proliferation, and scar formation and maturation [19]. Cardiac fibroblasts cooperate with many other cell types during these phases to facilitate wound healing. First, in the inflammatory phase, immune cells rapidly infiltrate the infarct area. Necrotic response neutrophils (principally leukocytes) followed shortly after by macrophages make up this immune cell phase[20]. This initial inflammatory phase clears necrotic myocytes and degrades the ECM via MMP secretion to enable tissue remodelling [21] [20]. During this time, immune cells secrete many pro-inflammatory cytokines, including IL-6, IL-1 $\alpha$  and tumour necrosis factor- $\alpha$  (TNF- $\alpha$ ) [21]. Resident cardiac fibroblasts are present and respond to this signal by secreting IL-1β, TNFα and IL-6 themselves[22]. This inflammation phase is important because blocking it impedes the rest of the fibrotic response and leads to an increased risk of cardiac rupture due to improper tissue

stabilization[23]. The inflammatory phase is immune-focused. Fibroblasts are not yet activated; they are in an anti-proliferative, anti-migratory, and anti-apoptotic stage. Instead, they support the immune function via cytokine secretion[20, 21].

The progression to the proliferative phase of the healing response marks a shift from proinflammatory to anti-inflammatory characteristics[20, 21]. Fibroblasts begin to activate and shift to proliferative and migratory phenotypes[21]. In this phase, the phenotype of fibroblasts can be referred to as "proto-myofibroblasts", in which they are proliferative, secrete ECM proteins (like collagens and periostin), and express cytoplasmic actin.[1] The tissue begins to stiffen as ECM begins to be replaced, and this further activates proto-myofibroblasts. At this stage, the transition form cytoplasmic actin expression to  $\alpha$ -SMA begins and gradually ramps-up as activation increases[24]. Cardiac fibroblasts are influenced by TGF- $\beta$ 1 production in the infarct environment by autocrine and paracrine mechanisms (from anti-inflammatory macrophages for example), to progress from the activated fibroblast to myofibroblast phenotype[21, 24]. Fibroblast activity increases from this point until the maturation phase, driving fibroblast activation and differentiation to myofibroblasts.

The maturation phase is marked by large increases in ECM protein production like type 1 and 3 collagen and fibronectin (FN), and a reduction in proliferation and migration marked my the increase of adhesion proteins like cadherin 2 and 11[25, 26]. This occurs as fibroblasts transition from the "proto-myofibroblast" phenotype to the myofibroblast phenotype. This is characterized by *de novo* expression of  $\alpha$ -SMA which is directly associated with a contractile fibroblast/myofibroblast phenotype [21]. Since  $\alpha$ -SMA is not induced in a switch-like fashion, fibroblast activation proceeds as a gradual shift from fibroblast to myofibroblast rather than a sharp transition. Therefore there are not simply two subpopulations of fibroblasts. There is a spectrum

of fibroblasts [27] that are at different stages of activation on their way to developing the maximal contractile and ECM-producing myofibroblast phenotype[20, 21, 28, 29]. Myofibroblasts are the principle cell type that contributes to the mature scar formation by secreting the most amounts of ECM proteins and contracting the tissue[20, 21, 28, 29]. Once the mature scar is formed, myofibroblasts transition toward two outcomes: apoptosis or tissue residence[30, 31]. The clinical concern in fibrosis resolution is that the programmed cell death that should happen with myofibroblasts does not typically occur in the heart[30]. Instead, pro-fibrotic effectors like the autocrine production of Ang II and the ever-increasing stiffness of the infarct environment result in prolonged myofibroblast survival and activity[30, 32]. Furthermore, the infarct zone is not isolated from the rest of the myocardium (chemically or from a tissue stiffness perspective). Throughout the wound healing response, potent fibroblast activation signals are diffuse throughout the tissue and stiff substrate interacts with the soft surrounding tissue. This promotes the activation of adjacent fibroblasts and contributes to the remodelling of the myocardium beyond the infarct[30, 32]

These activation stages and phenotypes can be applied to the cardiovascular pathologies described associated with HF. The fibroblast and myofibroblast are responsible for the poor outcomes associated with cardiac fibrosis, but as demonstrated above, it would be ill-advised to completely inhibit a critical part of the wound healing response in the heart. The challenge is to allow the fibroblast and myofibroblast to perform their tissue-stabilizing functions and promote the apoptosis and removal of the myofibroblast once a mature scar has formed.

# 1.4 GPCR Signalling pathways involved in cardiac fibrosis

The angiotensin II, type 1 receptor (AT1R) and the angiotensin II, type 2 receptor (AT2R) are associated with opposing functions in the heart. This introduction will focus on their effects on cardiac fibroblasts, but these receptors drive signalling events in many other cardiac cells as well. The angiotensin receptors are part of the G protein-coupled receptor (GPCR) receptor superfamily. These are membrane-integrated receptors that have 7 transmembrane helices spanning both sides of the plasma membrane. GPCRs are sometimes called 7-transmembrane receptors for this reason[33]. GPCRs have an outwardly-facing surface and an inward-facing surface to transduce ligand signals across the plasma membrane and drive intracellular signalling[3, 33, 34]. The cytoplasmic facing side of the GPCR is coupled to a family of proteins called the heterotrimeric G proteins. Heterotrimeric G-proteins are made up of one  $\alpha$ , one  $\beta$ , and one  $\gamma$  subunit. There are 16 G $\alpha$  subunits, 5 G $\beta$  subunits, and 12 G $\gamma$  subunits encoded in mammalian genomes[3, 33, 34]. These subunits can all form many heterotrimeric complexes with one another, and so the pool of possible G $\alpha\beta\gamma$  combinations is very large.

Classically, each GPCR was thought to be coupled to specific  $G\alpha$  subunits (**Table 1**), although this is likely an oversimplification as most GPCRs couple to multiple G protein partners.

Table1

labici				
GPCR	Canonical G protein partner			
AT1R, AT2R	Gαq			
$\beta_1 AR, \beta_2 AR$	Gαs (β <sub>2</sub> AR can couple to Gαi)			
$\alpha_1 AR$ , $\alpha_2 AR$	Gαq			
$ET_AR$ , $ET_BR$	Gaq/Gai			
Muscarinic recentors	Gαq: M1, M3, M5			
widscarmic receptors	Gα1: M2, M4			
$\beta_1 AR$ , $\beta_2 AR$ $\alpha_1 AR$ , $\alpha_2 AR$	Gαs (β <sub>2</sub> AR can couple to Gαi)  Gαq  Gαq/Gαi  Gαq: M1, M3, M5			

**Table 1: Canonical G protein partners.** AT1R = angiotensin II, type 1 receptor, AT2R= angiotensin II, type 2 receptor,  $\beta_1AR = \beta$  1 adrenergic receptor,  $\beta_2AR = \beta$  2 adrenergic receptor,  $\alpha_1AR = \alpha$  1 adrenergic receptor,  $\alpha_2AR = \alpha$  2 adrenergic receptor, ET<sub>A</sub>R = Endothelin A receptor, ET<sub>B</sub>R = endothelin B receptor

Once an agonist binds to the GPCR extracellular ligand binding domain, it induces a conformational change in the receptor that facilitates activation of GDP-bound heterotrimeric G protein [3, 34]. This ligand-bound state catalyzes the exchange of GDP for GTP and activates the G protein, in some cases causing its translocation into the cytosol. The G $\alpha$ -GTP at least partially dissociates from G $\beta\gamma$  subunits, and each proceeds to start its signalling cascades [3, 33, 34].

Each  $G\alpha$  subunit is associated with different downstream signalling cascades that result in changes in cellular biology and function.  $G\alpha_s$  (for "stimulatory") activates the enzyme adenylyl cyclase, which increases the concentration of cAMP in the cytosol[3, 34]. Increased cAMP binds to protein kinase A (PKA) which then phosphorylates many effectors that modulate cellular function and activates Epac1 which acts as guanine-nucleotide exchange factors for small G proteins like Rap [3, 34, 35]. The effects of increased cAMP levels are well understood to increase "sympathetic" cardiomyocyte outputs, but in fibroblasts, the role of cAMP signalling is less clear [35]. Signalling downstream of the  $\beta_1$  and  $\beta_2$ -adrenergic receptors showed that the activation of Epac1 and PKA leads to pro-fibrotic outputs like myofibroblast differentiation, collagen synthesis, proliferation and migration[35]. However,  $\beta_2$ AR signalling has also been shown to be anti-fibrotic, increasing collagen degradation and fibroblast autophagy[36]. Another  $G\alpha_s$ -coupled GPCR is the  $A_{2B}$  adenosine receptor[37-39]. Activation of the  $A_{2B}$ AR has anti-fibrotic effects via the inhibition of pro-fibrotic activation of the endothelin and Ang II receptors[37-39].

Activation of  $G\alpha_i$  (for "inhibitory")-coupled GPCRs reduces cAMP levels via inhibition of adenylyl cyclase.[33] It has been reported that the  $\beta_2AR$  can undergo a G protein switching phenomenon [40] and this has been observed in cardiomyocytes as well [35, 41]. This switching to an inhibitory G protein coupling has been shown to counteract the activation effects of  $G\alpha_s$ -coupled  $\beta_2AR$  activation in cardiomyocytes, but such G protein switching has not been demonstrated in cardiac fibroblasts [41].

Gα<sub>q</sub> is the principal G protein that regulates fibroblast activation. It is coupled to angiotensin receptors, endothelin receptors, and  $\alpha$ -adrenergic receptors ( $\alpha$ -AR) [3]. When  $G\alpha_q$ coupled GPCRs are activated,  $G\alpha_q$ -GTP dissociates and recruits phospholipase C- $\beta$  (PLC $\beta$ ) to the plasma membrane, where it cleaves phosphatidylinositol 4, 5 biphosphate (PIP2) into diacylglycerol (DAG) and inositol 1, 4, 5-triphosphate (IP<sub>3</sub>) [34, 42]. Increased IP<sub>3</sub> triggers the release of intracellular Ca<sup>2+</sup> from the endoplasmic reticulum, and increased Ca<sup>2+</sup> combined with DAG from PIP2 cleavage activates protein kinase C (PKC) isoforms that phosphorylate several signalling effectors[3, 34, 42]. Gaq is also well-reported to activate the MAPK pathway. In cardiomyocytes and cardiac fibroblasts [43], activation of GPCRs coupled to  $G\alpha_q$  results in activation of a cascade of protein kinases culminating in p38, ERK5, NFAT, and JNK activation, leading to increased phosphorylation of transcription factors altered gene expression of its target genes [44] [45]. Particularly relevant to cardiac fibroblasts and myofibroblasts is the role of the p38 MAPK pathway, which has been directly tied to the control of many fibroblast activation outcomes like  $\alpha$ -SMA and MMP transcription [43]. The AT1R can also couple to  $G\alpha_{12}$  and initiate signalling via the Rho or Rac pathways, which also contribute to p38, JNK, and MAPK signalling as described above.

## 1.4.2 Renin-Angiotensin-Aldosterone-System (RAAS) in cardiac fibroblasts

The RAAS plays a pivotal role in cardiac fibroblast (and cardiomyocyte) signalling. The cycle begins in the kidneys, where renin is produced and secreted [46]. Renin cleaves the peptide angiotensinogen into inactive angiotensin I [47]. The angiotensin-converting-enzyme (ACE) converts angiotensin I to angiotensin II, the most biologically active peptide hormone that drives many pathways in the cardiovascular system [47]. Systemically, Ang II causes increases in blood pressure, vasoconstriction, sodium retention, aldosterone production, cell proliferation (and hypertrophy of myocytes), and activation of oxidative stress in myocytes and fibroblasts [47]. Ang II primarily binds to its two receptors, the angiotensin II-type 1 and angiotensin II-type 2 receptors (AT1R and AT2R, respectively).

AT1Rs are associated with many adverse outcomes in heart failure. They are upregulated in hearts undergoing maladaptive remodelling, hypertrophy or recovering from ischemia [34]. These contributions to HF are driven by Ang II action on cardiomyocytes, as well as pro-fibrotic signalling driven by Ang II in fibroblasts [3]. In fibroblasts, Ang II binds to the AT1R and triggers the canonical Gαq signalling cascade. This is associated with increased production and secretion of extracellular matrix (ECM) components, proliferation, migration, production of cytokines and growth factors like TGF-β1 and aldosterone, and importantly, the activation and the conversion of activated fibroblasts to myofibroblasts[6, 48]. Fibroblasts show a hierarchy of pro-fibrotic signalling that coordinates the fibrotic response. Ang II increases the production of the potent cytokine TGF-β1 and it is believed that a significant portion of fibrotic outcomes in fibroblasts are due to the autocrine activity of this Ang II-induced TGF-β1 secretion [48, 49]. The AT1R also has mechanosensory functions that drive downstream signalling. Upon mechanical stimulation, the AT1R becomes activated and initiates further autocrine release of Ang II[3]. It is believed that in

this event, the AT1R adopts a conformation consistent with  $\beta$ -arrestin activity and therefore  $\beta$ -arrestin biased signalling is believed to be downstream of mechanosensitive AT1R activity [3, 50].

Ang II also binds to the AT2R, which is reported to have anti-fibrotic functions[51]. The AT2R is thought to couple to  $G\alpha_i$ , but AT2R activation does not affect adenylyl cyclase activity or cAMP levels [52]. Nor does it affect the direct mediators of  $G\alpha_i$  activity since it does not affect PLC activity [52]. AT2R likely acts via the activation of protein phosphatases that counter the protein kinase-driven signalling mediated by the AT1R [53].

# 1.4.3 Gβγ signalling

When activated by an extracellular ligand, the βy components of the G protein dissociate from the  $\alpha$  subunit as a heterodimer[33]. Due to the prenyl lipid modifications of the  $\gamma$  subunit, historically it was thought that  $\beta \gamma$  did not signal beyond the plasma membrane and acted only as a thermodynamic sponge that sequestered free Ga subunits back into their GDP-bound, inactive state to negatively regulate Gα signalling [54]. It was later discovered that Gβγ subunits directly activated Kir3 inwardly rectifying potassium channels, contributing to hyperpolarization of excitable cells [54, 55]. Gβγ proteins were also found to directly interact with Ca<sub>v</sub>2 voltagedependent calcium channels, thereby reducing the maximal amplitude of whole-cell current via voltage-dependent inhibition [54, 56]. A third role of canonical Gβγ signalling is activating the PLC $\beta$  enzyme[54]. Similar to the mechanism discussed for  $G\alpha_q$  activation,  $G\beta\gamma$  activates PLC $\beta$  to cleave PIP<sub>2</sub> into DAG and IP<sub>3</sub>, IP<sub>3</sub> increases intracellular Ca<sup>2+</sup> release from the ER, and both increased DAG and intracellular Ca<sup>2+</sup> activate PKC [3, 34, 42]. While both Gα<sub>q</sub> and Gβγ bind to PLC $\beta$ ,  $G\alpha_q$  binds with greater affinity, and each has its unique binding site on the enzyme[54, 57]. Interestingly, it was also observed that in vascular smooth muscle cells, inhibition of Gβγ subunits via electroporation of anti Gβ antibodies blocked the recruitment of PLC-β after Ang II stimulation

[58]. A fourth established regulatory function of G $\beta\gamma$  subunits is the binding to and activation of phosphoinositide 3 kinases (PI3Ks)[54]. PI3Ks are activated in response to survival signals, and G $\beta\gamma$  most selectively regulates the PI3K $\gamma$  class IB enzyme[59]. Finally, it was shown in cardiomyocytes that G $\beta\gamma$  subunits liberated specifically from G $\alpha_q$  coupled receptors increased autophosphorylation of ERK1/2 on Thr188, which translocated to the nucleus and controlled hypertrophic gene expression by two complementing mechanisms [44]. G $\alpha_q$  stimulates the RAF1/MEK/ERK1/2 pathway to enhance Thr188 auto phosphorylation and G $\beta\gamma$  independently stimulates the RAF1/MEK/ERK1/2 complex to contribute to the same outcome [44].

While these direct regulatory targets of G $\beta\gamma$  have been well established, other roles for G $\beta\gamma$  have been demonstrated in diverse cellular compartments, including the Golgi, the ER, the cytoskeleton, mitochondria, and the nucleus [60]. This plethora of non-canonical signalling reflects a broad diversity of G $\beta\gamma$  functions (reviewed in [54, 60]), but for this thesis, we will discuss mainly the nuclear roles of G $\beta\gamma$  subunits. G $\beta\gamma$  subunits have been shown to indirectly affect transcription in both positive and negative ways [60]. It was shown that inhibition of G $\beta\gamma$  reduced the G $\alpha$ s-mediated transcriptional activity downstream of thyrotropin receptor activation. In contrast, inhibition of G $\beta\gamma$  in CD4+ T cells led to an increase in mRNA of IL-2 and increased transcription due to NFAT activity [61, 62]. G $\beta\gamma$  has also been shown to act as a direct co-repressor on complexes that control transcription. It interacts with the adipocyte enhancer-binding protein (AEBP1) and with the AP-1 subunit to negatively regulate each of these complex's endogenous transcriptional activity[63, 64]. Finally, G $\beta\gamma$  has a repressive function on M3 muscarinic receptor-mediated Ca<sup>2+</sup> release and was permissive of ERK1/2 activation[65]. In that study, G $\beta\gamma$  also interacted with heterologous ribonuclear (hnRNP) proteins, which are transcriptional co-

regulatory elements [65]. Additionally, the signal transducer and activator of transcription protein (STAT) proteins may also be stimulated by  $G\beta\gamma$  pairings, implicating another co-transcriptional complex in the  $G\beta\gamma$  nuclear regulatory network [66].

## 1.5 TGF-β signalling

TGF-β is the most potent driver of fibroblast activation in the heart (and in other organs). The TGF-β receptor is not a GPCR, but rather a serine-threonine kinase receptor dimer. TGF-β ligands are activated in the extracellular space by enzymes like thrombospondin-1[67] and bind to the TGF-β type 1 and type 2 receptor, causing a conformational change that promotes the phosphorylation of the intracellular signal transducer SMAD proteins. SMAD2 and SMAD3 become phosphorylated and form a complex with SMAD4 in the cytosol. The SMAD2/3/4 complex then translocates into the nucleus and regulates target genes [68]. TGF-β target genes include ECM components like type 1 and 3 collagen and MMPs, cytoskeletal proteins like α-SMA, and pro-fibrotic cytokines like CTGF and IL-6 [68]. In addition to the pro-fibrotic signalling, TGF-β receptor and SMAD activation also upregulate transcription of SMAD6/7 which are endogenous inhibitors of the TGFB1/2R[68]. SMAD6/7 competes with SMAD2/3 for binding to the TGF-β receptors. when the inhibitor SMADs are bound, they cause receptor internalization and degradation, thus inhibiting further TGF-β/SMAD signalling [68].

## 1.6 Treatment options and pharmacological interventions in cardiac fibrosis

As discussed above, cardiac fibrosis manifests as a condition associated with other heart diseases, and therefore, currently approved treatments that affect cardiac fibrosis are often off-target effects of a drug used to treat other aspects of the heart disease. The treatment algorithm for

HF depends on which type of HF a patient has[13]. HFrEF has clear guidelines for recommended treatments, whereas HFpEF and HFmrEF have less clear treatment guidelines. Patients with preserved and moderately reduced ejection fractions will often continue to receive treatments for underlying pathologies (such as hypertension or arrhythmias) and will often be prescribed diuretics to reduce congestion symptoms[13]. Patients with reduced ejection fraction and who are symptomatic have a much more regimented treatment algorithm. Full clinical guidelines are referenced here[13], but the treatments for heart failure that also reduce cardiac fibrosis include angiotensin-converting enzyme inhibitors (ACE-I), angiotensin receptor blockers (ARBs), renin inhibitors aldosterone receptor blockers, and statins[6, 13].

## 1.6.1 ARBs, ACE-I, and Renin Inhibitors: Targetting the RAAS

As discussed above, the RAAS is a critical driver of both cardiomyopathies and cardiac fibroblast/myofibroblast activity. In various cardiomyopathies blocking the effects of renin, Ang II, and aldosterone using these agents improves cardiomyocyte outcomes[13]. Renin inhibition includes compounds that inhibit the production of Ang II from the RAAS-axis and block renin production [46]. Aliskiren is a renin inhibitor that is used in the treatment of hypertension since Ang II is a hypertensive agent [69]. By reducing the amount of available Ang II that is produced, AT1R activation is reduced and therefore pro-fibrotic signalling is reduced, including demonstrated reduction in ECM production and improvements *in vivo* on diastolic function in HF mouse models[70]. Additionally, studies on blocking the renin receptor using peptide antagonists showed that mice with induced MI had reduced infarct size, improved cardiac output, reduced collagen and fibrosis, and reduced production of pro-fibrotic TGF-β1 and ACE[70].

ACE inhibitors and angiotensin receptor blockers act via the same mechanism: reducing Ang II levels or effects in circulation and on the heart. ACE inhibitors inhibit the ACE from

converting Ang I to Ang II, and ARBs antagonize the AT1R (and to some extent the AT2R) to prevent Ang II activation of its receptors. Captopril, enalapril, lisinopril, and trandolapril are ACE inhibitors that have been shown to reduce fibrosis *in vivo* and cell culture by blocking the AT1R [71-74]. Blocking the AT1R also reduced TGF-β1 production and signalling, through mechanisms described above [71]. ACE inhibitors are beneficial for patients with HFrEF but data is inconclusive regarding their effectiveness under conditions of preserved ejection fraction[46]. Common ARBs include losartan, valsartan, candesartan, and irbesartan[46]. Finally, aldosterone receptors in the kidney can be antagonized using the anti-hypertensive diuretic spironolactone, an aldosterone receptor antagonist [46]. *In vivo* studies have shown that spironolactone treatment reduced interstitial and total fibrosis in a rat arterial hypertension model [75].

# 1.6.2 Statins: inhibition of RhoGTPases

As discussed earlier, the AT1R can also couple to  $G\alpha_{12}$  and signal through RhoGTPase/p38/ROCK signalling to drive fibrotic signalling. Specifically, statins can inhibit TBG- $\beta$  induced myofibroblast differentiation from resident cardiac fibroblasts [76] and fibroblasts from epithelial cell origins [77]. Statins also affect proliferation and migration phenotypes in cardiac fibroblasts [76]. DNA synthesis is reduced via putative ERK/AKT pathways [78], proliferation is reduced via RhoA geranylation inhibition [79], and migration is reduced via ROCK inhibition [80], all under treatment by various statins [81]. Finally, ECM deposition (procollagen mRNA transcription and collagen secretion) is reduced by statin treatment through various mechanisms, including p38 MAPK [82] and by interfering in the PI3K-AKT-SMAD3 TGF $\beta$  receptor activation [83]. Statins act through complex mechanisms, but all seem to be related to AT1R receptor activation via  $G\alpha_q$  and  $G\alpha_{12}$  mediated RhoGTPase activation.

# 1.6.3 Antagonizing TGF-β signalling

TGF-β receptor activation is a central regulator of cardiac fibroblast activation[20, 21, 28, 29]. However, there are no currently approved uses of TGFβ signalling blockade for cardiac fibrosis [46]. Pirfenidone is approved for the treatment of idiopathic pulmonary fibrosis, but its anti-fibrotic mechanisms are not well understood. In pulmonary fibrosis, it has been shown to reduce and reverse TGF-β-induced collagen type 1 and 3 production and TGF-β1 transcription itself, but not necessarily by being a TGF-β receptor antagonist [84, 85]. In animal trials of cardiac fibrosis (pressure overload injury in mice and induced MI and pressure overload in rats), treatment with pirfenidone was shown to reduce infarct size, reduce collagen deposition and improve overall survival [86-88]. Pirfenidone is currently still in phase 2 clinical trials for the treatment of cardiac fibrosis (Study SHZS- F647-PIN-202201) after a previous phase 2 trial (the PIROUETTE trial) concluded modest improvements in myocardial fibrosis [89].

# 1.7 The role of epigenetics and chromatin remodelling complexes on the transcriptional control of cardiovascular diseases

This thesis will investigate questions about how G protein subunits control transcription in cardiac fibroblasts. In unpublished work, we observed that genes controlled by the Smarca4 subunit of the mSWI/SNF chromatin remodelling complex were upregulated in  $G\beta_1$  knockout HEK 293 cell lines (**Fig. S1**, R. Martin, T. Hébert, J. Tanny, unpublished). This work also showed that  $G\beta$  subunits could be co-immunoprecipitated with Smarca4 in HEK293 cells (**Fig. S1**). We are therefore interested in investigating how the mSWI/SNF chromatin remodelling complex is involved in G protein-dependent modulation of transcription.

Chromatin remodelling complexes are a complex and elegant solution that evolution has provided to solve problems caused by the basic biophysical makeup of our DNA. The basic structural unit of chromatin is the nucleosome, which is composed of ~150 base pairs of DNA wrapped around an octamer of histone proteins. The octamer consists of two copies of each of the core histones H2A, H2B, H3, and H4 [90]. In humans, each nucleosome is connected by a DNA linker of around 45 base pairs[91]. As such, most of the DNA in the genome is wrapped around a nucleosome at a given moment. This poses a problem for factors that need to access genomic DNA in a nucleosome context [90]. Four different classes of chromatin remodelers have evolved to help circumvent this inaccessibility problem. These four classes are the SWI/SNF family, the iSWI family, the CHD family, and the INO80 family [90]. Chromatin remodelers use energy from ATP hydrolysis to cause a variety of structural rearrangements to the nucleosome (Diagram 1). These can include the movement of nucleosomes by sliding the nucleosome along the chromatin, replacing certain histones with histone subtypes that serve the specific needed function at that moment, or evicting a nucleosome completely form the chromatin (Diagram 1) [90]. All 4 chromatin remodelling complexes are reviewed well here [90], and for this thesis, we will only discuss the SWI/SNF family of remodelers.

The SWI/SNF complex was discovered in yeast, but we will be discussing the evolutionary homolog in mammals called the mSWI/SNF or BAF family of complexes [92]. The ATPase subunit for the mSWI/SNF family is Brg1, encoded by the Smarca4 gene. For the rest of this work, we will refer to this ATPase as Smarca4. Situations where the mSWI/SNF complex is needed to reorganize nucleosomes include nucleosome replacement in DNA replication, chromatin topology and sister chromatin cohesion[92]. The mSWI/SNF complex has 3 distinct subtypes: the cBAF, PBAF, and GBAF complexes[92]. These subtypes mostly share the same subunits. The

cBAF complex is characterized by having the ARID1A/B and DPF1, 2, and 3 subunits, whereas the PBAF complex instead has ARID2 and PHF10 subunits[93]. Finally, the GBAF complex is the most recently discovered and has the most unique subunits of the three[92, 93]. Each subtype of the mSWI/SNF complex has non-redundant functions tied closely to developmental stages or regions, as well as tissue specificity[94]. Since we are investigating the role of Smarca4 in this thesis, and all mSWI/SNF subtypes contain the Smarca4/Smarca2 ATPase, subtype specificity can be excluded for the purposes of this work.

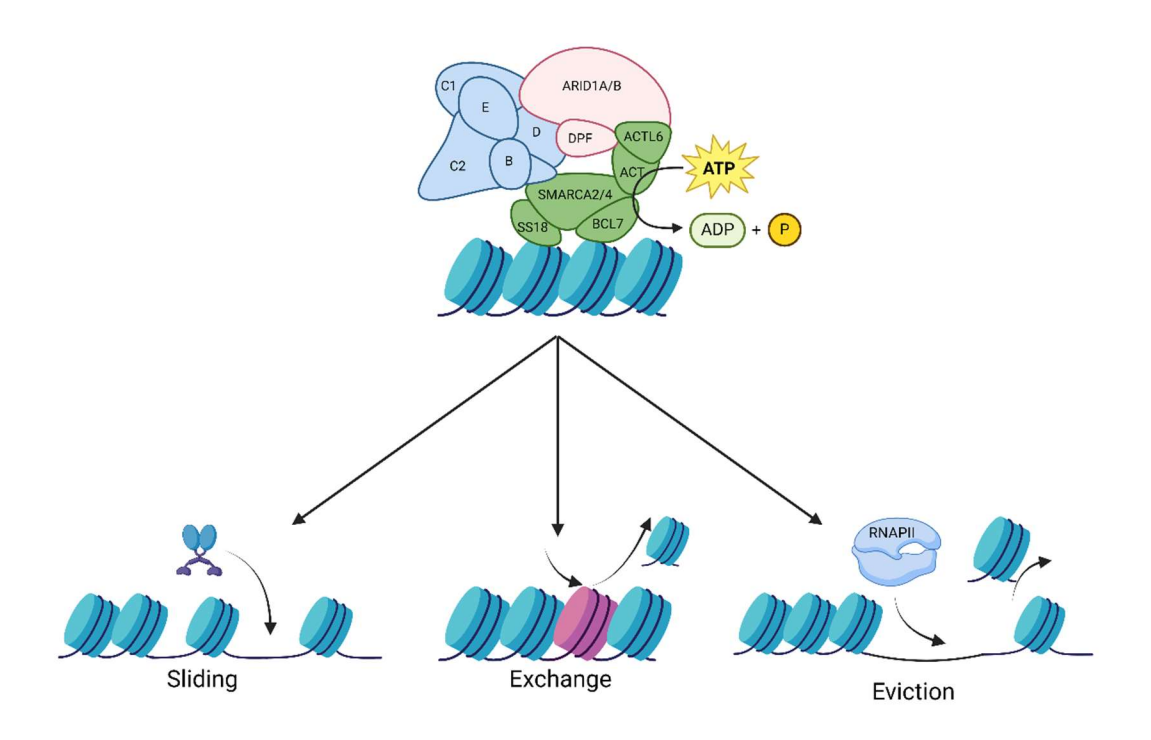


**Diagram 1: Schematic depicting mSWI/SNF functional outcomes**. Using the energy from ATP hydrolysis, the mSWI/SNF complex reorganizes nucleosomes via relocation, exchange, or complete eviction. Examples of potential functional outcomes resulting from this reorganization include transcription factors binding where slid nucleosomes were, the exchange of different nucleosome subtypes for different cellular functions, and RNAPII binding to accessible DNA after nucleosome eviction. Diagram made using BioRender.com.

Beyond chromatin remodelers, other epigenetic mechanisms play an important role in regulating gene expression by exerting control over the genome in terms of which genes are activated and deactivated depending on cellular demands. Common epigenetic modifications include methylation of DNA on the C-5 carbon of the cytidine ring (5mC) which represses genes upon which this mark is found [95]. In addition to DNA itself being modified, the tails of the histone proteins in the nucleosome octamers can be modified as well. Methylation, acetylation, and ubiquitylation are common chemical modifications on histone residues [96]. The best characterized activating histone modifications are H3K4me, H3K36me, H3K4ac, H3K9ac, H3K27ac, H3K36ac, and H2Bub1[96]. The best-characterised repressive modifications include H3K9me and H3K27me[96]. A complete list of histone modifications is well compiled and reviewed here [96].

# 1.7.1 The role of Smarca4 in cardiovascular development and disease

mSWI/SNF complexes are highly studied in embryonic development and cancer due to the vast control they exert over the activation and repression of gene expression programs [90, 93]. In cardiac development, genes such as tbx1, tbx5, tbx20, gata4, and gata6 encode transcription factors that are all implicated in normal cardiac development[97]. Congenital mutations in the subunits of the mSWI/SNF complex have been implicated in mid-gestation embryonic lethality due to drastic cardiovascular defects, and many studies have demonstrated that Smarca4 is required for viable cardiac development (although not Smarca2)[97, 98]. For instance, it was previously thought that the GATA4 transcription factor was a "pioneer factor", implying that it could activate cardiac development genes from silenced heterochromatin without the assistance of chromatin remodelling factors [99]. Contrary to this, recent work has shown that GATA4 could not activate

cardiac genes without the presence of the mSWI/SNF subunits Smarca4 and Baf60 [100], upending a previously held notion of the pioneer factor function of GATA4[98].

Beyond development, the mSWI/SNF complex is also involved in cardiovascular disease. During cardiomyocyte hypertrophy, a fetal-like gene expression program is reinstated [101]. Due to the large-scale reprogramming roles of the mSWI/SNF complex, it has been shown that the Smarca4 subunit is required for hypertrophy and to revert the myosin heavy chain expression to a more fetal-like state in these cardiomyocytes in pressure overload [102]. This myosin-switching phenomenon is associated with cardiomyocyte disfunction and cardiac fibrosis[102]. Furthermore, the Smarca4 subunit has been implicated with cardiac fibroblast activity and differentiation[103]. Analysis of publicly available single-cell RNA seq data implicated Smarca4 as a factor that was significantly upregulated in activated fibroblasts, and overexpression of Smarca4 led to increased fibroblast proliferation, migration, Col1a1, Col3a1, and α-SMA expression[103]. Another study in mice corroborated the role of Smarca4 in heart failure via other mechanisms. In an inducible, cardiomyocyte-targetted Smarca4/Smarca2 double knockout mouse line, knockout mice rapidly developed fatal defects in cardiac function that resulted in lethality within 22 days of induction of Smarca4/Smarca2 knockdown [104]. The knockout mice rapidly developed left ventricular dysfunction associated with bradycardia, DCM, and hypertrophic cardiomyopathy [104]. Electrophysiological repolarization defects were also present, particularly elongated QT interval and abnormal ST segments [104]. Mechanistically, the depletion of Smarca4 subunits caused decreased expression of connexin genes and increased expression of c-Myc, both of which are associated with cardiac dysfunction and serious defects in cardiac electrophysiological conduction [104]. Elevated Smarca4 expression has also been linked to thoracic aortic aneurisms through upregulation of long non-coding RNA [105]. Additionally, Smarca4 is upregulated and recruited

by NF-κB to the promoters of calmodulin-family genes during atherosclerotic stimulation of endothelial cells [106]. Depletion of Smarca4 in these endothelial cells reduced atherosclerotic phenotypes and expression profiles [106].

Smarca4 also modulates the development and response to cardiac reperfusion injuries via multiple epigenetic mediators [107]. Ischemia-reperfusion injury is associated with fibrotic infarct remodelling[108]. Depletion of Smarca4 in mouse endothelial cells was shown to reduce fibrotic outcomes [108]. This mechanism involved Smarca4 interacting with and enhancing the function of the H3K9 demethylase JMJD2B [108]. This led to the increase of gene expression associated with immune cell interactions with endothelial cells and worsened the reperfusion injury outcomes [108]. Additionally, Smarca4 has been shown to activate NADPH oxidase transcription via KDM3A, an H3K9 demethylase, leading to cardiac damage by reactive oxygen species after reperfusion injury [109]. In this same model, the knockdown of Smarca4 led to increased repressive H3K9 dimethylation at the NOX promoter [109]. Given these findings, it is evident that Smarca4 and mSWI/SNF are critical to the development of cardiovascular diseases

# 1.7.2 Epigenetic control of myofibroblasts

Epigenetic modifications play a large role in the biology of myofibroblasts. The Smarca4 subunit (and broadly the mSWI/SNF complex) also interacts with modified histones, and interestingly, is known to exclusively interact with acetylated lysine 14 of histone H3 (H3K14ac) [110]. There is no reported overlap between Smarca4 histone modification selectivity and fibroblast activation, but reviews identify that little is known currently about epigenetic control of fibrotic gene expression, and this is an area for further research.

While DNA methylation is a well-studied control mechanism in many diseases, not much is known about how 5mc incorporation affects fibrotic gene expression in myofibroblasts [111]. Much more is known about other histone modifications, however. First, TGF-\(\beta\)1 stimulation activates p300 which is a histone acetyltransferase. TGF-\beta1 stimulation promoted H4 lysine acetylation and activation of histone acetylation caused by p300 on histone H4 lysine residues at pro-fibrotic genes (Col1A2) [112]. Contrastingly, HDAC4 is a histone deacetylase that removes activating histone acetylation, and HDAC4 activity has been shown to reduce α-SMA expression, antagonizing the TGF-β response [113]. Repressive H3K9 methylation was shown to silence the transcription of PPARy receptors and therefore worsen fibrotic outcomes increasing collagen secretion and necrosis [114]. Finally, H3K27ac is associated with super-enhancer localization of Brd4 that drives P-TEFb phosphorylation of RNAPII and activates transcription[115]. Inhibition of Brd4 via the selective inhibitor JQ1 reduced α-SMA and Serpine1 transcription in TAC-induced mice[116]. In lung fibroblasts, JQ1 reduced secretion of IL-6, production of collagen and  $\alpha$ -SMA, and fibroblast contraction and proliferation[117]. This diverse list of epigenetic modifications implicated in fibrosis indicates that epigenetics exerts well-coordinated control fibrotic transcriptional programs.

## 1.8 Linking Gβγ signalling to transcriptional control of cardiac fibrosis

The work in this thesis was principally designed as a follow-up to a recent publication in our labs that showed Gβ1 subunits interact with RNA polymerase II (RNAPII) in the nucleus of rat neonatal cardiac fibroblasts (RNCFs) and regulate fibrotic transcription and protein expression[118]. First, we showed that the knockdown of Gβ1 led to enhanced fibrotic gene expression in response to Ang II (assessed using a commercial qPCR array). This was recapitulated at the protein level using liquid chromatography-mass spectrometry (LC-MS) experiments, in

which Gβ1 knockdown enhanced Ang II-dependent accumulation of proteins involved in fibroblast activation compared to the control siRNA condition.

Strikingly, chromatin immunoprecipitation coupled with sequencing (ChIP-seq) analysis revealed an enrichment of FLAG-tagged  $G\beta_1$  at the transcription start site of fibrotic genes when the RNCFs were treated with Ang II for 75 minutes. To test the effect of removing  $G\beta_1$  on this transcriptional function, we performed siRNA knockdown and analyzed RNA polymerase II (RNAPII) occupancy by ChIP-seq.  $G\beta_1$  knockdown enhanced RNAPII occupancy at fibrotic genes, both in the absence and presence of Ang II treatment. We further found that RNAPII could be co-immunoprecipitated with Flag- $G\beta_1$ . This co-immunoprecipitation was increased with Ang II and decreased, or completely abrogated, with transcriptional inhibitors iCdk9 and DRB. This recent publication is the first reported transcriptional regulatory role of  $G\beta\gamma$  subunits in cardiac fibroblasts suggesting that  $G\beta\gamma$  subunits interact with chromatin itself to control fibrotic gene expression.

#### HYPOTHESIS AND AIMS

To summarize the work in our labs that preceded and inspired this thesis, we have demonstrated that G $\beta\gamma$  subunits act in cooperation with RNAPII to control fibrotic transcription and protein expression[118]. As well, in unpublished work, we observed that genes controlled by the Smarca4 subunit of the mSWI/SNF complex were upregulated in G $\beta_1$  knockout HEK 293 cell lines (R. Martin, T. Hébert, J. Tanny, unpublished). In HEK 293 cells, overexpressed Flag-G $\beta_1$  co-immunoprecipitated with overexpressed Smarca4 from nuclear lysates, and the amount of co-immunoprecipitated proteins increased with a carbachol treatment (a G $\alpha_q$ -coupled M3 muscarinic receptor agonist). We knew that G $\beta_1$  was interacting with RNAPII in the nucleus but did not know how that interaction actually controlled the changes in fibrotic gene expression reported in 2023. This G $\alpha_q$ -dependent Smarca4-G $\beta_1$  interaction observed in HEK 293 cells that mirrored the G $\alpha_q$ -dependent interaction between G $\beta_1$  and RNAPII in RNCFs led us to hypothesize that:

Gβγ subunits act as transcriptional modulators of the cardiac fibrotic response via interactions with the Smarca4 subunit of the mSWI/SNF complex to alter RNA polymerase II activity.

My M.Sc. thesis has 3 aims:

- 1) To develop a reliable and efficient primary-cell culture system wherein G $\beta$ 1, G $\beta$ 2, and Smarca4 subunits are knocked down using siRNA.
- 2) To characterize the effect that these siRNA knockdowns have on basal and Ang II-induced fibrotic outcomes and myofibroblast phenotypes.
- To investigate the transcriptomic changes in basal and Ang II-induced RNCFs under Gβ<sub>1</sub>,
   Gβ<sub>2</sub>, and Smarca4 knockdown conditions

#### MATERIALS AND METHODS

# 2.1 Isolation and culturing of Rat Neonatal Cardiac Fibroblasts

Cardiac fibroblasts were isolated from 1-3 day old neonatal Sprague Dawley rats (Charles River, Saint-Constant QC, Canada). Rats were housed 12 pups per litter with one 300 g mother rat. Pups were delivered to the McGill McIntyre Medical Building Animal Facility and pups were immediately transferred to a portable, filtered top cage to be brought to the euthanasia room. Pups were kept together with litter-mates and kept warm during the euthanasia procedure. A cotton swab soaked in 70% ethanol was used to sterilize the neck of the pup and the pups were euthanized by decapitation. The thoracic cavity was opened via an incision down the sternum and the heart was removed with forceps. The hearts were placed in 7 mL cold, unsupplemented HBSS (Wisent, 311-511-CL) until the full litter of 12 pups was euthanized. Using small surgical scissors, the heart was crosshatched to increase the surface area for the enzymatic digestions. Crosshatched hearts were placed in a 0.1 % trypsin (Wisent, 325-043-CL) solution dissolved in HBSS and rotated in trypsin solution overnight (16 hours).

The hearts were then removed from trypsin and subjected to mechanical and enzymatic digestion in a 1 mg/mL collagenase (Bishop, 9001-12-1) solution. Briefly, 5 mL of DMEM low glucose (Wisent, 319-010-CL) supplemented with 7% Fetal bovine serum (FBS) (Wisent 098150) and 1% penicillin/streptomycin (P/S)(Wisent, 450-201-EL) was added to the trypsin tube to deactivate the trypsin. The deactivated trypsin media was aspirated out of the 50 mL tube and replaced with 5 mL of the collagenase solution. This was shaken horizontally at a frequency of 2.5 Hz in a 37°C water bath to dissociate the individual cells physically and enzymatically from the underlying tissue. The 5 mL of media containing a mixture of myocytes, fibroblasts and other cell types in the heart was removed from the tube, leaving the remainder of the hearts in the tube, and

5 mL of fresh collagenase solution was added again, and the process repeated a total of 5 times. Each 5 mL removal of cell suspension was filtered through a 40 nm sieve into a clean 50 mL tube to total 25 mL of suspended cell mixture. This was centrifuged to pellet the cell mixture and the collagenase digestion media was removed. The cell pellet was washed once with 20 mL of cold HBSS low glucose and centrifuged again. The HBSS wash media was aspirated off the pellet and the pellet was thoroughly dissociated in 20 mL 37 °C DMEM low glucose supplemented with 7 % FBS and P/S. 10 mL of the cell mixture was transferred to 10 cm tissue culture treated, uncoated plastic plates (VWR, 10062-880) and incubated in a cell culture incubator set to 37 °C and 5% CO<sub>2</sub>. After allowing fibroblasts to adhere to the plates (75 minutes), cardiomyocytes and other cell types that remained in suspension were removed. The fibroblasts were washed 3 times with warm DMEM + 7% FBS to remove leftover myocytes and left in the cell culture incubator for 48 hours to proliferate. After this point, siRNA treatments and/or Ang II/losartan treatments were performed (see respective methods sections).

Rat mothers were donated to the CMARC (Comparative Medicine and Animal Research Centre) at McGill University or if their health status did not allow this, were either euthanized by CO<sub>2</sub> asphyxiation as per approval by the McGill Facility Animal Carre Committee in compliance with the Canadian Council of Animal Care guidelines (AUP: MCGL-5187).

# 2.2 Fixed Transfection of RNCFs on plastic plates with siRNA

48 hours after RNCF isolation, the DMEM + 7%FBS + P/S was removed and the RNCFs in the 10 cm plates were treated with 2mL of warm trypsin/EDTA (2.25%/2.21mM) for 5 minutes. 8 mL of DMEM supplemented with 2.5% FBS was added to the trypsin media to deactivate the trypsin and the fibroblasts were pipetted up and down with a 10 mL serological pipet 4 times to generate a single cell suspension. Cells were counted using the BioRad TC-20 automated cell

counter and a live cell count was determined via 0.2 μM trypan blue (GE, SH40003.01) staining. In tissue culture compatible 6-well plates (Thermo Scientific, 130184), 250,000 RNCFs were seeded and allowed to adhere for 24 hours in DMEM supplemented with 7% FBS and 1% P/S. 24 hours later, at a target confluency of 70%, media was exchanged for siRNA transfection mixtures. siGENOME Smartpool siRNA against Gβ1 (Dharmacon, SO-3148576G), Gβ2 (Dharmacon, SO-3114119G) or Smarca4 (Dharmacon, SO-3001156G) was suspended in nuclease free water at 20uM as per manufacturers instructions. siRNA was diluted in unsupplemented DMEM low glucose to a concentration of 25 or 50 nM as per experimental conditions in a 1:1 ratio with lipofectamine 2000 (Thermo Scientific, 11668500). The DMEM growth was exchanged for 1 mL of the lipofectamine:siRNA mixture and the RNCFs were allowed to incubate with the lipofection reagents for 5 hours. Once this was complete, the lipofection reagents were aspirated off the cells and DMEM low glucose with 7% FBS and P/S was added to the cells to grow and recover. 24 hours later, the DMEM growth media was replaced with unsupplemented DMEM low glucose for 16 hours overnight to serum starve the fibroblasts before agonist treatment.

#### 2.3 Suspended Transfection of RNCFs on plastic plates with siRNA

siRNA: lipofectamine mixtures were prepared as described for the fixed transfection protocol and mixed with the appropriate number of isolated RNCFs in a well of a 6-well plate, and the volume was topped up to 1 mL with media. 1 mL of the transfection mixture was added to the well next, yielding a final volume of 2 mL per well. The intermediate stock concentration of the lipofection mixture was made double the final target concentration in a stock (target siRNA concentration described in each experiment in *Results*) so that when diluted in a 2 mL final volume with the cells, the final siRNA concentration was the correct target. The siRNA and RNCF suspension was incubated for 5 hours in a cell culture incubator, during which time the suspended

cells attached to the plastic plate and were lipofected. After 5 hours, the media containing the lipofection reagents was aspirated off and replaced by 2 mL of DMEM low glucose supplemented with 7% FBS and 1% P/S for 24 hours. 24 hours later, this growth DMEM media was replaced by DMEM + 1% P/S (no FBS) to serum starve the fibroblasts overnight (16 hours). The following morning, the serum starvation media was replaced by the agonist/antagonist media as described in the respective assay section.

#### 2.4 Scratch assays

Serum starvation DMEM media for transfected RNCFs was replaced by DMEM low glucose (no FBS, with 1% p/s) with or without 10 uM losartan potassium (Sigma-Aldrich, 61188-100MG). After 30 minutes of losartan treatment, the media was removed, and a sterilized ruler was placed across the opening of the 6-well plate. Three swift, firm, evenly spaced scratches were made vertically and three were made horizontally perpendicular to the vertical ones. The scratches were made using a long 10 uL pipette tip. This resulted in a 3 x 3 hash pattern scratched out of the monolayer of transfected, losartan-treated RNCFs. 1 mL of unsupplemented DMEM media was added to the well and swirled to wash away debris. This was replaced with the assay media (DMEM low glucose supplemented with 1 % P/S) containing either 10 µM losartan, 1 µM Ang II (Sigma-Aldrich, A9525), or combined Ang II and losartan at their respective concentrations.

The 6-well plates were placed in the Cytena Cellcyte X automated microscope (Cytena, C2111137) and images were captured every hour for the first 6 hours, then every 2 hours for the remaining 18 hours to total 24 hours of scans. The microscope scanned in a 4 x 4 grid, taking 16 images in the centre of the well and therefore generating 16 fields of view per well. The scratches were made in a 3 x 3 hash pattern to maximize the likelihood of a scratch being fully visualized in a field of view. Once the images were acquired, the CellLink (Cellcyte Studio 2.6.0) software

exported the images as TIFF image stacks which were imported to ImageJ. A scratch assay analysis plugin for image J created by Suarez-Anedo and colleagues [119] was used to extract the scratch area in each image of the image stack in mm<sup>2</sup> and the percentage of the field of view. This scratch area was then plotted over time in GraphPad Prism (GraphPad Prism version 10.0.0 for Windows) and a linear regression analysis was run on each field of view. Slopes of the linear regression were measured and plotted for each condition. This value is the rate of scratch area closure in mm<sup>2</sup>/hour and it was compared between the conditions outlined in whichever experimental set up was described in the *Results* section.

Scratches performed with Hoechst nuclear stain (Thermo Scientific, H3570) proceeded as described above, except with the addition of the nuclear stain in a 1:10,000 ratio. For each time point, a brightfield and a blue, fluorescent image were taken to measure nuclear staining. These images were then analyzed by the CellLink built-in analysis software to identify unique objects in bright field or fluorescent images, mark them with a virtual overlay mask, and count the individual objects. The calculated count values were plotted against confluency measurements in GraphPad Prism and a Pearson correlation analysis was performed.

For scratch assays testing FBS concentration, there was no losartan pre-treatment. Instead, fibroblasts were trypsinized after the 48-hour recovery from isolation and plated at 250,000 cells per well on uncoated 6-well plates (as described previously) or on 6-well plates coated with human plasma fibronectin. They were allowed to grow directly to a monolayer since this experiment had no siRNA treatment. The plates were serum starved as described above and the scratches were made directly after the unsupplemented DMEM serum starvation media was removed. The media was replaced by DMEM low glucose supplemented with the 0 %, 2 %, 5 %, 7 %, and 10 % FBS

(v/v%) and 1% P/S and the 6 well plates were placed in the microscope for the imaging program as described above.

For scratch assays testing cytosine arabinoside (Ara-C, Sigma Aldrich, C1768-500MG), the same procedure was followed as the cells treated with losartan and Ang II described above. The above conditions were duplicated and one set of conditions had 10 µM Ara-C added at the time of losartan treatment. From that point on, any media being added to the Ara-C conditions, as described in the procedures above had Ara-C supplemented to it. The scratch closure rate for the Ara-C experiment is described with a half-life, which is another metric exported from the GraphPad Prism linear regression analysis described above.

For scratch assays including TGF-β1 (ThermoFisher, PHG9214), the same procedures were followed for the preparation of RNCFs for scratch assays to test FBS concentrations. No siRNA knockdown was performed. After serum starvation, no losartan pretreatment was performed. Instead, scratches were made after serum starvation and 40 pM TGFβ-1 or 1 uM Ang II was added to DMEM low glucose with 1% P/S and the respective treatments were added to the scratched RNCF monolayers. Images were acquired and analyzed as described above.

#### 2.5 Proliferation Assays

Proliferation assays were performed in 6 well plates with RNCFs prepared via the suspended transfection and treated with losartan, Ang II, and respective vehicle controls as described above. The 6-well plates were placed in the CellCyte X microscope to grow. A program was run that captured a set of 9 brightfield images in a 3x3 grid for each well of the 6 well plates every hour for the first 6 hours, then every 2 hours for the remainder of the 24-hour timepoints. The same built-in confluence mask analysis as described in the scratch assay section above was

used to measure confluence at each time point. This confluence percentage was exported to GraphPad prism, and a mean confluence at each time point was calculated form the 9 fields of view. This mean confluence was plotted over time and a linear regression analysis was performed, as before. The slope of the regression (percent confluence change per hour) was plotted between treatment conditions as reported in the *Results section*.

# 2.6 Western blots for knockdown validation

Cells were grown in whichever format as described in the respective experiment in *Results*. Assay media was aspirated off the growing surface and cells were washed once with cold, nuclease-free PBS. For 10 cm plates, 500 uL of RIPA (1% Igepal CA630, 50 mM Tris-HCl pH7.4, 150 mM NaCl, 1 mM EDTA, 1 mM EGTA, 0.10% SDS, 5% Sodium Deoxycholate, 1x protease inhibitor) lysis buffer was added to the media-free plate. Cells were lifted and mixed with the lysis buffer using a rubber cell scraper. The lysate was added to 1.5 mL microcentrifuge tubes. Lysates were homogenized using a probe sonicator (Mandel Sonicator ® 3000) at 3W power 3 times for 5 seconds with 30 sec rests on ice. Samples were spun in a microcentrifuge (Eppendorf, Centrifuge 5425/5425R) at maximum speed and the supernatant was transferred to a new 1.5 mL microcentrifuge tube. Total protein was quantified using the fluorescence-based Pierce<sup>TM</sup> BCA kit (Thermo Scientific, 23225) as per manufacturer instructions. 20 µg of protein lysates were added to an equal volume of 2X Laemmli buffer supplemented with 5% β-mercaptoethanol and heated for 15 minutes at 65°C before SDS-PAGE. SDS-PAGE was performed as described previously [65]. For Gβ1, Gβ2, and Smarca4 siRNA knockdown validations, protein lysates in Lammeli buffer were loaded onto 10% Tris-glycine gels and run on a Bio-Rad Protean® (Bio-Rad, 525BR) gel electrophoresis apparatus for 15 minutes at 100V followed by 1 hour at 140V. Proteins were transferred to a PVDF membrane (GE, A10083114). in cold transfer buffer (2.91 g Tris, 1.47 g

Glycine, 450 mL ddH2O, 50 mL 100% MeOH) at 12V for 1 hour with constant stirring in a Bio-Rad Protean® Transfer Tank. Membranes were soaked in 5% skim milk powder in TBST (8.78g NaCl, 10mL 1M Tris pH 8.0, 0.5 mL Tween-20, all dissolved in 1L ddH<sub>2</sub>O) for blocking for 3 hours, then incubated overnight in the primary antibody against pan-Gβ1-4 (BD, #610288) or Smarca4 (Cell Signalling, D1Q7F). Anti-pan-Gβ1-4 and Anti-Smarca4 were used at a concentration of 1:1000. Antibodies against loading controls of β-tubulin (Invitrogen, 32-2600) or GAPDH (Invitrogen, AM-4300) were used at a concentration of 1:500. The membrane was incubated in appropriate secondary antibody for 30 minutes (rabbit 1:20,000, Sigma-Aldrich, A0545-1mL; mouse 1:20,000, Sigma-Aldrich, A9917-1mL). Membranes were treated with GE ECL Select (GE, RPN2235) and chemiluminescence was detected using the GE Amersham Imager 600. Western blots were quantified using ImageJ [120].

# 2.7 Western blots for collagen secretion

900  $\mu$ L of the growth media was removed from the relevant cell culture and added to 1.5 mL microcentrifuge tubes. The conditioned media was spun for 5 minutes at maximum speed in a microcentrifuge. The supernatant was transferred to new 1.5 mL microcentrifuge tubes and 10  $\mu$ g of BSA (Bioshop, ALB005.100), 100 uL of 0.2% w/v sodium deoxycholate, and 245  $\mu$ L of 100% Trichloroacetic acid (TCA) were added to the sample. After incubation at 4 ° C overnight, precipitated proteins were spun in a microcentrifuge at maximum speed for 15 minutes. The supernatant was removed and the pellet was washed twice with 1mL ice-cold 100% acetone. Pellets were dissolved in 21  $\mu$ L of Lammeli buffer and 3  $\mu$ L of 1.5 M Tris pH 8.8. The pellet was placed in a bath sonicator for 5 seconds per sample at 3 W with a 30-second cool down in between each of 3 sonication cycles. Sonicated protein samples were heated for 90 seconds at 70 ° C and run on an 8% acrylamide gel as described above. Nitrocellulose membranes (Bio-Rad, 1620115)

were used instead of PVDF to enable total protein quantification by Ponceau S (Sigma-Aldrich p3504-50G) staining. Immunoblot images were quantified using ImageJ and bar plots were made using Graphpad Prism 10.

#### 2.8 RNA extraction and RT-qPCR

Using a standardized protocol for 10 cm and 6-well plates, TRI reagent® RNA Isolation Reagent (Sigma, T9424) was added to each well/plate and cells were lifted and lysed with a rubber cell scraper. Suspensions were transferred to a 1.5 mL microcentrifuge tube and vortexed for 5 seconds. 200 uL of Bromochloropropane was added and lysates were spun at 12,000 rpm for 15 minutes at 4°C, and the aqueous, upper phase containing RNA and trace DNA was digested with DNAse1. cDNA synthesis was primed with random hexamers (IDT, 51-01-18-01) using M-MLV reverse transcriptase. Sequences are provided in **Table S1**. For qPCR, cDNA was diluted to 5 ng/uL and stored at -20 °C until used. cDNA was added to the reaction well at a concentration of 5 ng/uL, BrightGreen 2X qPCR Mastermix – No Dye kit (Applied Biological Materials, MasterMix-S-XL) at 1X and forward and reverse primers at 30 nM. The reaction plate was centrifuged in a plate microcentrifuge to collect all reaction reagents at the bottom. qPCR was performed in triplicate using a ViiA 7 Real-Time PCR System (Thermo Scientific). Amplification results were analyzed via the 2-ddCt method [121].

$$dCT_{G\beta1} = \left(Ct_{G\beta1\,from\,G\beta1\,siRNA} - Ct_{GAPDHfrom\,G\beta1\,siRNA}\right)$$

$$ddCT_{G\beta1} = dCT_{G\beta1} - Ct_{G\beta1\,from\,Ctrl\,siRNA}$$

$$Fold\,Change = 2^{-ddC}\,_{G\beta1}$$

$$Knockdown\,\% = (1 - fold\,change) * 100$$

$$dCT_{Serpine1\,from\,Ang\,II\,condition} = \left(Ct_{Serpine1\,from\,Ang\,II} - Ct_{GAPDHfrom\,Ang\,II}\right)$$

$$ddCT_{Serpine1\,from\,Ang\,II\,condition} = dCT_{Serpine1\,from\,Ang\,II\,condition} - Ct_{Serpine1\,from\,Vehicle\,condition}$$

$$Fold\,Change = 2^{-ddCT_{Serpine1\,from\,Ang\,II\,condition}$$

Normalized fold change values were plotted in GraphPad Prism 10 and any statistical analyses were performed as described in the experimental results

# 2.9 qPCR mRNA primer design

Primers were designed using NCBI Primer BLAST. The parameters were as follows:

Parameter	Setting
PCR Product size	50 -150 bp
Primer melting temperature range	59°C - 60°C - 61°C
Exon junction span	Primer must span an exon-exon junction
Database	Refseq RNA (refseq_rna)
Organism	Rattus norvegicus
Primer GC content	40-60%
Salt correction formula	Schidkraut & Lifson 1965

**Table 2: Settings for NCBI Primer BLAST.** 

Primer pairs were selected based on minimizing the predicted PCR product size and self-3' complementarity. Primer sequences are listed in **Supplementary Table 1.** 

# 2.10 Morphology microscopy image acquisition

To evaluate the fibroblast morphology of TGFβ-1 and Ang II treated RNCFs, the Leica Dmi1 microscope was used. Images were downloaded using the LAS-EZ software (Leica, version 3.4).

#### 2.11 Immunofluorescent microscopy image analysis

Immunofluorescent analysis of α-SMA and Ki-67 was performed on paraformaldehyde (PFA) fixed RNCFs and imaged using the Revvity OperaPhenix plus microscope. RNCFs were

seeded in 96 well, black-walled, clear bottom optical plates (Thermo Scientific Nunc, 165305) at a density 10 000 cells per well and left to attach and grow in DMEM low glucose supplemented with 7% FBS and 1% P/S for 24 hours. This growth media was replaced by FBS-Free DMEM with 1% P/S for 16 hours overnight to serum starve. After 16 hours, serum-free media was replaced by fresh serum-free media supplemented with 1% P/S and 1 uM Ang II and cells were incubated for 6 hours. After 6 hours, the media was removed and cells were fixed in 2% PFA for 10 minutes. Fixed cells were washed in 1 X PBS. 50 μL of 0.3% Triton-X (Sigma-Aldrich, X100) was added to each well to permeabilize the RNCFs for 10 minutes. The RNCFs were then blocked with 5% (% w/v) BSA for 2 hours. After blocking, the RNCFs were incubated in the primary antibody of interest, and diluted in 5% BSA. Anti-Ki-67 (BD, 550609) was diluted at 1:200, anti-α-SMA (Sigma-Aldrich, A2547-100UL) was diluted at 1:1000, and anti-vimentin was diluted at 1:1000. Ki-67 + vimentin or α -SMA + vimentin antibodies were mixed and the RNCFs were incubated in the primary antibody mixture overnight at 4°C. The following day, Alexafluor 488 (Invitrogen, A11034) and AlexaFluor647 (Invitrogen, A21239) diluted 1:1000 in 5% BSA were added to the wells, with mouse and rabbit species reactivity corresponding to the combined primary antibodies on the cells. The plates were incubated for 3 hours in the dark at room temperature. Secondary antibody mixtures were removed, plates were washed with 1X PBS and 1:10 000 Hoechst nuclear stain was added for 10 minutes. Hoechst was removed and plates were washed with 1x PBS once more. The plates were imaged immediately using the Opera Phenix plus microscope.

### 2.12 RNA isolation for RNA sequencing

For the RNA sequencing experiment, we prepared RNCF conditions in the same way as the suspended transfection methodology described above. After 6 or 24 hours of Ang II treatment, RNCFs in 6 well plates were lysed using the RNEasy Mini kit (Qiagen, 74104) and Qiashredder

Homogenization kit (Qiagen, 79645) as per manufacturer instructions. RNA samples were quantified using the Nanodrop 2000 (Thermo Scientific) and aliquoted into 4 x 150 ng aliquots. An additional aliquot was generated for quality control purposes and analyzed on an Agilent 2100 Bioanalyzer (Agilent, G2939A).

Samples were run by Dr. Nicolas Audet on the Agilent 2100 Bioanalyzer to verify the minimum RIN score for cDNA library generation. Once all samples passed this quality check, cDNA library generation proceeded using the NEB Next Ultra II Directional RNA Library Prep Kit for Illumina (NEB, E7760L). First, spike-in RNA was added using the ERCC RNA Spike-in Mix (Invitrogen, 44567-40). Then, RNA was subjected to poly-adenylation pulldown selection via the poly-A enrichment kit provided with the NEB Next Ultra II Directional RNA Library Prep Kit for Illumina (NEB, E7760L). Poly-A selected RNA was subjected to fragmentation, Illumina adaptor ligation, priming with NEB Next multiplex Oligos for Illumina (NEB, E6440S) and PCR amplified for 8 cycles. An aliquot of the prepared cDNA library was set aside for a final bioanalyzer quality control. The remaining cDNA was stored at -80°C until all samples passed the fragmentation and contamination thresholds in the Bioanalyzer QC, at which point they were shipped to the BC Genomics and Cancer research centre for sequencing. cDNA libraries were sequenced using the Novaseq 6000 platform (Illumina). Sequencing was paired-end and performed at a pooled depth of 1.6 billion reads for 67 samples.

# 2.13 RNA Sequencing Data processing and bioinformatics

FASTQ files were subjected to adaptor trimming and filter of low quality and duplicate reads using fastp (v0.23.4, [122]. Then, a FastQC (v0.12.1) report was run on the forward and revere trimmed fastp output files. Our sequences likely had sequence overamplification but other than PCR amplification flags, our FASTQ files passed this QC. Next, sequences were aligned to

the Rattus norvegicus genome (GRCr8, GenBank NCBI # GCA\_036323735.1) using STAR (v2.7.11b). Individual count matrices were generated using FeatureCounts (v2.0.1). Counts were summarized into 1 text file and exported for further analysis.

Once counted, count files were separated by timepoint (6 and 24 hours) using python scripts. Count files were divided into two groups: one with count files organized by siRNA and one with count files organized by treatment. Specifically, each count subfile was split into 4 individual count files, each one containing all the count information for one siRNA (ctrl siRNA, Gβ1 siRNA, Gβ2 siRNA, and Smarca4 siRNA) or one treatment (Vehicle, losartan, Ang II, and Ang II + Losartan). For each count file, a DESeq annotation file was created to input into the DESeq package information describing the individual conditions, siRNA, treatment, replicate and timepoint for each sample in a count file. Creating the annotation files and separating the count were all achieved using Python scripts.

Differential expression analysis proceeded using the DESeq2 (v1.42.1) package. DESeq results outputs were shrunken using the DESeq function IfcShrink to better estimate count abundances for visualizations[123]. Lists of differentially expressed genes were output from R and Venn diagrams were generated (https://bioinformatics.psb.ugent.be/webtools/Venn/). From the lists of up and downregulated genes, GO term enrichment analysis was performed using the EnrichGO function of the clusterProfiler package (v4.10.1). Significant GO terms for biological processes, molecular functions, and cellular compartments were generated and plotted using GOplot (v1.0.2). Volcano plots were generated using EnhancedVolcano (v1.20.0) from the LFC-shrunk fold change results. Before generating heat maps, however, it is important to remove batch effects from the DESeq 2 results. The LFC outputs from DESeq2 have already had the litter/batch effect removed as a part of the differential expression design we created, but the heatmaps

generated from count scores and expression levels do not have this controlled for. Additionally, visualization is more accurate if the fold change results are variance stabilized transformed, so the vst function of DESeq2 was used. The limma package (v3.58.1) was used to remove effects from the different replicates. Heatmaps were generated using pheatmap (v1.0.12). All of the above analyses were performed for each branch of the analysis (siRNA groups and treatment groups) and a combination of the results are reported in *Results*.

#### RESULTS

# Results Section 1- Developing and optimizing a knockdown protocol to investigate the effects of G proteins and chromatin remodelers on the fibrotic response using siRNA

Section 1 of this thesis outlines methodological and tool development processes that were undertaken to investigate the roles of G $\beta$  subunits and the Smarca4 subunit on the cardiac fibrotic response. *Section 1* will cover the optimization of protocols for transient knockdown of the genes of interest in primary cardiac fibroblasts using siRNA [124] and the subsequent validation of their efficacy.

#### 3.1 Determining plating conditions for optimal knockdown of G\beta and Smarca4 subunits

To investigate the roles of  $G\beta$  subunits and Smarca4 on the fibrotic response, a protocol for reliably and reproducibly knocking down these genes of interest was developed. We chose to use siRNA as the knockdown tool because of its strengths as a transient intervention and as a follow-up on previous work done using siRNA in RNCFs in the lab[118]. Three parameters were optimized in the development of the knockdown protocol: cell plating methodology, siRNA concentration, and knockdown duration.

# 3.1.1 siRNA lipofection performed on fixed RNCFs grown on plastic yields low knockdown efficiency

The first methodological question that was answered was to determine whether the RNCFs grown on plastic were a flexible system that could handle multiple techniques for siRNA lipofection to guide the development of downstream assays. For instance, being able to transfect RNCFs after they have adhered to the plate would enable scratch wound healing assays (discussed later) since a target confluency must be reached during peak knockdown. We tested 25 nM or 50

nM siRNA transfected using lipofectamine 2000 on RNCFs that had been plated at a density of 250,000 cells per well of a 6-well plate. siRNA and lipofectamine transfection reagents were left incubating on the cells overnight. Knockdown efficiency was validated using western blotting and qPCR. The results of the three independent experiments to determine knockdown efficiency are shown in **Table 3**.

Table 3 A

Replicate	siRNA concentration	Time post- Knockdown	Percent of targets knocked down by qPCR	Percent of targets knocked down by western blot			
Gβ1 knock	Gβ1 knockdown on Fixed RNCFs						
1	25 nM	48 hours	13 %	Not determined			
1	50 nM	48 hours	25 %	Not determined			
2	50 nM	48 hours	22 %	20%			
2	50 nM	72 hours	16 %	9%			
3	50 nM	48 hours	Not determined	52%			
3	50 nM	72 hours	Not determined	27%			

B

Replicate	siRNA concentration	Time post- Knockdown	Percent of targets knocked down by qPCR	Percent of targets knocked down by western blot		
Smarca4 knockdown on Fixed RNCFs						
1	25 nM	48 hours	Not determined	17.4 %		
1	50 nM	48 hours	Not determined	71.5 %		
2	25 nM	48 hours	19 %	Not determined		
2	50 nM	48 hours	5 %	Not determined		
3	50 nM	48 hours	18 %	Not determined		
3	50 nM	72 hours	5 %	Not determined		

Table 3. Summary of siRNA target knockdown percentage by qPCR and western blot on adherent RNCFs. siRNA concentration, time since knockdown and replicate number are reported. A)  $G\beta_1$  knockdown efficiency. B) Smarca4 knockdown efficiency. qCPR percentage is shown as 1 minus target gene fold change (determined by the  $2^{-ddCt}$  method described in *Methods*. Western blot percentages are reported as (band intensity of target in the Ctrl siRNA condition)/(band intensity of KD condition)\* 100.

To test different knockdown conditions, the efficacy of 25 nM and 50 nM siRNA concentrations were tested 48 or 72 hours after transfection. Either qPCR or western blot were used to determine knockdown efficiency. Both Gβ1 and Smarca4 were knocked down most effectively using 50 nM siRNA and assaying 48 hours after transfection with a maximal efficiency of 52% and 72% respectively. Neither siRNA was physiologically effective after 72 hours and 25 nM siRNA concentration performed worse than 50 nM siRNA in all attempts except one Smarca4 trial. This being said, as seen in the 5-20% knockdown efficiency in **Table 3**, it is evident that at the mRNA or protein level, knocking down genes on already adherent RNCFs is not the most effective way to achieve substantial levels of target knockdown.

# 3.1.2 siRNA lipofection performed on RNCFs in suspension yields more efficient target knockdown

The previous section outlined methodological alterations to previously in-use siRNA lipofection protocols to knock down target genes in adherent RNCFs rather than RNCFs in suspension. Suspension-based transfection had been used before in the Hébert and Tanny labs but could not be used for scratch assays which require adherent cells. To move the project forward, since other planned assays did not require adherent cells, we proceeded with transfecting cells in a liquid cell suspension. To begin, knockdown was first established in 10 cm plates for practicality purposes, followed by optimization of transfection in 6 well plates to set the stage for the bulk of the results in this thesis. First, a pilot trial of the suspended transfection protocol yielded strikingly successful knockdown of G $\beta$ 1 in RNCFs using 50 nM siRNA lipofection reagents, allowing for expanded knockdown trials of G $\beta$ 1, G $\beta$ 2 and Smarca4. In 3 independent experiments, G $\beta$ 1 and Smarca4 were both efficiently knocked down using a suspended transfection protocol after 48 hours of transfection in a large format 10 cm plate system (**Fig. 1a**). Maximum knockdown was

observed at the mRNA level for both G $\beta$ 1 and Smarca4 at 92% and 89% respectively (**Fig. 1 c-d**). At the protein level, Smarca4 was knocked down by 64% (**Fig. 1b**). The G $\beta$ 1 knockdown western blots showed a 23% reduction in quantified western blots (**Fig. 1a**). However, the only reliable antibody available at the time of this experiment was a pan-G $\beta$  antibody. This means the western blot signal visualized represented multiple G $\beta$  subunits. Given the strong qPCR knockdown, we were confident that the seemingly low G $\beta$ 1 KD on the western blot was due to the detection of non-targetted G $\beta$  subunits.

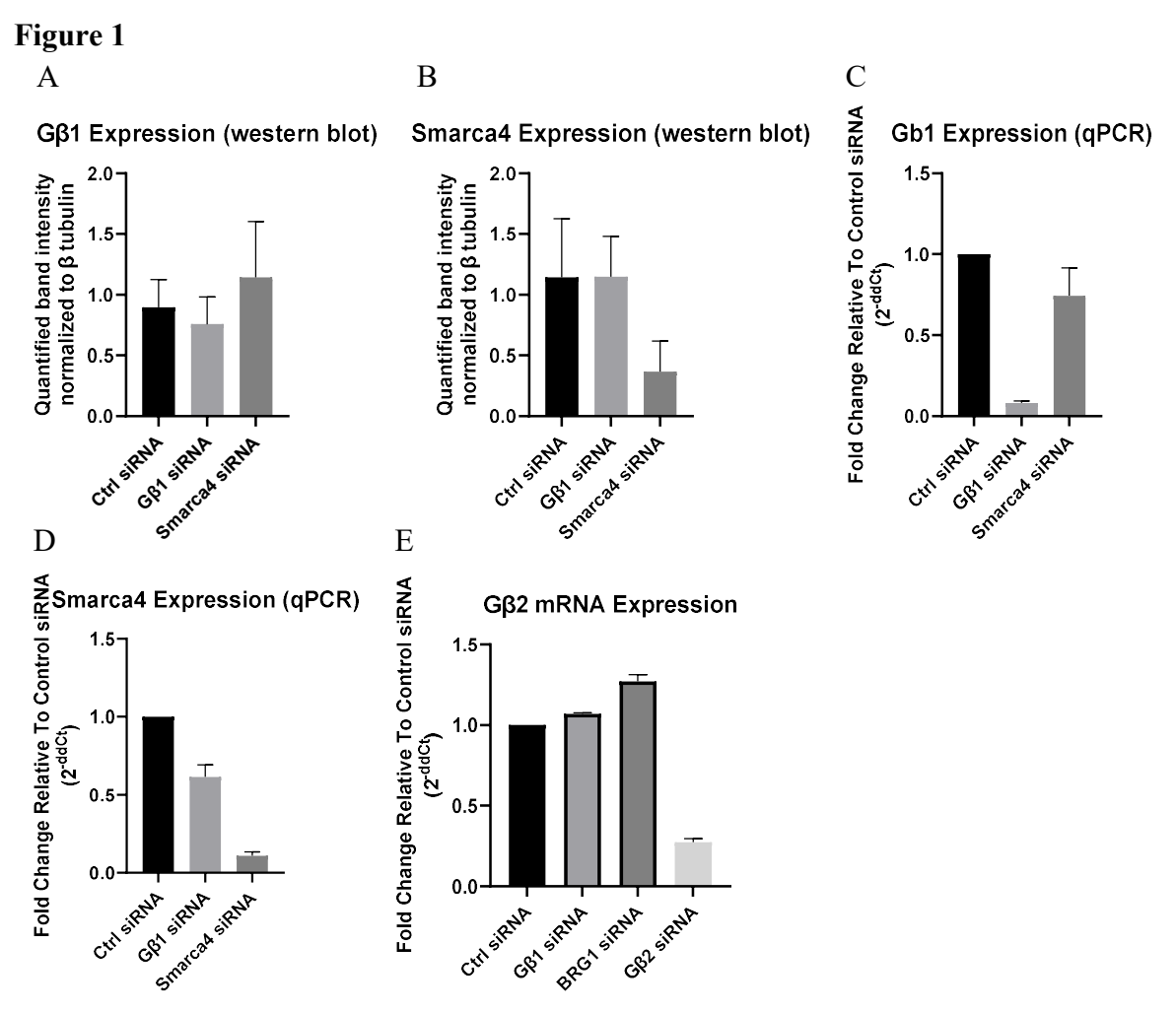


Figure 1. Quantification of mRNA and protein of suspended RNCFs. A-B) Quantification of western blot G $\beta$ 1 and Smarca4 knockdown. C-E) quantification of mRNA knockdown of G $\beta$ 1, Smarca4, and G $\beta$ 2. Representation of n=3 independent knockdowns (Mean +/- SEM)

### 3.2 siRNA knockdown optimization for phenotypic assays

Since RNA sequencing and large-scale phenotypic assays were the goal of this project, we proceeded to scale down the RNCF knockdown system from 10 cm plates to 6-well plates. This knockdown validation was combined with measures of fibrotic gene expression via qPCR which will be discussed in *Results Section 3*. The knockdowns were carried out using 50 nM siRNA against G $\beta$ 1, G $\beta$ 2, Smarca4, or a non-targetting control siRNA (Ctrl siRNA). These experiments were the first to include Ang II and losartan (an AT1R antagonist) treatments in combination with the siRNA knockdown. Each siRNA was tested in combination with the following treatments: Vehicle treated (DMEM), 10  $\mu$ M losartan alone, 1  $\mu$ M Ang II alone, or both Ang II and losartan. RNCFs were pre-treated with losartan for 30 minutes before Ang II treatment, and RNA was collected 6 hours and 24 hours after the addition of Ang II. The knockdown validation results are shown in Table 4.

Table 4

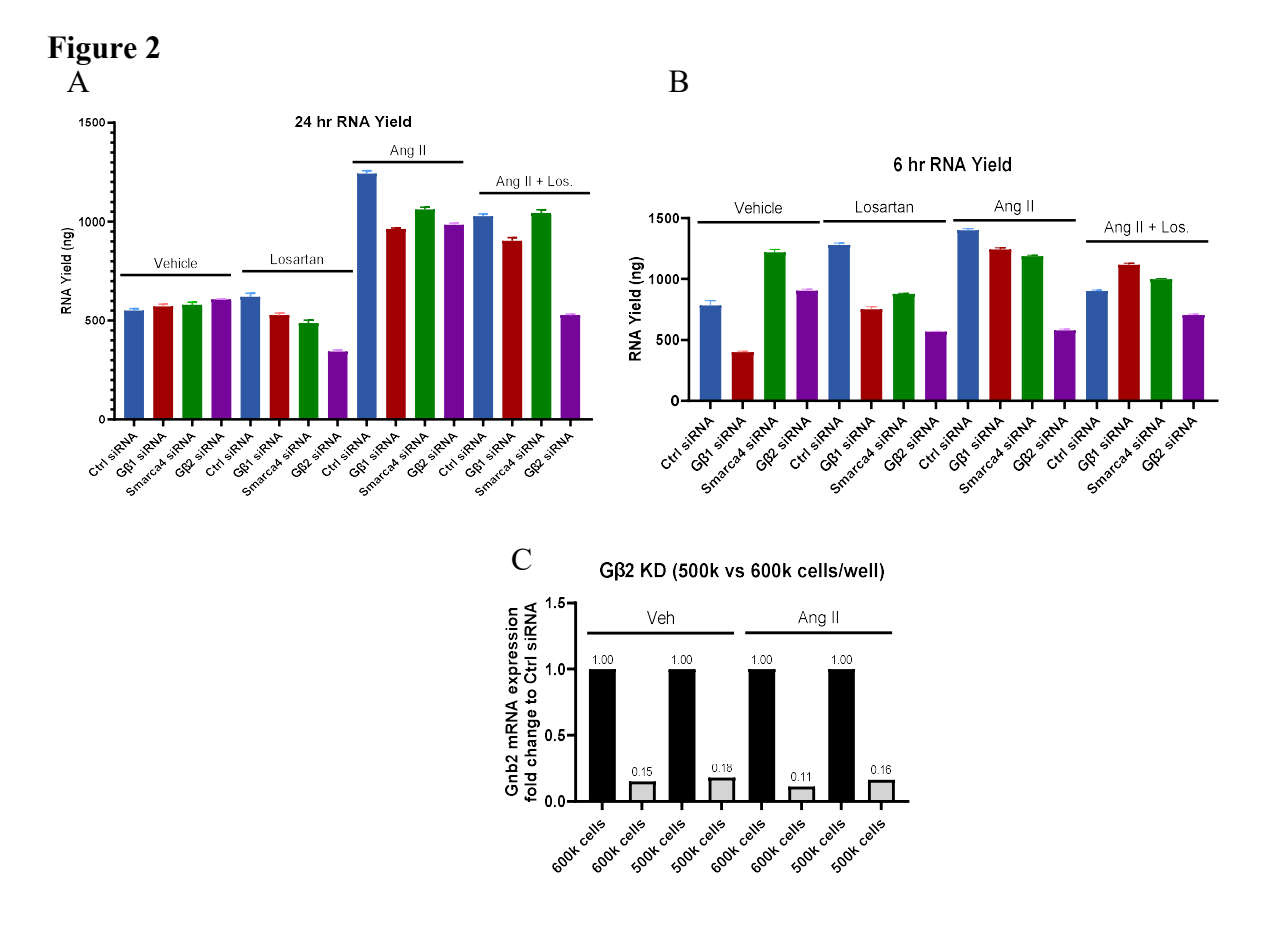
6 hours			24 hours		
siRNA	Treatment	KD %	siRNA	Treatment	KD %
Gβ1 siRNA	Vehicle	83%	CO1 'DNIA	Vehicle	46%
	Losartan	87%		Losartan	51%
	Ang II	85%	Gβ1 siRNA	Ang II	55%
	Ang II + Los.	87%		Ang $II + Los$ .	49%
	Vehicle	86%	Gβ2 siRNA	Vehicle	78%
Gβ2 siRNA	Losartan	85%		Losartan	79%
	Ang II	86%		Ang II	86%
	Ang II + Los.	62%		Ang $II + Los$ .	71%
Smarca4 siRNA	Vehicle	48%		Vehicle	30%
	Losartan	52%	C	Losartan	26%
	Ang II	87%	Smarca4 siRNA	Ang II	36%
	Ang $II + Los$ .	83%		Ang $II + Los$ .	-18% *

Table 4. Quantification of siRNA knockdown percentages for suspended transfection in 6-well plates to be used for phenotypic tests (not scratch assays) by qPCR. Percentages are shown as 1 minus target gene fold change (determined by the 2-ddCt method described in *Materials and Methods*.

These results showed that, as expected, siRNA knockdown was more efficient at the earlier timepoint (6 hours after Ang II treatment) and knockdown efficiency diminished at the second timepoint (24 hours after Ang II treatment). We also note that Gβ2 is the most effectively knocked-down subunit across all conditions, while Smarca4 is the most difficult to knock down. Nevertheless, we accepted these limitations and proceeded with the examination of phenotypic and qPCR analyses of fibrotic processes and gene expression.

#### 3.3 siRNA knockdown validation for RNA sequencing

Preceding the RNA sequencing experiment of the previously described combinations of siRNA and drug treatments, a third round of siRNA knockdown optimization was performed. In this round, seeding density was the last parameter that was optimized for RNA sequencing to balance the maximization of RNA yield and siRNA knockdown of the target mRNA from 6-well plates. Three different seeding densities were tested: 400 000, 500 000 or 600 000 cells per well. We found that 400 000 cells per well yielded effective siRNA-mediated knockdown, but we could not obtain enough RNA from each well of the 6-well plate to generate large enough cDNA libraries for RNA sequencing. Both 500 000 and 600 000 cells per well yielded enough RNA and had acceptably effective siRNA knockdown efficiency to satisfy both parameters. (Fig. 2)



**Figure 2. 6 and 24-hour quantification of RNA yield from lysis using Qiagen RNeasy Isolation columns. A-B)** 500,000 cells per well, RNA content is mean +/- SD for 3 technical replicates of RNA quantity. **C)** Knockdown validation of 500,000 and 600,000 cells by qPCR, the same method as in Figure 1.

RNA was validated for knockdown efficiency via qPCR before sequencing. RNCFs were treated with siRNAs against G $\beta$ 1, G $\beta$ 2, or Smarca4 and Ang II or losartan in 4 independent experiments as described above. Based on the qPCR knockdown validation of each of these 4 experiments, the 2-3 replicates with the best knockdown efficiency for each condition were selected for RNA sequencing. **Table 5** summarizes the pooled knockdown efficiency shown in **Fig. 3** for the samples chosen for sequencing. The best knockdown was seen in G $\beta$ 2 siRNA conditions, followed by G $\beta$ 1, and Smarca4 was the most difficult to knock down. Based on the above-described validations, the best knockdown obtainable for Smarca4 was around 50-60% at 6

and 24 hours after Ang II treatment. We did not see changes in the targeted knockdown genes with Ang II or losartan treatment which is ideal since this isolates the effects of treatment and siRNA knockdown from one another and enables analysis of these two interventions without complication caused by Ang II changing G protein or Smarca4 expression levels.

Table 5

6 hours			24 hours		
siRNA	Treatment	Pooled KD %	siRNA	Treatment	Pooled KD %
	Vehicle	61%		Vehicle	77%
Gβ1 siRNA	Losartan	66%	Gβ1 siRNA	Losartan	69%
	Ang II	75%	Opi sikiva	Ang II	69%
	Ang $II + Los$ .	60%		Ang $II + Los$ .	57%
Gβ2 siRNA	Vehicle	88%		Vehicle	77%
	Losartan	88%	CQ2 aiDNA	Losartan	77%
	Ang II	86%	Gβ2 siRNA	Ang II	75%
	Ang $II + Los$ .	73%		Ang $II + Los$ .	56%
Smarca4 siRNA	Vehicle	58%		Vehicle	50%
	Losartan	50%	Smarca4	Losartan	46%
	Ang II	57%	siRNA	Ang II	64%
	Ang II + Los.	46%		Ang $II + Los$ .	52%

Table 5. Quantification of siRNA knockdown percentages for RNCFs to be used in RNA sequencing experiment by qPCR. Percentages are shown as 1 minus target gene fold change (determined by the 2<sup>-ddCt</sup> method described in *Material and Methods*.

# Figure 3

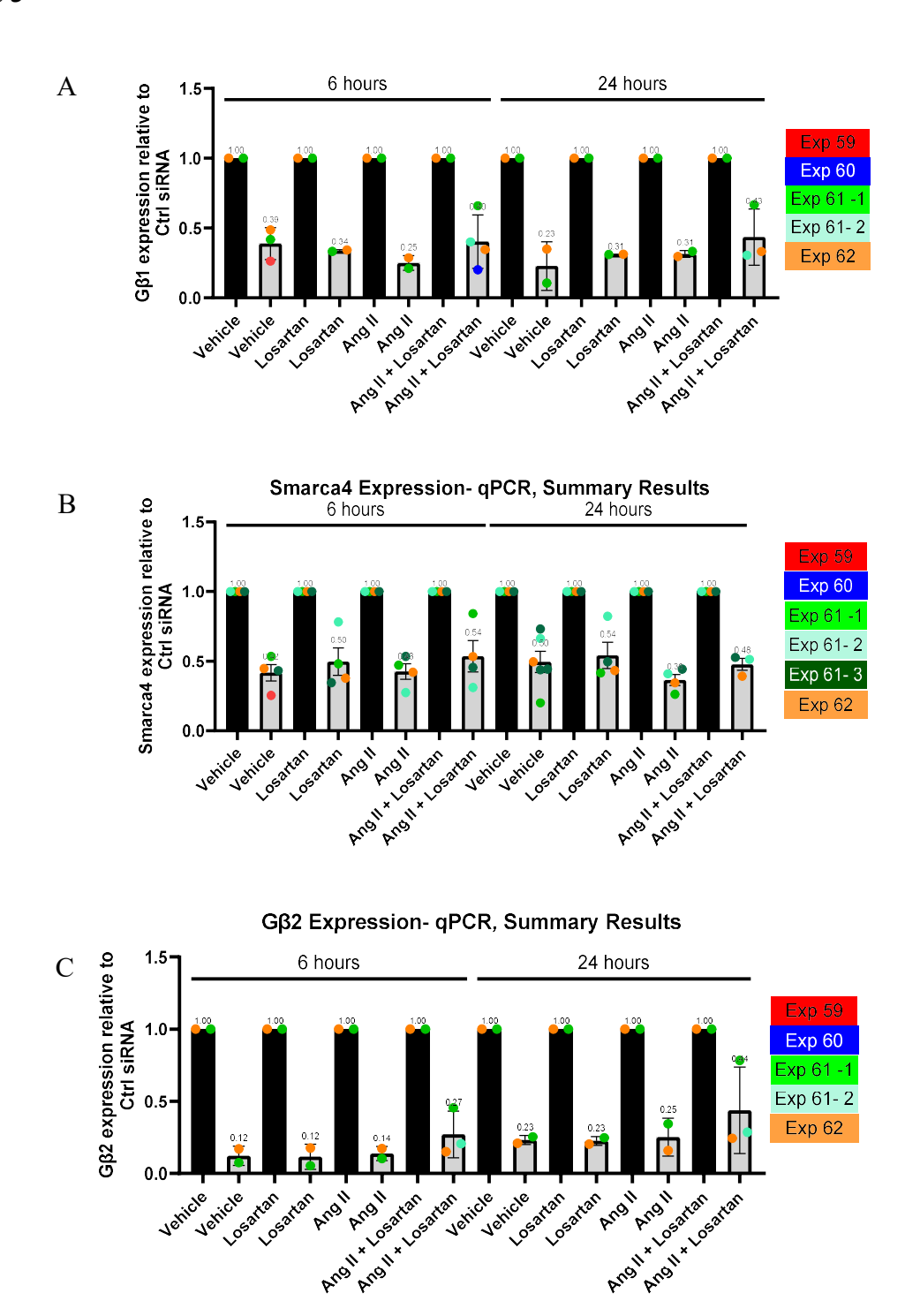


Figure 3. qPCR quantification of siRNA target gene knockdowns for RNA seq samples. Bars representative of mean +/- SEM of the n=4 knockdown trials. A) G $\beta$ 1 knockdown, B) Smarca4 knockdown, C) G $\beta$ 2 knockdown. Exp 59, 60, 61, and 62 refer to the litter of rats/the "n". Exp 61 qPCR has additional repeats as indicated by the suffix 1 or 2.

# <u>Results Section 2: Investigating the phenotypic effects of knocking down Gβ subunits and Smarca4 on the fibrotic response</u>

Once the siRNA knockdowns had been validated in the 6-well plate system with Ang II and losartan treatments, we were able to evaluate the effects of these knockdowns on the Ang II response in RNCFs. Different aspects of the fibrotic response were evaluated, including growth, migration, ECM production, and grading of the extent of the fibroblast-to-myofibroblast transition. These outcomes were evaluated via division rate, migration rate, collagen secretion, and intracellular a-SMA production.

#### 3.4 Ang II induces proliferation via division and not cell migration in scratch assays

Ang II drives fibroblast and myofibroblast division, and it is reported that activated fibroblasts exhibit increased migration rates in response to Ang II [6, 48]. To test this phenotypic output, we performed a series of scratch assays as a model of the wound healing response. Since it is generally reported that Ang II mediates many aspects of its pro-fibrotic stimulation via the synthesis and autocrine signalling of TGF-β1we compared 1 μM Ang II to 50 pM TGF-β1 in a scratch assay without FBS in the media to see how wound closure changes in response to different pro-fibrotic agonists. In this trial, the RNCFs did not migrate into the gap, however, we did see distinct morphological differences between the RNCFs treated with Ang II versus TGF-\beta1 (Fig. 4). Compared to vehicle-treated samples, Ang II treatment did not change the morphology of the fibroblasts greatly, however, TGF-β1 treatment resulted in a notable dendritic and spiked morphology. This morphology induced by TGF-β1 is indicative of an advanced myofibroblast phenotype. The dendritic shape is likely a result of myofibroblast contraction along a-SMA fibres. Since this was not observed in the Ang II treated samples, we can reason that the TGF-β1 treatment of our RNCF model rapidly advances the myofibroblast phenotype. Because of this rapid advancement, combined with the fact that the TGF-β1 receptor is not a GPCR, we elected to

proceed without TGF-β1 treatments combined with siRNA knockdown. However, this TGF-β1 trial showed us that our RNCFs could be induced easily into a quite advanced myofibroblast state, which led us to hypothesize that we were perhaps working with a fibroblast system with high baseline fibrotic "tone".

# Figure 4

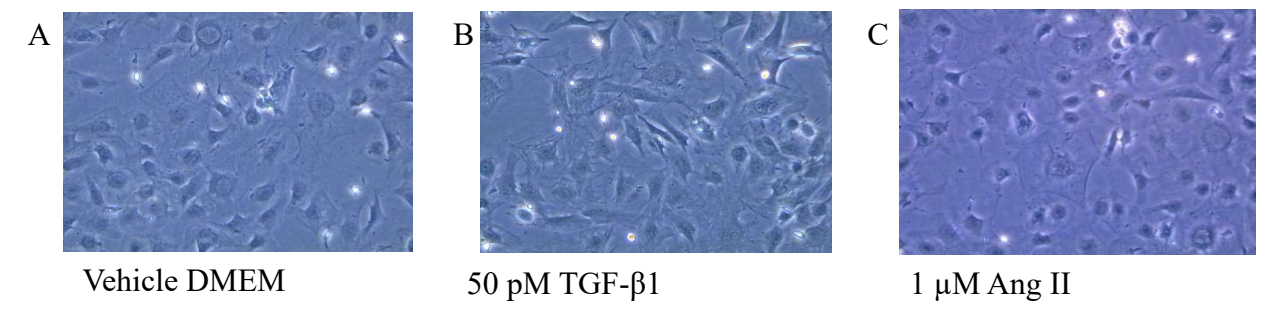


Figure 4. Brightfield images of RNCFs under different agonist treatments. A) Vehicle treatment (serum-free DMEM), B) 50 pM TGF-β1, and C) 1 μM Ang II to identify morphological differences.

With these optimizations complete, we proceeded with a pilot experiment to investigate the effect of knocking down G proteins and Smarca4 on the wound closure aspect of the fibrotic response. We also tested the impact of inhibiting proliferation with the mitotic inhibitor Ara-C. The scratch assays with siRNA knockdowns were inconclusive since the scratches did not close and therefore, we could not extract closure rate data. We did observe reduced confluence in the Ara-C treated conditions (Fig. S4), prompting the transition to a proliferation assay instead of the scratch assays

# 3.5 RNCF proliferation is potentially accelerated by G\(\beta\)1 knockdown in this RNCF model

It was previously discussed that fibroblasts exist across a vast spectrum of activation states. A hallmark of activated fibroblasts and myofibroblasts is accelerated proliferation [6, 48]. To test the effects of the siRNA knockdown of G $\beta$ 1, G $\beta$ 2, and Smarca4 on the Ang II response, we first

showed that our RNCFs proliferate in response to Ang II, instead of the cells simply migrating across the plate. This was tested with a live cell immunofluorescence growth assay where the number of nuclei stained with Hoechst nucleic acid stain was tracked over 24 hours of growth in response to 1 µM Ang II. When nuclei count was plotted against cell confluence, a Pearson correlation of 0.95 was measured (**Fig. 5**). This indicates that mitotic divisions contribute significantly to RNCF confluency, not simply locomotive migration.

Figure 5

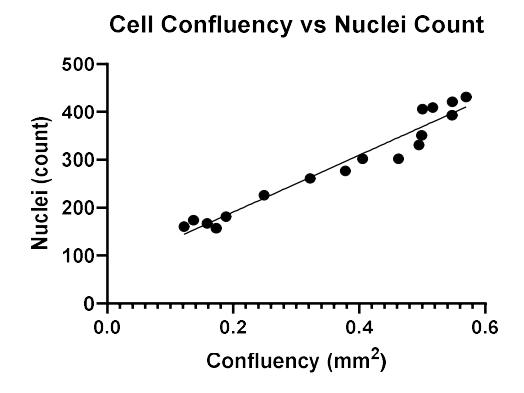
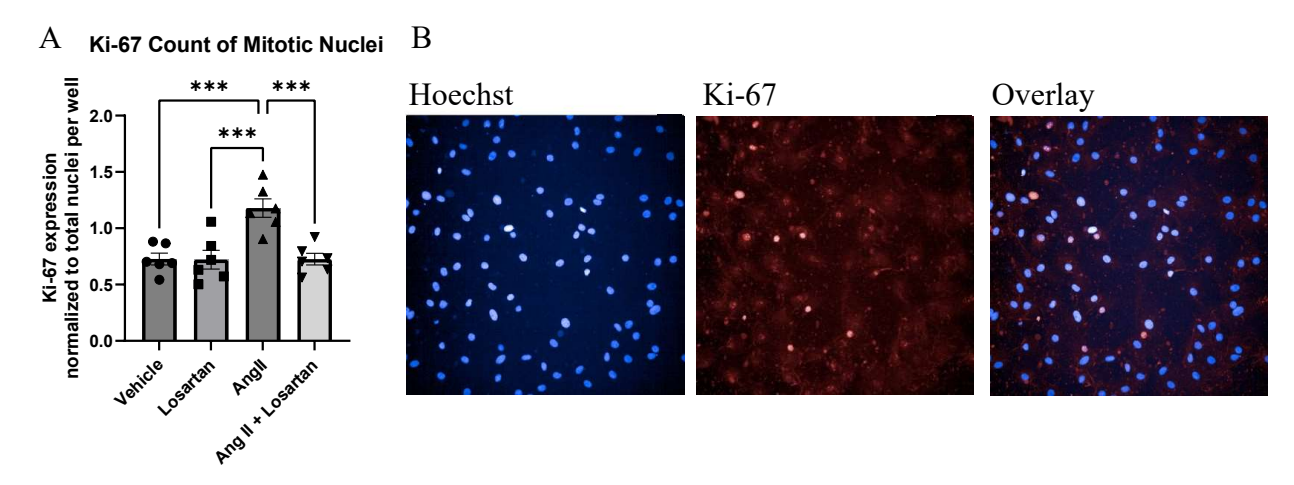


Figure 5. Pearson correlation plot of RNCF nuclei versus confluency. RNCFs were treated with Ang II for 24 hours. Nuclei and confluency were measured using the CellcyteX microscope. R = 0.95, indicating a strong relationship between nuclei count and confluency.

Another indicator that these RNCFs are more proliferative rather than migratory was shown in an immunofluorescence staining assay of Ki-67, a chromosomal stabilization protein expressed in cells actively undergoing mitosis [125]. RNCFs were plated in 96-well plates, treated with Ang II, losartan, both Ang II and losartan or their negative control vehicle (at the same concentrations as previously described) and were incubated for 6 hours. Cells were fixed and stained with an anti-Ki-67 antibody. Ki-67 positive nuclei were counted and plotted (**Fig. 6a**). Ang II treatment shows increased Ki-67 positive nuclei and losartan treatment significantly blocks this increase by 1-way ANOVA (with Dunnett's correction, **Fig. 6a**).

### Figure 6



**Figure 6. Assessment of mitotic divisions via Ki-67 immunofluorescence. A)** quantification of Ki-67 positive nuclei normalized to total nuclei per well (bars =mean +/- SEM. One-way ANOVA: p=0.0002, F=10.91). **B)** representative immunofluorescent images showing the overlay of Ki-67 positive nuclei on Hoechst stained nuclei.

The Ki-67 results confirmed that our RNCF system is at a stage of myofibroblast differentiation that is non-migratory, but still actively proliferative. Therefore, we proceeded to test if Ang II would increase the RNCF proliferation rate, instead of the migration rate, using the same automated microscopy system used in the scratch assays. This time, confluency was tracked over 24 hours instead of tracking the RNCF migration into a gap. Chronologically, by this time we had optimized all siRNA knockdowns and determined that the best knockdown was obtained via lipofection of suspended RNCFs (see section 1.2). Therefore, we tested how the Ang II-induced proliferation rate changed between  $G\beta1$ ,  $G\beta2$ , and Smarca4 siRNA-treated conditions. Our RNCF system responds to Ang II by increasing proliferation after 6 and 24 hours of treatment (**Fig. 7**). Further, this increase was blocked by the AT1R antagonist losartan (**Fig. 7**). When comparing different siRNA knockdowns,  $G\beta1$  knockdown showed a trend towards increased proliferation when compared to the Ang II treated siRNA control condition (**Fig. 7a**). This effect was only observed after 6 hours of Ang II treatment; the different siRNA knockdowns did not differentially affect the proliferation rate after 24 hours of Ang II (**Fig. 7b**). These results are in contrast to the

scratch assays where Ang II did not reliably increase the migration rate of the RNCFs in our model. As mentioned above, locomotive migration of fibroblasts is different from cell division, and in the context of a fibrotic response, reflects a fibroblast that is farther activated along the myofibroblast activation spectrum. Taken together, it seems like Gβ1 knockdown shows a trend towards increased proliferation rate at 6 hours and not 24 hours, and that this proliferation is indeed mitotic divisions, not migration.

Figure 7

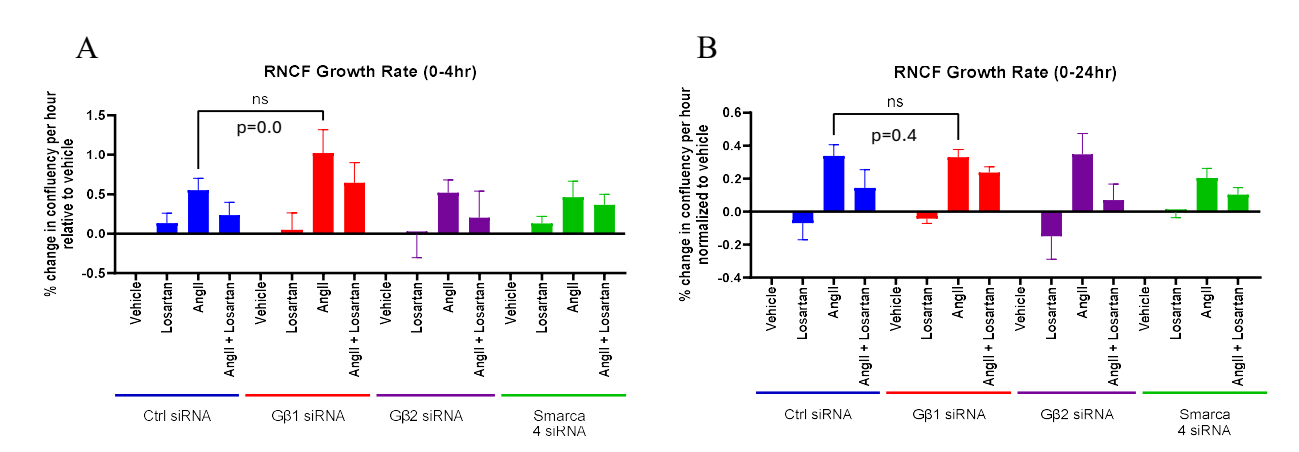


**Figure 7. Quantification of RNCF proliferation, induced by Ang II and measured between siRNA treatments.** Bars are the mean of n=4 biological replicates, mean +/- SEM. A) growth rate in the first 6 hours of Ang II treatment (One-tailed, unpaired t test, p=0.09, t=1.415, df=10). B) growth rate in all 24 hours of Ang II treatment (One-tailed, unpaired t test, p=0.47, t=0.07860, df=6).

#### 3.6 Ang II treatment increases 24-hour collagen secretion but not collagen mRNA transcription

As reported in *section 1.2*, we validated siRNA knockdown conditions for phenotypic assays. The growth assays shown in **Fig. 7** were done with these knockdown conditions. The system validated in section 1.2 was set up in such a way that multiple outputs could be evaluated from the same cells, particularly, growth rate, secreted collagen, and gene expression via qPCR. This section will discuss the collagen secretion assays performed on these cells. After the growth

data was collected and before cell lysis for qPCR gene expression analysis, a sample of the conditioned media in which the RNCFs were growing was collected and the collagen content in the media was quantified by western blot. From pilot experiments where we tested 24 hours of Ang II stimulation, we found increased secreted collagen (**Fig.8**)

Figure 8

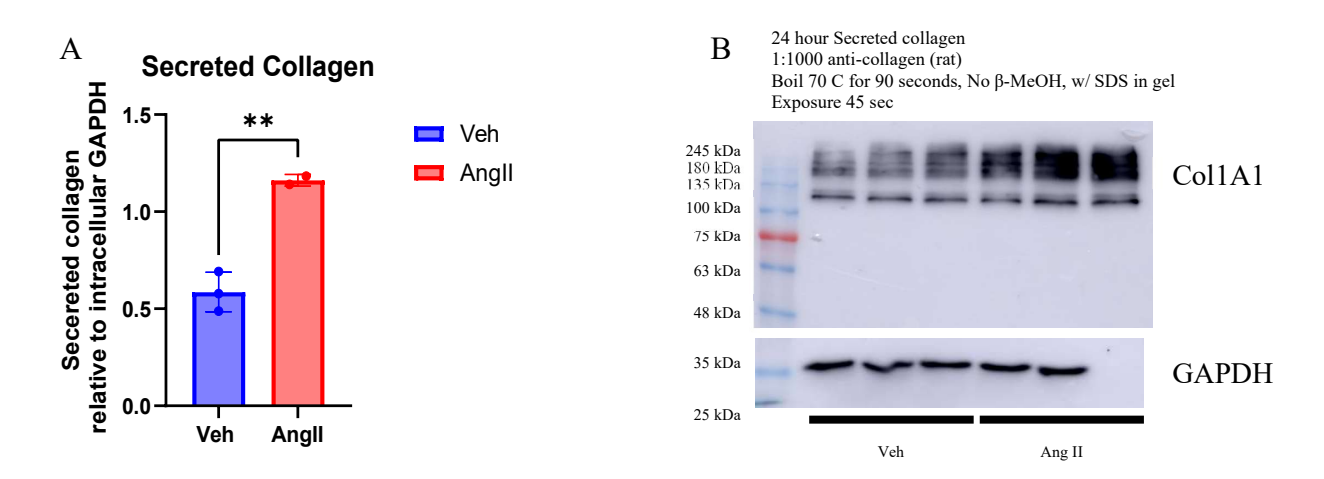
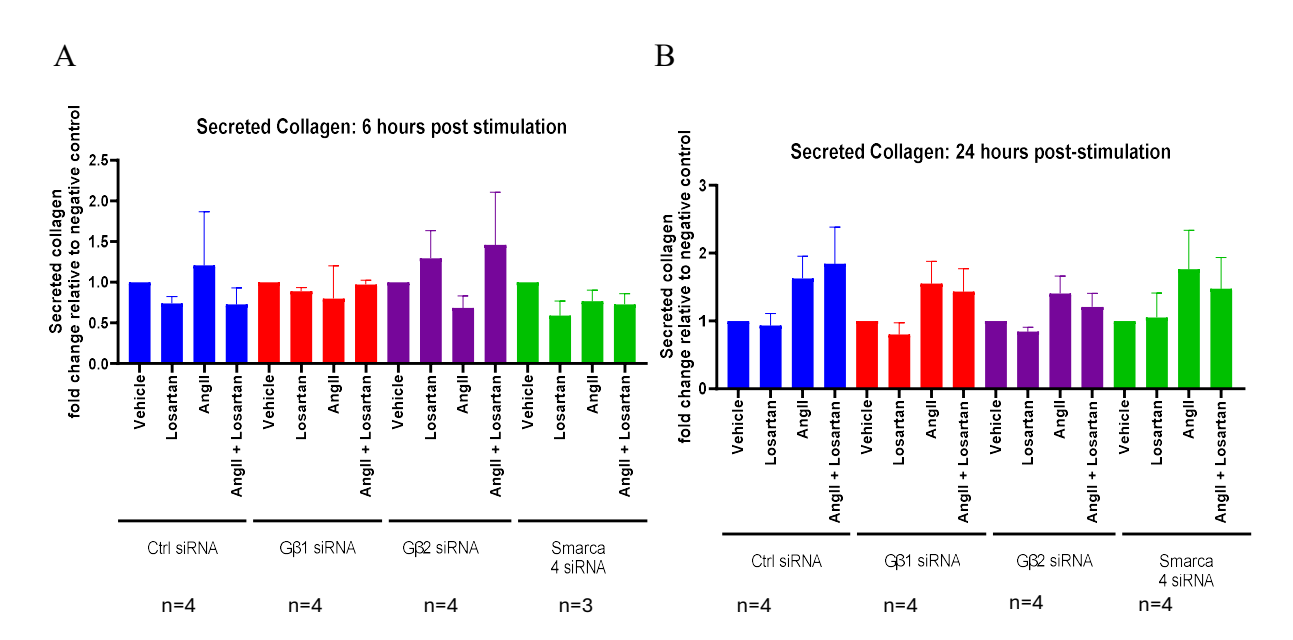


**Figure 8.** Ang II-mediated collagen secretion pilot A) Quantification of secreted collagen western blot showing Ang II induction of collagen secretion after 24 hours of stimulation (bars = Mean +/- SEM of n=2, 3 replicates, one-tailed t test, p = 0.0099, t=3.763, df=4). B) Western blot of secreted collagen from which the quantities in A) were measured. Antibody recognizes the c-propeptide of Col1A1. Lane 6 omitted due to missing loading control.

With this validation done, we proceeded with the full collagen secretion experiment including the siRNA knockdowns. We found that after 6 hours of Ang II treatment, collagen secretion was not significantly increased, and any changes in immunoblotted type 1 collagen were not affected by losartan antagonism (**Fig. 9**). Only after 24 hours, like the pilot western blot, did we see changes in collagen secretion to the extracellular space induced by Ang II stimulation (**Fig. 9a-b**). This suggests that 6 hours may not be enough time for sufficient collagen to accumulate in the media and be detected by immunoblotting in response to Ang II stimulation, so we performed qPCR at the same 6 and 24-hour time points to assess if Col1A1 gene expression matched the

secreted collagen patterns. To our surprise, we did not see a similar response between the western blots and the qPCRs. Instead, there was a slight increase in Col1A1 expression at 6 hours of Ang II (Fig 9c) and an unclear response at 24 hours (Fig 9d). We also saw no consistent effects of Gβ1 or Gβ2 knockdown (Fig. 9 c-d). We did not have enough of the Smarca4 KD RNA left to assess collagen mRNA production in this condition. This indicates that our cells may be at a stage that does not respond to Ang II agonism by increasing type 1 and 3 collagen production and secretion but advances the fibrotic response via other outputs. This would be consistent with the results that our RNCFs do not migrate but instead proliferate in response to fibrotic stimuli. This could further indicate that our RNCFs, at their stage of myofibroblast activation, are no longer secreting large amounts of type 1 collagen, but instead are responding to fibrotic stimuli in other ways (further expanded on in the RNA sequencing data of *Section 3*).

Figure 9



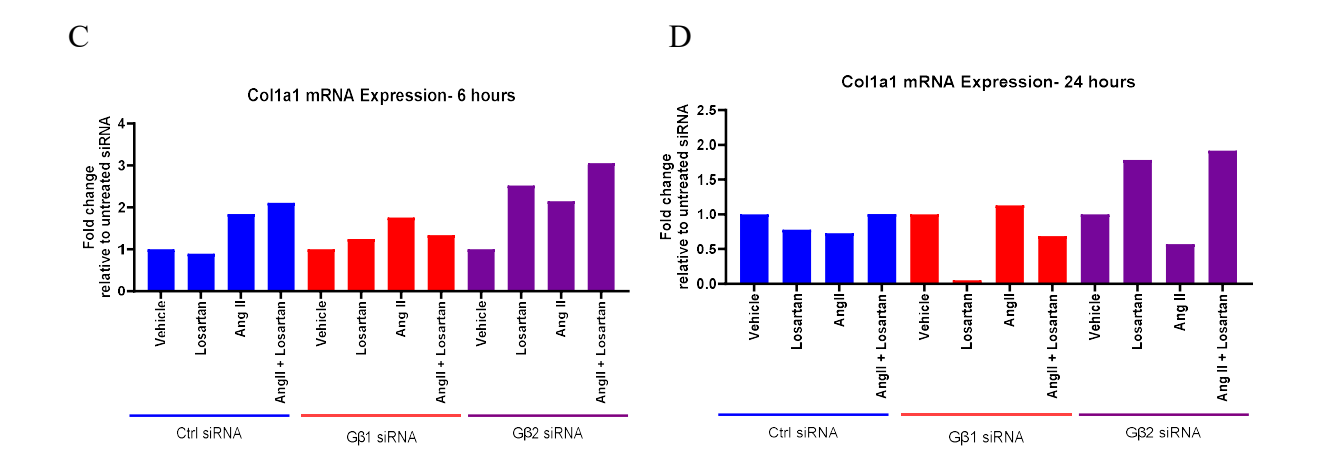


Figure 9. Western blot and qPCR analysis of collagen type 1 secretion. A-B) Western blot summary of secreted Col1A1 in n=4 independent experiments, between siRNA and treatment conditions (not significant by 1-way ANOVA). C-D) qPCR quantification of Col1A1 mRNA for G $\beta$ 1 and G $\beta$ 2 siRNA, between treatments (not significant by 1-way ANOVA). C,D are n=1, therefore no error bars could be calculated and statistical testing is not possible.

#### 3.7 Our RNCF model shows attributes of an advanced myofibroblast state

As previously discussed, as fibroblasts proceed along their activation spectrum, they gain more smooth muscle characteristics as they develop into myofibroblasts. The stereotypic hallmark of this is *de novo* and increasing expression of the smooth muscle cytoskeletal protein  $\alpha$ -smooth muscle actin ( $\alpha$ -SMA). At this point in our investigations, it was clear that our RNCFs responded to Ang II expectedly for some outputs and unexpectedly for others. As a final verification of the essential myofibroblast characteristics of the model before proceeding to RNA sequencing, we wanted to test if the RNCFs responded to Ang II by increasing a-SMA production. Immunofluorescent staining of  $\alpha$ -SMA proteins in RNCFs after 24 hours of Ang II stimulation showed an increase in  $\alpha$ -SMA protein (**Fig. 10, a-b**). This increase in intracellular  $\alpha$ -SMA indicates that our RNCF system responds to Ang II via increasing proliferation and some fibrotic protein expression ( $\alpha$ -SMA, but not all common fibrotic responses, notably lacking in migration and collagen secretion). With these results in mind, we proceeded to investigate how the siRNA

knockdown of G $\beta$ 1, G $\beta$ 2, and Smarca4 altered the fibrotic transcriptional response to Ang II to better understand how our RNCF system models fibrosis and how transcription is affected by G $\beta$  and mSWI/SNF subunits.

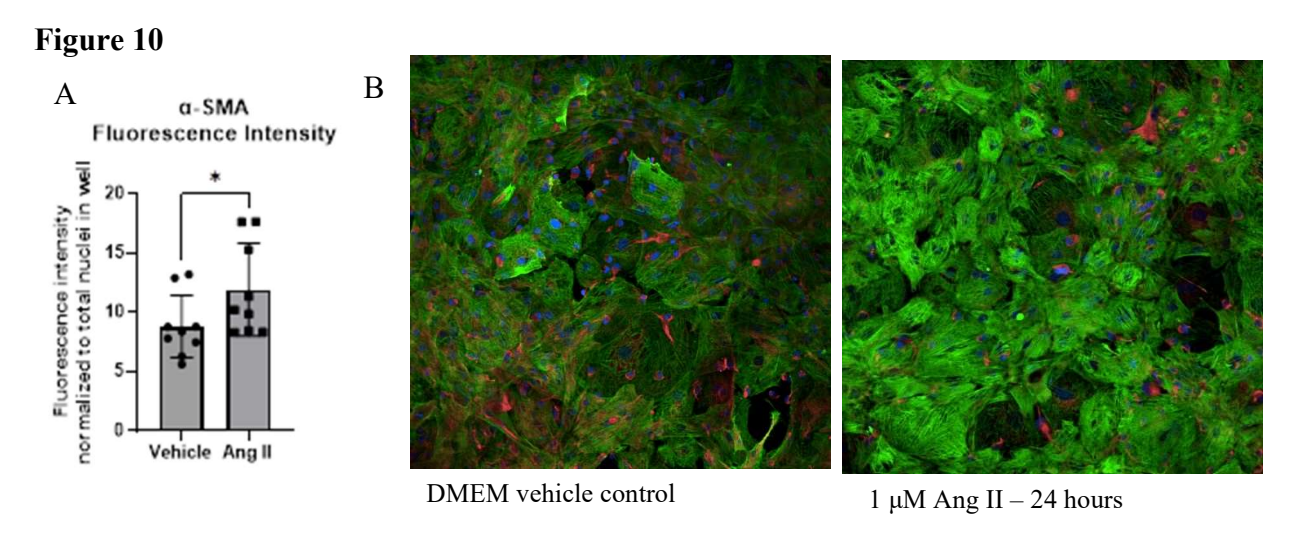


Figure 10. Quantification of α-SMA fluorescence intensity. A) summary of fluorescent signal intensity for anti-α SMA normalized to total nuclei (p = 0.0335, t=1.964, df=16) n=1 biological replicate, n=9 technical replicates, bar represents mean +/- SD). B) representative immunofluorescent images illustrating α SMA in green, vimentin in red, and nuclei in blue. The right panel shows higher α-SMA intensity under Ang II stimulation than the right panel which is unstimulated.

# Results Section 3: Profiling the role of G protein and mSWI/SNF subunits on the transcriptional response to Ang II

Section 2 demonstrated that in response to Ang II, our RNCFs activate certain common fibrotic endpoints, but not others. The specific combination of these indicates that our fibroblasts likely reflect a myofibroblast differentiation state. In profiling these fibrotic outputs, most did not show an effect of knocking down the G proteins and Smarca4 subunits, except for proliferation rate. Mitotic proliferation, locomotive migration, and collagen secretion are all outputs that result far downstream of a chorus of other contributing intracellular events that precede and enable the output. The work preceding this thesis showed that Gβγ subunits interact with transcriptional and

chromatin regulatory machinery to modulate the cellular response to Ang II. Evidently, our system may not be sensitive enough, or the effects of this  $G\beta\gamma$ -mSWI/SNF interaction may not be potent enough to be seen in our system at the phenotypic output level. Therefore, focusing on changes in the transcription of the genes involved in regulating the Ang II fibrotic response brings our investigation closer to the source of this interaction. To circumvent these confounding influences on investigating the phenomenon under question in this thesis, *Results Section 3* investigates gene expression changes at the mRNA level

#### 3.8 qPCR profiling of select pro-fibrotic and transcriptionally relevant genes

As described in the collagen secretion assays, once we had validated a reliable knockdown of Gβ1, Gβ2, and Smarca4 in 6-well plates, we created an experimental layout that enabled the measurement of RNCF proliferation rate, measurement of secreted collagen, and mRNA profiling of genes of interest all from the same cells. We collected the mRNA from the RNCFs treated with our panel of siRNAs after 6 and 24 hours of Ang II stimulation (after collagen-containing media was collected). We then performed qPCR to measure the relative abundance of two fibrotic genes of interest: connective tissue growth factor (CTGF) and Serpine1 (the gene that encodes the plasminogen activator inhibitor-1 protein, PAI-1). All qPCR results in this section were obtained by Giada Castagnola, a U3 undergraduate research trainee under my supervision. CTGF was chosen because, in our previous work in RNCFs, we showed by chromatin immunoprecipitation that Gβ1 localizes to this pro-fibrotic gene in an Ang II-induced manner [118]. Additionally, in this same paper, we showed by LC-MS that Serpine 1/PAI-1 was enriched in samples where G\beta 1 was knocked down and treated with Ang II [118]. We saw an increase in Serpine1 expression induced by Ang II at 6 and 24 hours of stimulation, but we did not see an increase in CTGF at either time point (Fig. 11 a-d). Furthermore, we did not see changes in either gene's transcript levels between

siRNA conditions. This led us to conclude that CTGF might be implicated in the same mechanism that caused our RNCF system to not respond to Ang II in the scratch wound healing assays and collagen secretion experiments. Conversely, Serpine1 expression may be involved in the same pathways that resulted in increased α-SMA production and mitotic growth in response to Ang II discussed before. The conclusion of these qPCR results supports the proposition that this RNCF model displays a mosaic of fibrotic responses due to its position along the fibroblast-to-myofibroblast activation spectrum.

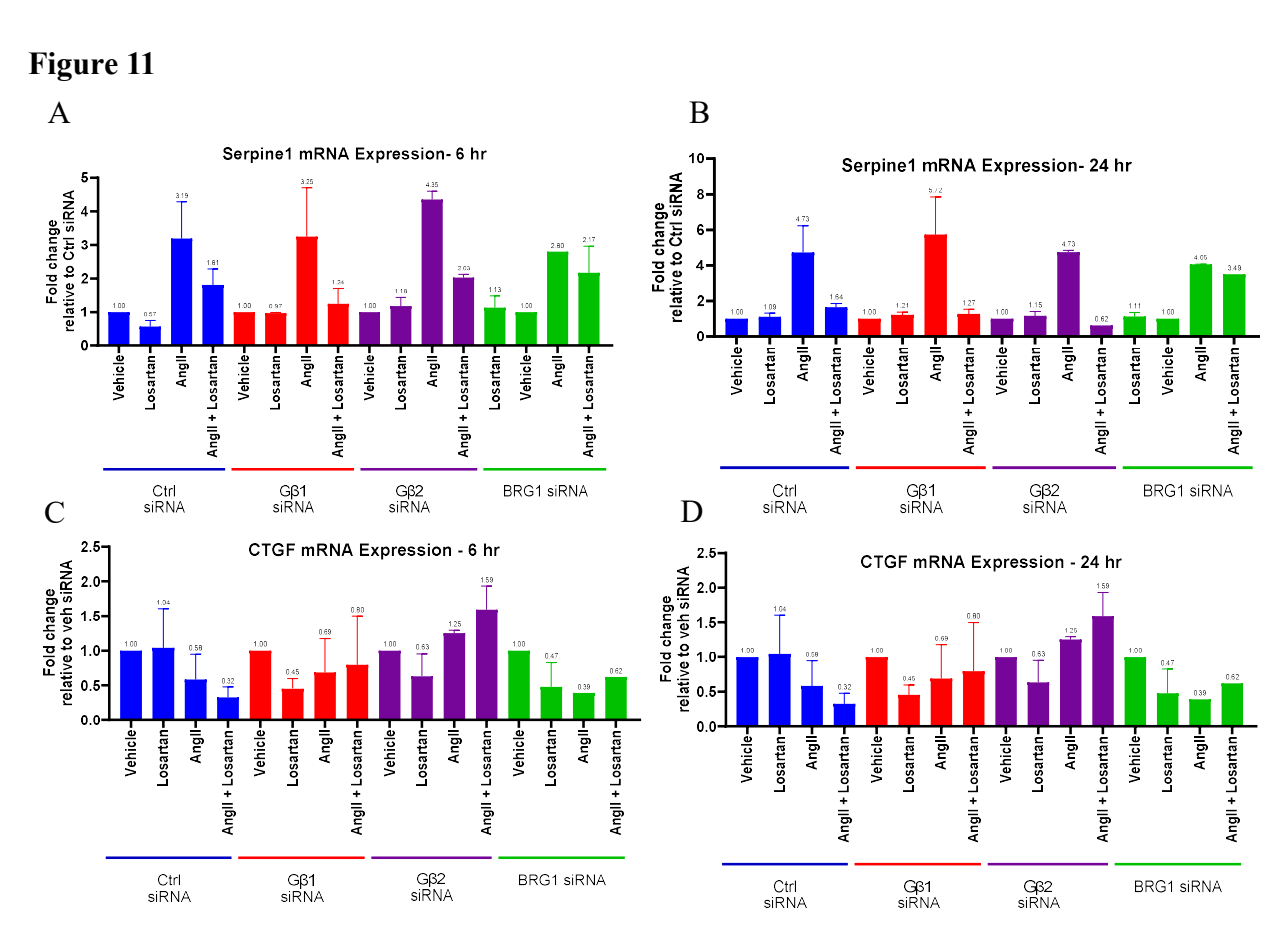


**Figure 11. qPCR quantification of 6 and 24-hour Ang II-treated RNCFs, expression between siRNA knockdowns.** Bars represent mean +/- SEM of n=4 independent experiments. **A-B**) 6 and 24-hour Serpine1 mRNA expression. **C-D**) 6 and 24-hour Serpine1 mRNA expression.

# 3.9 Profiling the transcriptomic changes of $G\beta$ and mSWI/SNF knockdown on Ang II-induced transcription via RNA sequencing

To proceed with broad transcriptomic analyses, we prepared the same set of siRNA and treatment conditions as described for other phenotypic endpoints. RNCFs were treated with siRNA to knock down G $\beta$ 1, G $\beta$ 2, and Smarca4 and were treated with Ang II, losartan, or co-treated with both. RNA was collected at 6 and 24 hours post-Ang II treatment. cDNA libraries were generated for each RNA sample and the samples were sequenced using Illumina sequencing.

Before differential expression analysis, principle component analysis (PCA)was done on the sequenced libraries to ensure reliable conclusions could be drawn. As shown in the PCA plots in Figure 12, we had a very significant separation of clusters by batch (litter of rats). In this situation, 73% of the total variance was attributed to the presence of variability from litters at 6 hours (Fig. 12a) and 66 % at 24 hours (Fig. 12b). In volcano plots not shown, we also saw hundreds of differentially expressed genes between comparisons of the different litters. This was corrected by including batch as a variable in the design of the DESeq object and batch effect removal by the limma package. PCA plots plotted after the litter effect was corrected show the amount of variation attributed to PC1 dropped to 37% (6 hours) and 53% (24 hours). Now, the two main factors contributing to the variation are siRNA and agonist/antagonist treatments. PC1 is likely the variance due to the "Treatment" factor: Vehicle, losartan, Ang II or Ang II + losartan. PC2 is likely the variance due to the siRNA factor: Ctrl, G $\beta$ 1, G $\beta$ 2, and Smarca4 siRNAs. You can see this because the x-axis clusters group by treatment (Fig. 12c-d) and the y-axis clusters group by siRNA (Fig. 12 e-f). This is a dramatic improvement to non-batch corrected reads and is not unique to our experimental model. Many reports show in animal work, the litter effect is very significant, and in some cases greater than the biological effects of the interventions [126-128].

Therefore, it is always critically important that litters be controlled for in studies like ours, and that comparisons be made within a litter as much as possible.

Figure 12

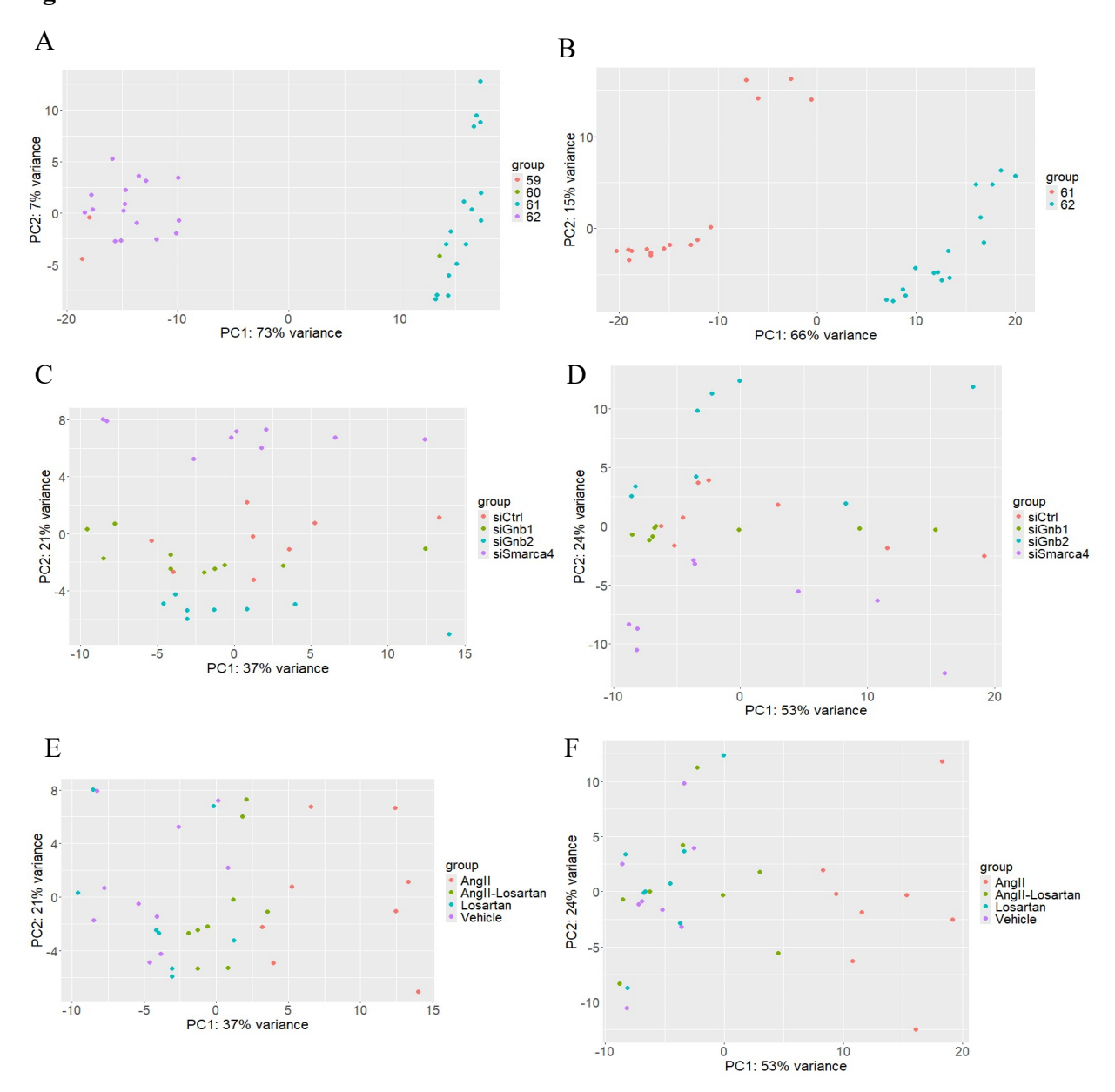


**Figure 12.** PCA analysis of sequencing conditions, before (A, B) and after batch effect removal (C-F). A,C,E) 6 hours Ang II. B, D, F) 24 hours Ang II. A-B) show samples labelled by replicate to illustrate the batch effect. C-D) show samples labelled by treatment to show x-axis groupings of treatment (PC1). E-F) show samples labelled by siRNA to show y-axis groupings of siRNA (PC2).

First, we validated the experimental setup conditions by showing the siRNA knockdown of G $\beta$ 1, G $\beta$ 2, and Smarca4 in each of their respective conditions was achieved at both 6 and 24 hours (**Fig. 13**). The lowest knockdown efficiency was Smarca4 and the highest was G $\beta$ 2 knockdown, which is consistent with our qPCR validations. Further, the 24-hour timepoints showed a slight reduction in knockdown efficiency, also consistent with the qPCR validation.



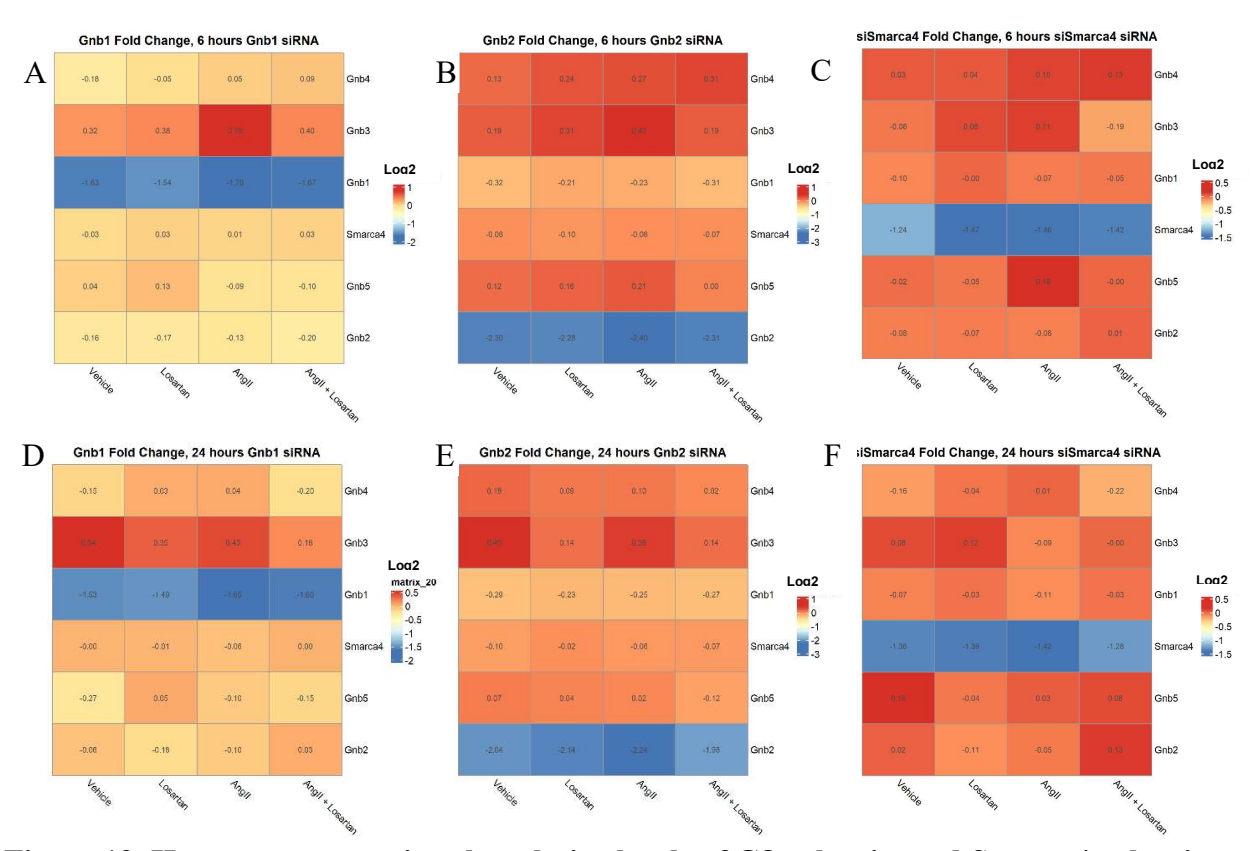


Figure 13. Heatmaps comparing the relative levels of Gβ subunits and Smarca4 subunits to show knockdown fold changes between 6 and 24 hours. A, D show Gβ1 knockdown, B, E show Gβ2 knockdown, C, F show Smarca4 knockdown. Log2FC is relative to Ctrl siRNA.

Next, we showed that treatment with Ang II had the expected gene expression outcomes. Among the Ang II treated conditions, at 6 and 24 hours, Ang II drove an upregulation of many genes, which was blocked by losartan pretreatment at both 6- and 24-hour timepoints (**Fig. 14**). Notably, the losartan negative control conditions resembled the Ang II + losartan conditions with

high concordance, indicating that the antagonism of the AT1R was effective. Furthermore, when looking at the total number of differentially expressed genes, Ang II treatment causes the most differentially expressed up and down genes, relative to far fewer differentially expressed genes in the vehicle, losartan, and combination Ang II + losartan conditions (**Fig. 14**). Notably here, we did not see the previously hypothesized broad increase in upregulated transcripts when G $\beta$ 1 was knocked down and treated with Ang II or basally in the vehicle-treated condition. Instead, we saw that knocking down G $\beta$ 2 resulted in the most potentiation of the Ang II transcriptional response (**Fig. 14**). At 6 hours of AngII treatment, the individual siRNA knockdowns did not result in significant differences in the number of up or downregulated genes (**Fig. 14**). After 24 hours, we see that G $\beta$ 2 siRNA resulted in a 47 % increase in total upregulated transcripts and a 78 % increase in total downregulated transcripts relative to control siRNA. Further, as expected, 24 hours of Ang II treatment resulted in more up and down-regulated transcripts than 6 hours (**Fig. 14**).

Figure 14

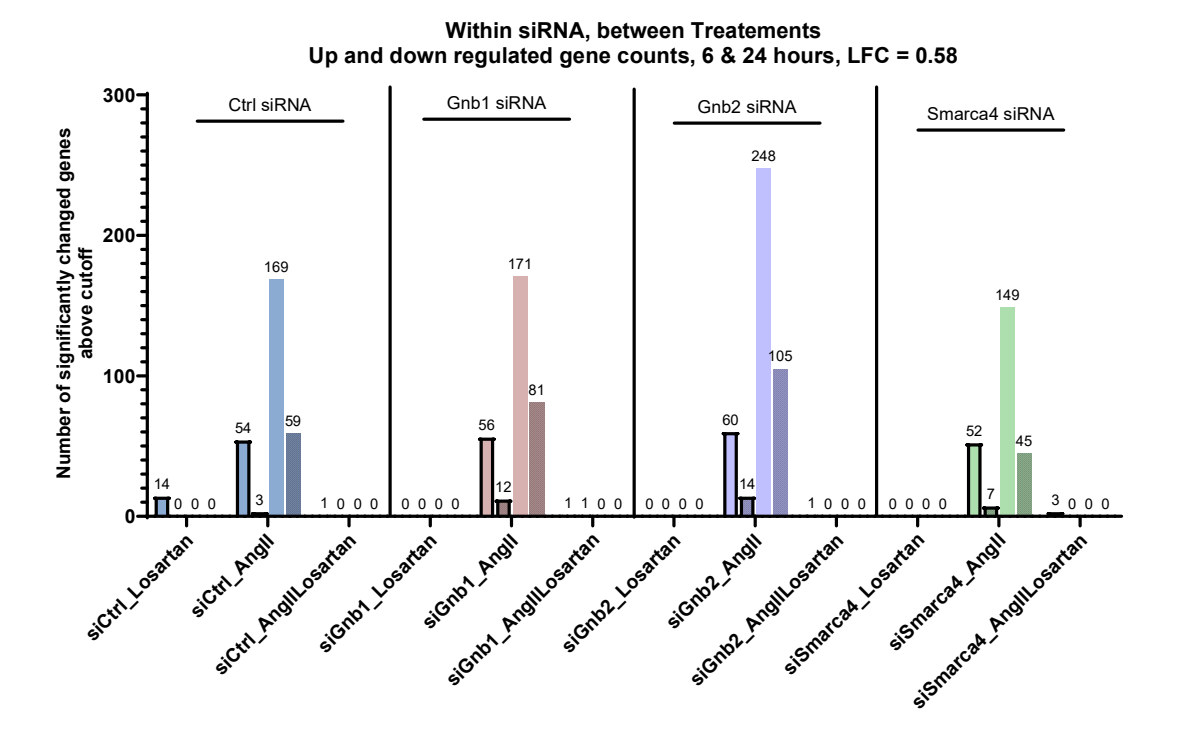


Figure 14. Quantity of up and down-regulated differentially expressed genes induced by Ang II and antagonized by losartan between siRNA treatments. Bars are sums of the genes significantly changed, p adj. < 0.05 and Log2FC > +/- 0.58 (fold change > +/- 1.5 fold). Shaded bars indicate downregulated genes, clear bars indicate upregulated genes. Bold-outlined bars are 6 hours, no-outline bars are 24 hours

First, we examined some individual differentially expressed genes to determine if our gene expression results from the qPCR assays were consistent with these RNA sequencing data. We observed the same patterns as in the qPCR experiments: Serpine1 and  $\alpha$ -SMA both respond strongly to induction by Ang II at 6 and 24 hours (**Fig. 15a-b**). Type 1 and type 3 collagen do not respond to Ang II induction at 6 hours (**Fig. 15a**), but Col1A1 does at 24 hours (**Fig. 15b**). There is not an obvious link between an individual siRNA and a directional change in gene expression of these individual fibrotic. In the log2FC heat map for expression changes after 6 hours of Ang II, there are no subclusters identified under the Ang II parent cluster (**Fig. 15a**). At 24 hours, GB1

and G $\beta$ 2 siRNA form a subcluster under the Ang II cluster, but the log2FC is less than the control siRNA condition, indicating an opposite effect on expression as predicted for this gene (**Fig. 15b**). These experiments are useful as corroboration of prior qPCR assays, but the strength of the RNA seq is to perform exploratory investigations of how G $\beta$ 1, G $\beta$ 2 and Smarca4 control expression of fibrotic genes beyond a select few canonical genes.

Figure 15

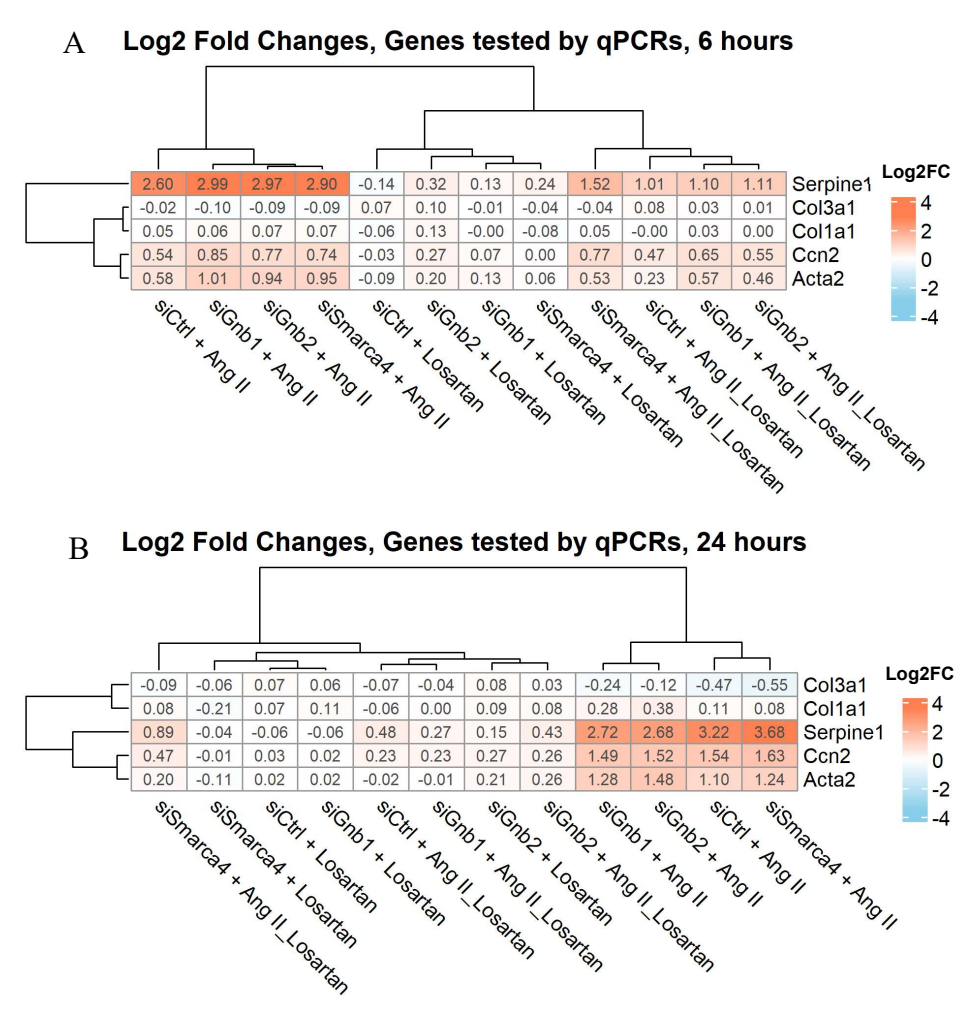


Figure 15. Log2FC heatmaps comparing genes that were assessed in the qPCR assays at A) 6 hours of Ang II and B) 24 hours of Ang II treatment, validating section 2 qPCR and collagen secretion results. Pink indicates a positive Log2FC, and blue indicates a negative Log2FC. Dendrograms were constructed using hierarchical clustering.

Since G $\beta$ 1 has been demonstrated as a transcriptional regulator, it is important to investigate how the other G protein subunit abundances change when altering G $\beta$ 1 abundance. Particularly if the G $\alpha$  abundances change, other GPCR signalling can be altered. Alternatively, it could illustrate compensatory mechanisms that the RNCFs have activated in response to the siRNA. When profiling the G $\beta$  subunits, we only saw changes in the targeted G $\beta$  proteins. No other G $\beta$  subunits compensated for the loss of G $\beta$ 1 or G $\beta$ 2, nor did other G $\beta$  subunits decrease (**Fig. 16a-b**) G $\gamma$  subunit changes are also illustrative to track since G $\beta$  and G $\gamma$  subunits are in obligate dimers. In the G $\beta$ 1 siRNA conditions, G $\gamma$ 12 expression was reduced in response to G $\beta$ 1 knockdown at 6 and 24 hours (**Fig. 16 c-d**). G $\alpha$  subunits mostly did not change. An interesting response is that G $\alpha$ 12 expression slightly increased with G $\beta$ 1 siRNA at 6 and 24 hours and decreased with G $\beta$ 2 siRNA at 6 hours only. (**Fig. 16 e-f**). Largely, G protein abundances were not altered, however, the G $\alpha$ 12 and G $\gamma$ 12 changes could illustrate avenues for future mechanistic investigation.

At this stage, we split the analysis into two paths to interrogate different factors of the differential expression analysis. The first way looked within each siRNA group and compared differentially expressed genes between treatment conditions (vehicle, losartan, Ang II, and Ang II + losartan). The second way looked within each treatment condition and compared differentially expressed genes between the different siRNAs. The first method allows us to see the effect that an siRNA had on potentiating or blunting the Ang II response. The second method enables a direct assessment of how each siRNA changes the differentially expressed genes. An example of the first method is looking within all G $\beta$ 1 siRNA treated samples, and comparing what each treatment does. An example of the second method is looking within all Ang II treated samples, and comparing what each siRNA does. Combining results from both analysis methods in the forthcoming section

enables a comprehensive investigation of how gene expression is regulated in our RNCF system. In the following sections, heatmaps generated from the first method will have a colour scale from sky blue to pink and heatmaps from the second analysis method will have a colour scale from turquoise to orange.

Figure. 16

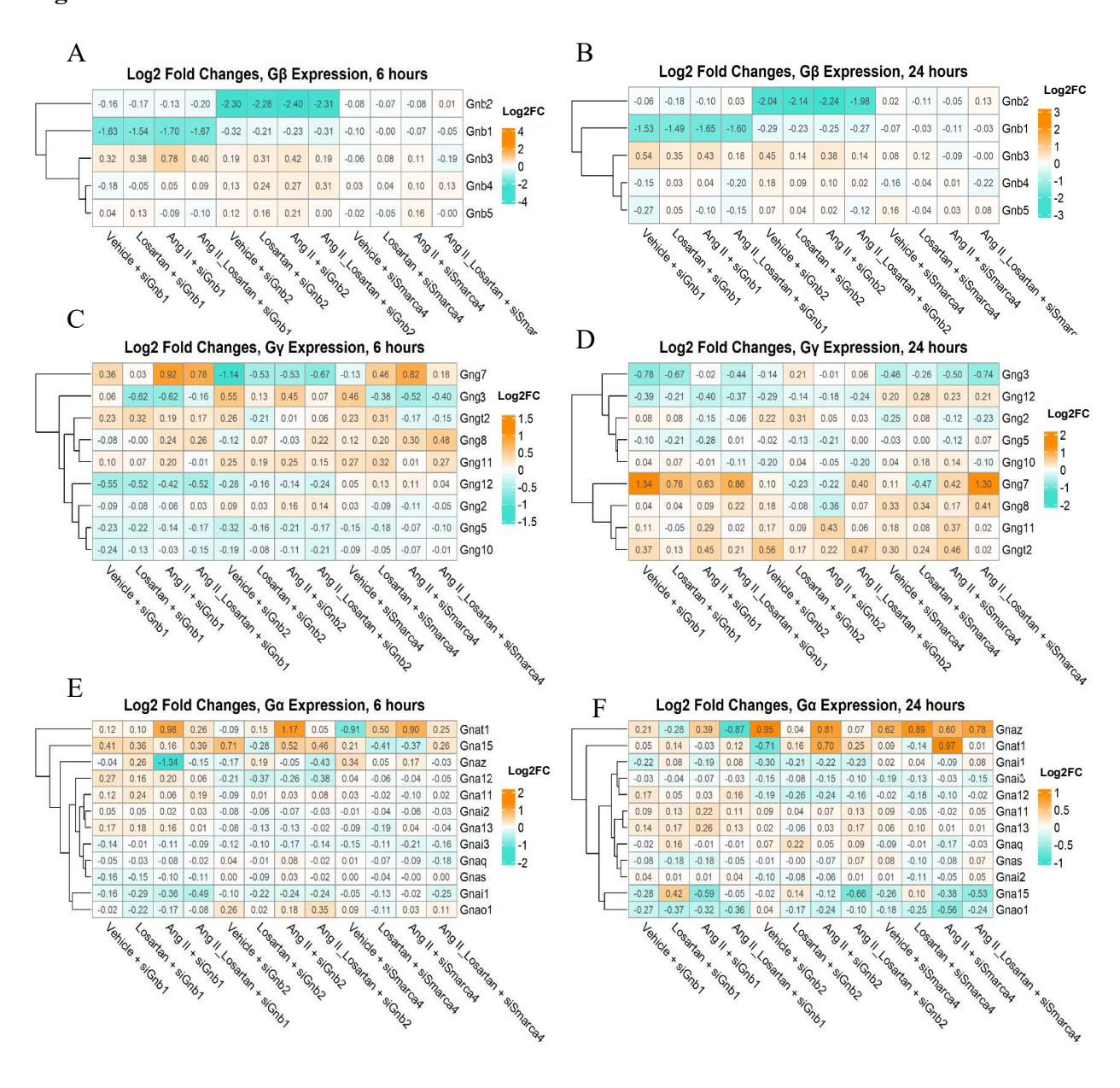
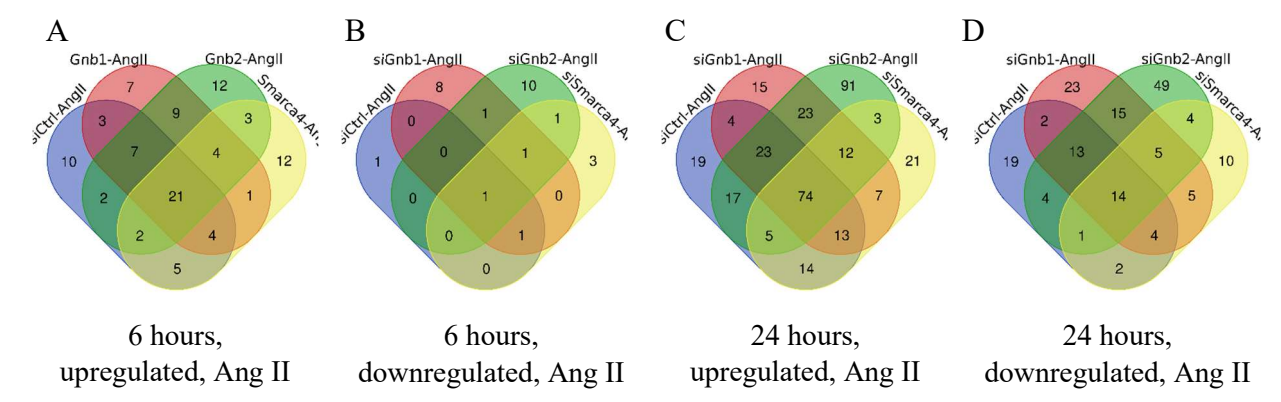


Figure 16. Log2FC heat maps comparing relative expression of G protein subunits between siRNA treatments. A-B) G $\beta$  subunit expression levels between conditions show minimal changes outside of the KD targets, C-F) G $\gamma$  and G $\alpha$  subunit expression levels between conditions indicate potential regulation of G $\gamma$  transcription from G $\beta$ 1 and G $\beta$ 2. Orange indicates a positive Log2FC, and turquoise indicates a negative Log2FC. Dendrograms were constructed using hierarchical clustering.

# 3.9.1 Investigating the effects of G $\beta$ 1, G $\beta$ 2 and Smarca4 on the Ang II induced fibrotic gene expression

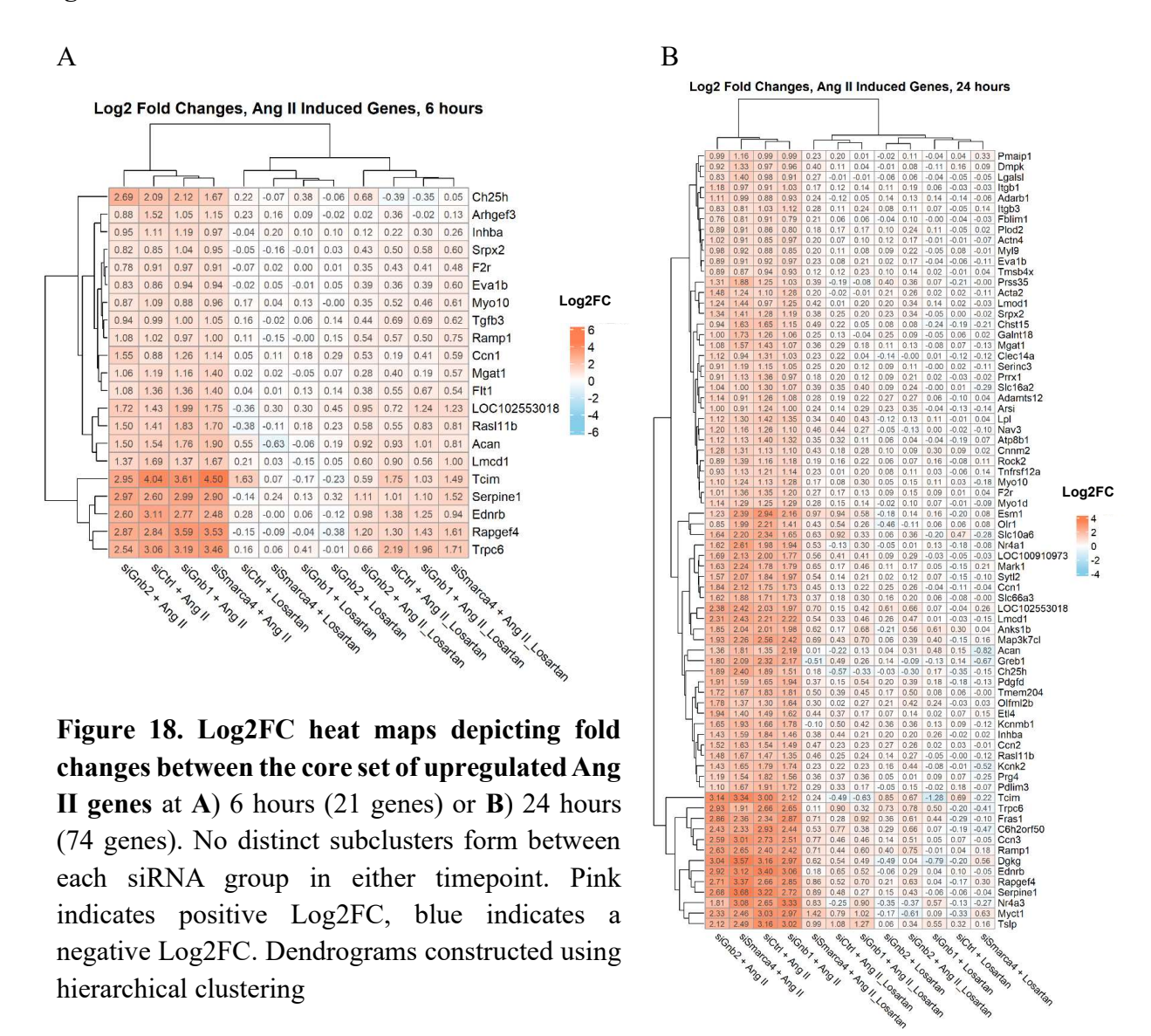
Up and down-regulated genes for each differential expression analysis were grouped into Venn diagrams of overlapping up- or down-regulated genes for each Ang II condition. These Venn diagrams help show what effects each siRNA has on the Ang II response by showing the genes induced by Ang II within each siRNA condition. Each differential expression was made with reference to the vehicle control condition of that siRNA group. The 6- and 24-hour Venn diagrams show a conserved Ang II expression response between all siRNAs that increases with treatment time (Fig. 17). Additionally, there are notable sets of uniquely changing genes in each siRNA condition (Fig. 17). This tells us that while a majority of the Ang II-induced genes are not changing with different siRNA knockdowns, there are still unique changes in the Ang II response attributed to each knockdown. The pattern is somewhat reversed for the downregulated genes. The commonly downregulated genes by Ang II among all siRNA is a smaller group than the uniquely downregulated genes (Fig. 17).



**Figure 17.** Venn diagrams containing counts of differentially expressed genes induced by **Ang II,** showing overlap between siRNA treatments. A) 6 hours, upregulated, AngII; B) 6 hours, downregulated, AngII c) 24 hours, upregulated, AngII and D) 24 hours, downregulated, AngII. The overlap shows a large, conserved Ang II response between all siRNA conditions.

Once again, we don't see the G $\beta$ 1 siRNA group exhibiting the highest number of uniquely up or downregulated genes in response to Ang II as hypothesized. Instead, we see the same pattern mirrored in *Figure 14*, where G $\beta$ 2 siRNA has the largest impact on expression changes. This led us to further investigate the commonly upregulated genes in the Venn diagrams (21 genes for 6 hours and 74 genes for 24 hours). When the Log2fold changes of these top changing genes were plotted in a heat map (Fig 18), dendrogram clustering suggests that G $\beta$ 1 and Smarca4 siRNA may be similarly affecting the expression of these 21 genes at 6 hours (greater than G $\beta$ 2 and control siRNA) but at 24 hours, G $\beta$ 1 clusters with the control siRNA, indicating G $\beta$ 1 has transcriptional effects at the 6-hour but not at the 24-hour time point (Fig. 18). This is consistent with the hypothesis from our previous work[118] that shows G $\beta$ 1 acting as a transient break on fibrotic transcription.

Figure 18



## 3.9.2 Gene Ontology pathway analysis of Ang II-induced gene expression

Using the same lists of up and down regulated genes, we performed Gene Ontology (GO) pathway analysis to determine which biological processes, molecular pathways, and cell components are enriched among Ang II-regulated genes in control and knockdown conditions (**Figs. 19-22**).

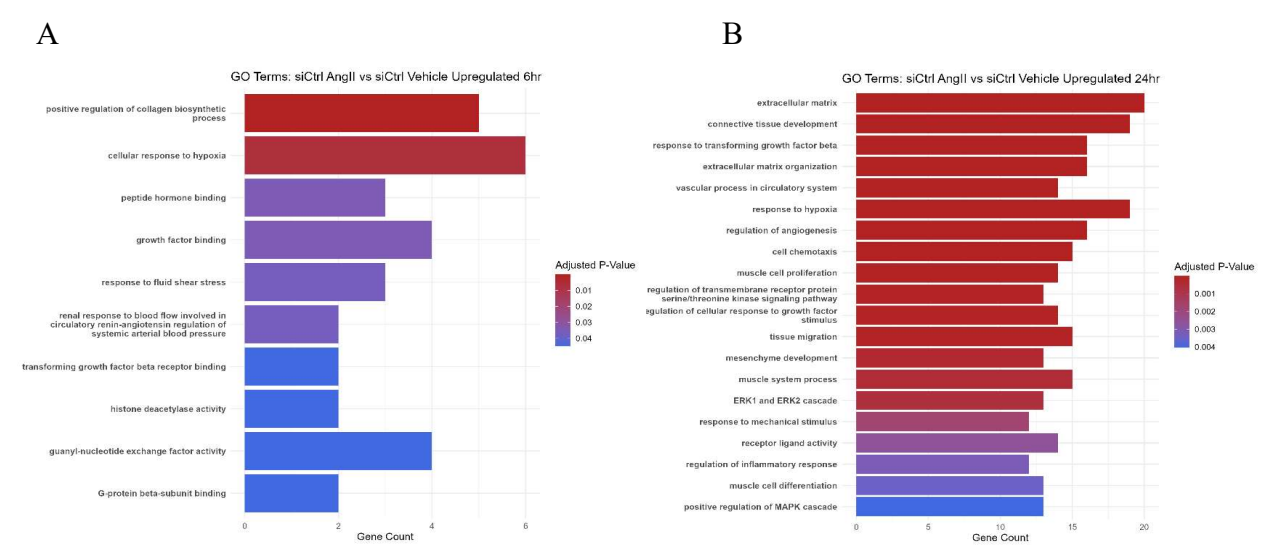


Figure 19. Summary bar plots of GO terms enriched in Ang II-treated samples vs vehicle-treated samples, within the Ctrl siRNA conditions at A) 6 hours indicating a baseline level of fibroblast function and B)24 hours indicating a highly activated network of fibroblast activation. Top 20 GO terms, ordered by significance: p adj. < 0.05

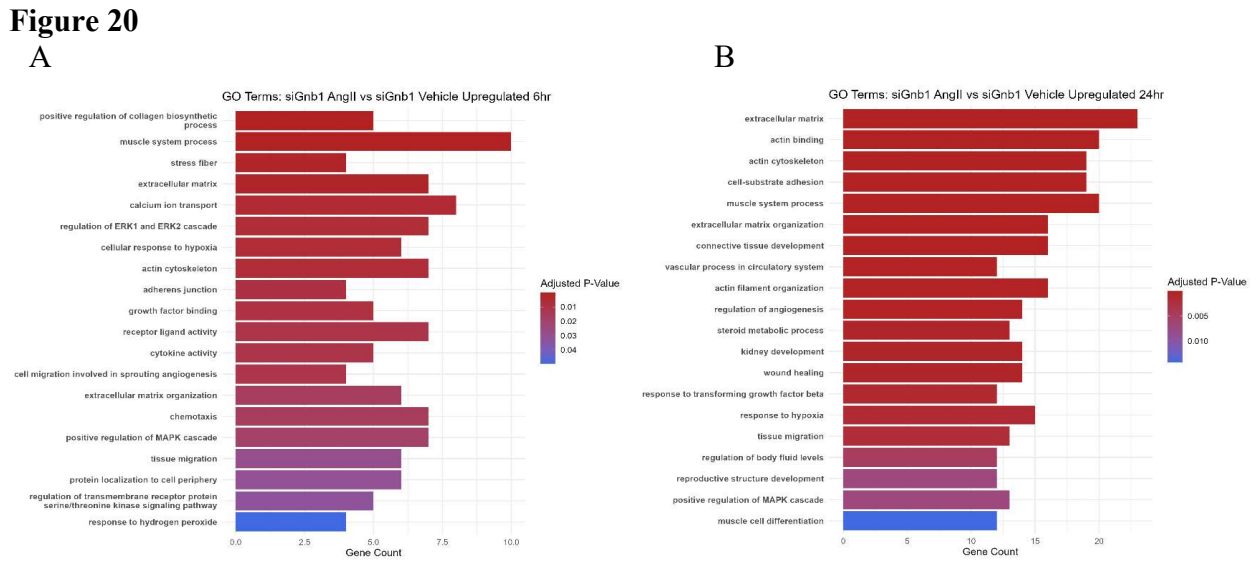


Figure 20. Summary bar plots of GO terms enriched in Ang II-treated samples vs vehicle treated samples, within the G $\beta$ 1 siRNA conditions at A) 6 hours indicating more activated fibroblast induction pathways and B)24 hours indicating a highly activated network of fibroblast activation consistent with other KDs. Top 20 GO terms, ordered by significance: p adj. < 0.05



ive regulation of MAPK cascade

tein localization to cell periphery

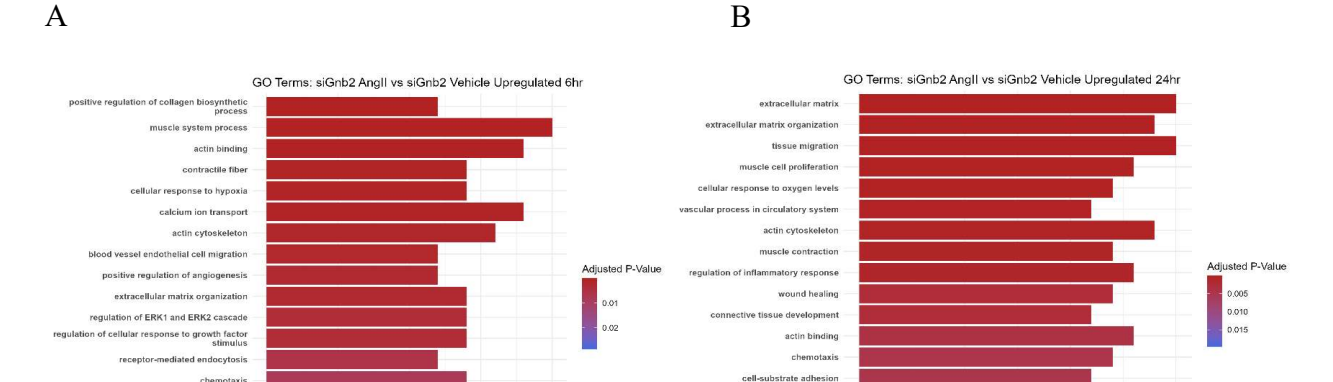


Figure 21. Summary bar plots of GO terms enriched in Ang II-treated samples vs vehicle-treated samples, within the G $\beta$ 2 siRNA conditions at A) 6 hours indicating more activated fibroblast induction pathways and B)24 hours indicating a highly activated network of fibroblast activation consistent with other KDs. Top 20 GO terms, ordered by significance: p adj. < 0.05

sponse to external stimulus actin filament organization

muscle cell differentiation positive regulation of MAPK cascade

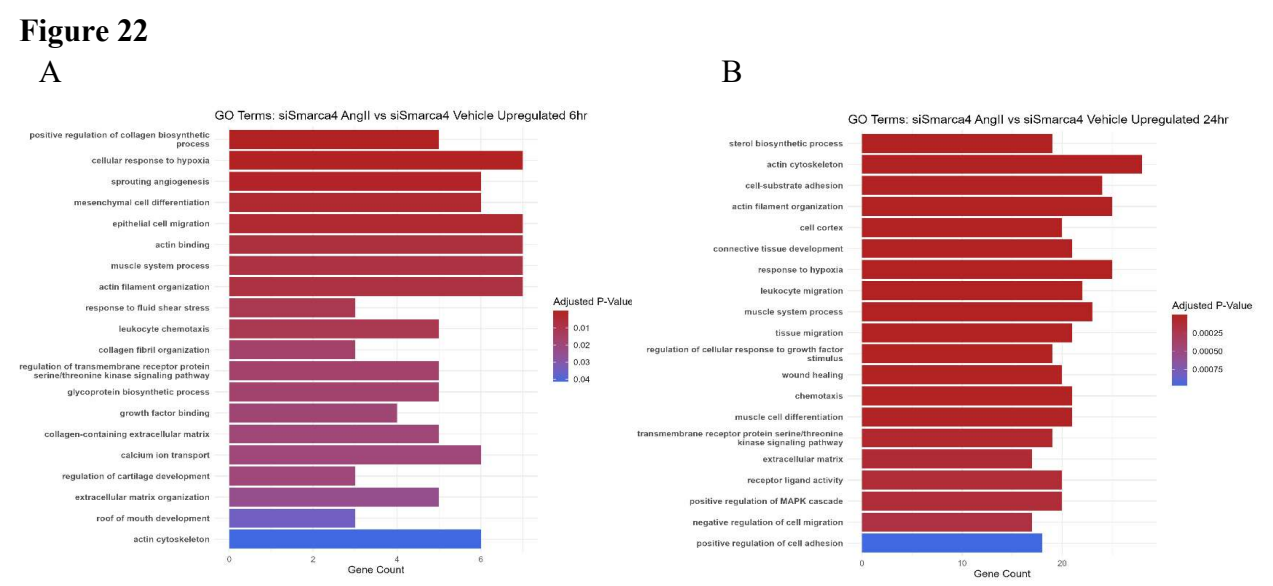


Figure 22. Summary bar plots of GO terms enriched in Ang II-treated samples vs vehicle-treated samples, within the Smarca4 siRNA conditions at A) 6 hours indicating more activated fibroblast induction pathways and B)24 hours indicating a highly activated network of fibroblast activation consistent with other KDs. Top 20 GO terms, ordered by significance: p adj. < 0.05

Across all comparisons, processes related to collagen biosynthesis and response to hypoxia were enriched significantly (**Fig. 19-22**). At 6-hour conditions, we see each knockdown may be upregulating different pathways in response to Ang II. For Gβ1 siRNA, we see muscle contraction and muscle system process pathways enriched (**Fig. 20a**). This is interesting because as fibroblasts become activated, they gain smooth muscle characteristics, implying these may be fibroblasts that have increased activation. To better understand these muscle contraction and muscle system process GO terms, we plotted the 10 genes that were included in them: Ednrb, Lmcd1, Nr4a1, Flt1, Nr4a3, Acta2, F2r, Ccn2, Rem1, and Tpm4 (**Fig. 23a**). Whereas most of the genes that map to this term are induced by Ang II in control and knockdown cells, Acta2, Tpm4, and Ccn2 are only induced above the Log2 fold-change cutoff in the knockdowns (LFC>0.58, fold change >1.5.).

Figure 23

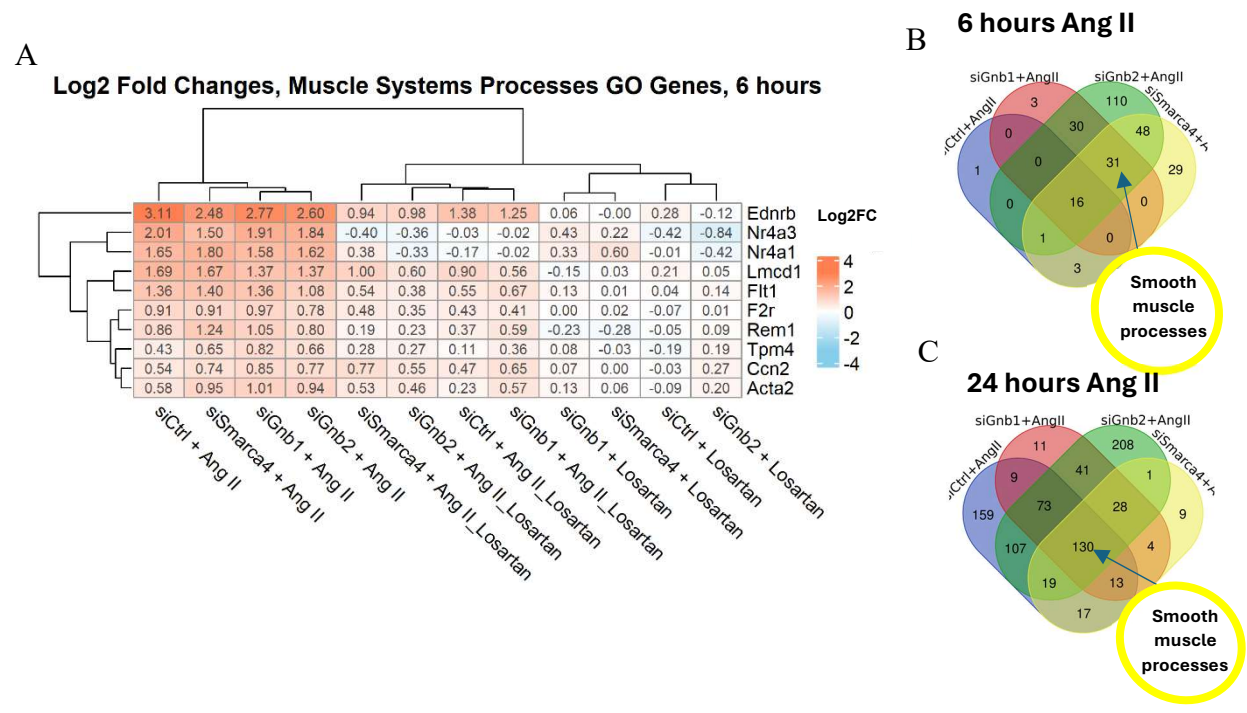


Figure 23. Log2FC heat map and Venn diagrams depicting the genes upregulated in the Muscle Systems Processes GO term between treatments and siRNA conditions. A) Log2FC heat map depicting 6-hour changes in muscle system genes. Pink indicates a positive Log2FC, and blue indicates a negative Log2FC. Dendrograms were constructed using hierarchical clustering. B-C) Venn diagrams illustrating which subset of upregulated genes these GO terms are found in.

These muscle systems/related terms are also seen in the Gβ2 knockdown and the Smarca4 knockdown at 6 hours. All three knockdown conditions show a similar profile of increased GO terms associated with fibrotic gene expression (Fig.20a, 21a, 22a). Interestingly, knocking down Gβ2 resulted in the largest number of significantly enriched GO terms (237) relative to the other knockdown conditions at 6 hours (Fig 21a, 23b). At 6 hours, Smarca4 knockdown resulted in 128 upregulated terms (Fig. 23b), the vast majority of which are overlapping with both Gβ1 and Gβ2 or uniquely overlapping with Gβ2. To summarize, upregulated GO terms are widely shared between knockdown conditions, with Gβ2 and Smarca4 sharing the most overlap in upregulated terms. Further, all three knockdown conditions show a similar profile of increased GO terms, including terms like muscle system processes and actin cytoskeleton regulation which are associated with fibrotic gene expression.

Proceeding to the 24-hour samples, the notable first finding is that all siRNA conditions (including the Ctrl siRNA RNCFs) treated with Ang II now show the upregulated muscle system process GO terms that only the G protein knockdowns showed previously (**Fig. 19b, 20b, 21b, 22b** and **Table S2**). Furthermore, all conditions now have additional GO terms related to classical fibrotic outcomes: ECM regulation, cell-matrix adhesions, and response to TGF-β1 among others (**Fig. 19b, 20b, 21b, 22b, 23c**). Of note are upregulated GO terms in the Gβ2 siRNA conditions that seem to be related to sterol and cholesterol metabolism (**Fig. 20b**). This is still present in the Gβ1 GO terms, however, there is a stronger upregulation via fold change, and therefore more significant p value for the sterol and cholesterol terms in the Gβ2 siRNA conditions. The 24-hour Ang II treated Smarca4 siRNA samples showed the same GO term profile as the 24-hour Gβ1 siRNA samples (**Fig. 21b**).

In the 24-hour Ang II treated GO terms, we see interesting differences in the downregulated terms as well (Table S3). Ctrl siRNA-treated samples show downregulated terms associated with extracellular matrix organization. Gβ1 siRNA shows downregulated terms related to immune system processes (neutrophil and granulocyte movement, chemokine responses) (Table S3). Additionally, Smarca4 siRNA seems to be downregulating developmental and apoptotic responses after 24 hours of Ang II treatment (Table S3). Clearly, knocking down Gβ1, Gβ2 and Smarca4 alters their transcriptional response to Ang II by up and downregulating processes that may be related to fibrotic outcomes. These GO term results allow us to understand the broader changes in activities of the RNCFs due to our interventions and have shown us differences between the knockdown conditions that the previous analyses before this RNA seq section were not precise enough to illustrate.

# 3.9.3 Effects of siRNA knockdown on basal gene expression in RNCF model

While we previously discussed the effects of siRNA on potentiating the Ang II transcriptional response and how that relates to transcriptional control and fibrotic gene abundance, another aspect of the siRNA knockdown is how siRNAs change basal gene expression without Ang II stimulation. These results are found in our negative control for Ang II (the vehicle treatment) comparing each siRNA. We calculated Log2 fold change values between vehicle-treated, control siRNA and vehicle-treated, G $\beta$ 1, G $\beta$ 2, and Smarca4 siRNA. We first investigated the quantity of significant up and down-regulated genes among the vehicle-treated conditions between siRNAs (**Fig. 24**)

Figure 24

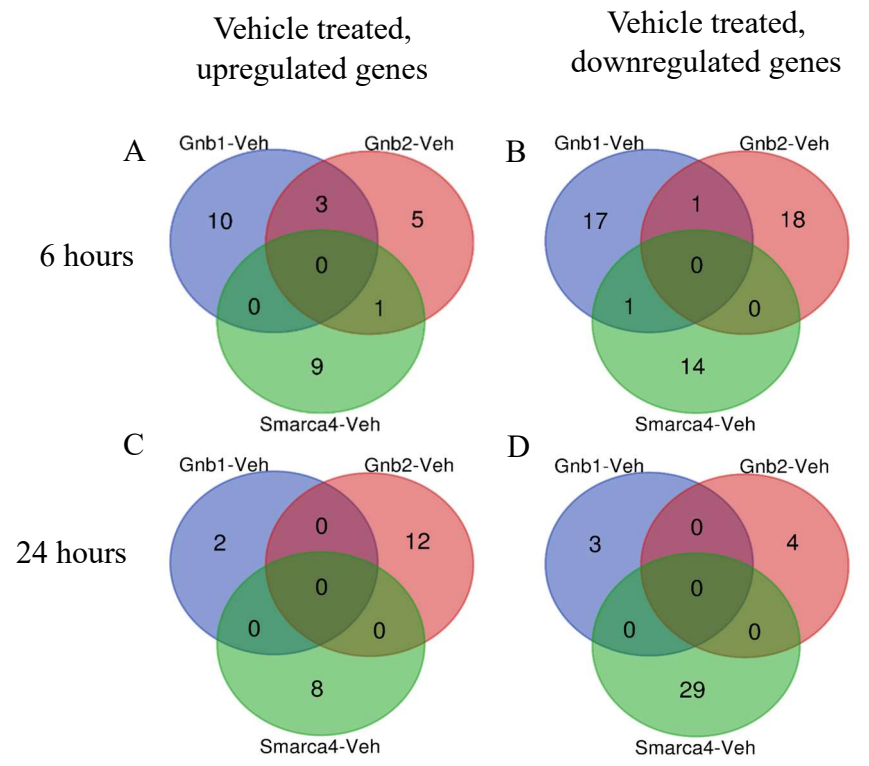


Figure 24. Venn diagrams containing counts of differentially expressed, up and downregulated genes caused by siRNA treatments at basal conditions. A-B) 6 hours C-D) 24 hours. The lack of overlap indicates each siRNA regulates mostly independent processes.

As seen in the Venn diagram and lists of changing genes (**Fig. 24-26 and Table S4**), knocking down our genes of interest has appreciable and significant changes to certain genes under basal conditions. Additionally, we saw nearly 0 overlapping up or downregulated genes in this analysis (**Fig. 24**). As expected, our siRNA target genes were significantly downregulated (**Fig 25-26, Table S4**). However, interestingly, we noticed genes associated with fibrotic processes downregulated in these lists as well: Col4a1, Col1a1, Col12a1, Acta2 (α-SMA), and Serpini1 to name a few (**Fig 25-26, Table S4**). We decided to do GO term enrichment analyses on these gene lists as well to see which pathways and cellular processes may be altered basally.



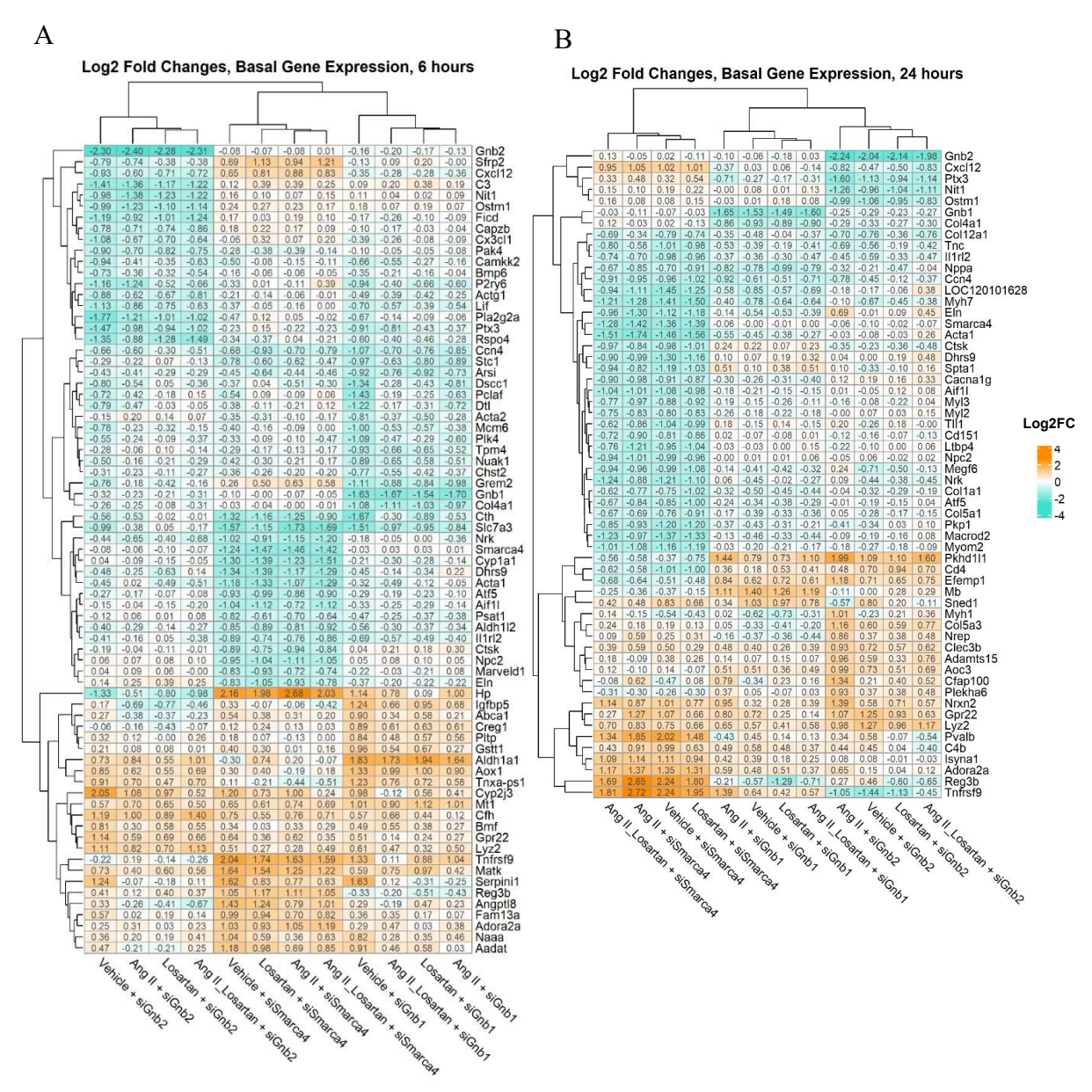


Figure 25. Log2FC heat maps depicting all up and down regulated genes at basal conditions between siRNA conditions. Clear clusters form in up and down regulated genes between siRNA treatments and between columns. Orange indicates positive Log2FC, turquoise indicates a negative Log2FC. Dendrograms constructed using hierarchical clustering

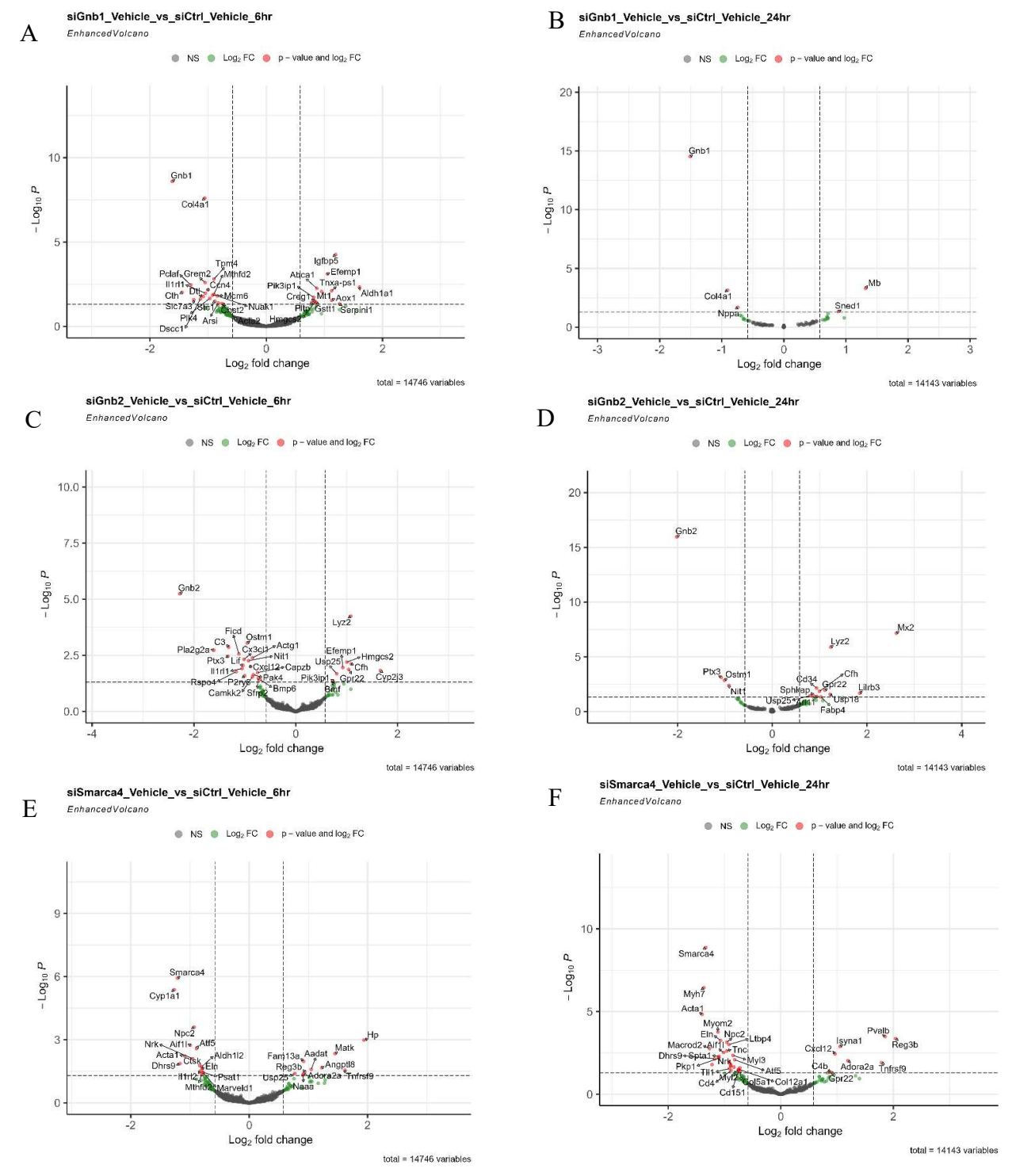


Figure 26. Volcano plots showing significantly up and downregulated genes between siRNA treatments at basal conditions. Log2FC cutoff is 0.58 (fold change +/-1.5), adjusted p value cutoff = 0.05. A, C, E) 6-hour timepoint. B, D, F) 24 hour timepoint

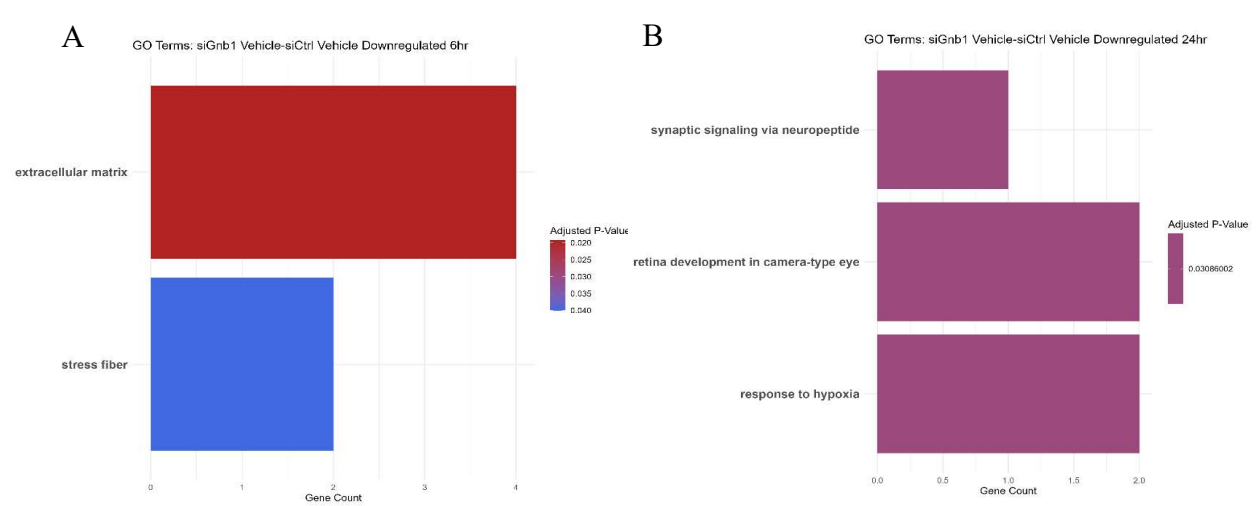


Figure 27. Summary bar plots of GO terms downregulated in Gβ1 siRNA-treated conditions vs Ctrl siRNA-treated conditions under basal conditions A) 6 hours indicating deactivation of fibrotic pathways B) 24 hours indicating little relevant changes due to inappropriate tissue localization of terms. GO terms significant by p adj. < 0.05.

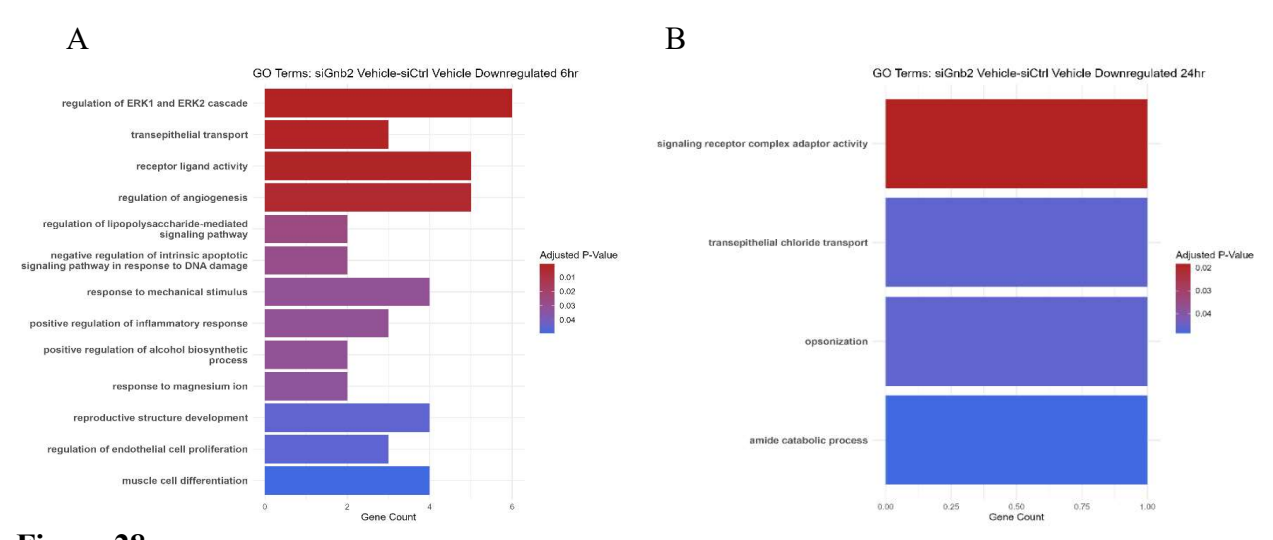


Figure 28

Figure 28. Summary bar plots of GO terms downregulated in G $\beta$ 1 siRNA-treated conditions vs Ctrl siRNA-treated conditions under basal conditions. A) 6 hours indicating deactivation of fibrotic pathways B) 24 hours indicating little relevant changes due to low gene count. GO terms significant by p adj. < 0.05.

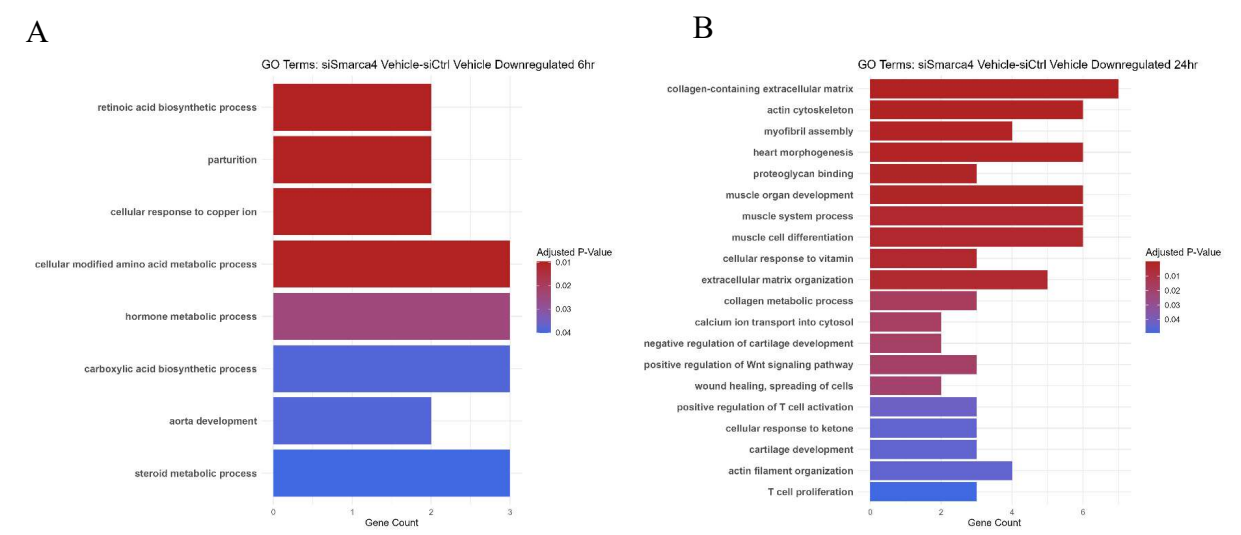


Figure 29. Summary bar plots of GO terms downregulated in Smarca4 siRNA-treated conditions vs Ctrl siRNA-treated conditions under basal conditions. A) Imprecise GO terms indicate weaker applicability of 6-hour GO terms and B) 24 hours indicating extensive downregulation of fibrotic processes. GO terms significant by p adj. < 0.05.

The GO term results show an interesting pattern among the downregulated genes in the knockdown conditions. Gβ1 siRNA reduced the expression of genes related to the extracellular matrix, actin filament formation, and stress fibre regulation (Fig 27a). At 24 hours, these processes were no longer seen in the downregulated GO terms, instead, only 1 fibrotic gene, Col4a1, was downregulated (Fig 27b). Gβ2 siRNA basally downregulated GO terms related to growth factors, cell adhesion, muscle cell development, and ERK1/2 signalling cascades (Fig 28a). Similar to Gβ1 siRNA these terms are all associated with fibrotic activities of fibroblasts. At 24 hours, only 1 gene was found in each significant GO term, and the GO terms were fairly non-specific to a specific category of processes (Fig 28b). Finally, for Smarca4 siRNA, we see a lot of metabolism and (embryonic) development genes downregulated at 6 hours of vehicle treatment (Fig 29a). At 24 hours, we see many terms related to cardiac function, myofibril contraction, muscle system processes and cardiac muscle cell development (Fig 29b).

The 6-hour Gβ1 siRNA RNCFs basally increase a few terms related to cholesterol metabolism (Table S5), and only terms related to striated muscle contraction are upregulated at 24 hours (Table S6). Gβ2 siRNA and Smarca4 siRNA did not generate any upregulated GO terms at 6 hours of vehicle treatment. After 24 hours of vehicle treatment, RNCFs treated with Gβ2 siRNA had upregulated GO terms related to protein de-ubiquitination and type 1 interferon responses (Table S6). Finally, Smarca4 siRNA showed a basal increase in GO terms also related to immune system processes after 24 hours (Table S6). Taken together, knocking down Gβ1, Gβ2 and Smarca4 affect basal transcription of certain biological processes, particularly by downregulating these pathways.

# 3.9.4 Evaluating the changes from siRNA knockdown on Ang II-induced myofibroblast differentiation

An unanswered question out of the phenotypic results from section 2 was still why our phenotypic results didn't match up with "stereotypical" myofibroblast expression patterns. We compared the Log2FCs of a panel of genes, collected from multiple myofibroblast reviews[1, 6, 17, 26, 27, 29, 30, 48, 129-132], canonically involved with myofibroblast characterization of fibroblasts and found results that closely corroborate our phenotypic results, while potentially supporting the hypothesis that G $\beta$  subunits negatively regulate the fibrotic response. Particularly interesting is that only a small subset of these genes was appreciably upregulated by Ang II (five out of 20). Further, as we saw before, at 6 hours Serpine1 was the strongest upregulated gene, followed by Ccn1, Ccn2 (CTGF), Edn1, and Acta2 ( $\alpha$ -SMA) (**Fig. 30a**). At 24 hours, the same genes upregulated at 6 hours were still upregulated, as well as Edn1 and Itgb1 (**Fig. 30b**). Interestingly, the five the genes affected by Ang II displayed potentiation of the Ang II response in siRNA knockdown conditions versus the control siRNA conditions, indicating that a portion of the

fibrotic response is rewired by knocking down these subunits (**Fig. 30a**). The heterogeneity of myofibroblasts could explain why only a subset of these canonically reported genes are upregulated. Consistent with the GO analysis presented above, this siRNA-dependent effect is not seen at 24 hours (**Fig. 30**).

Figure 30

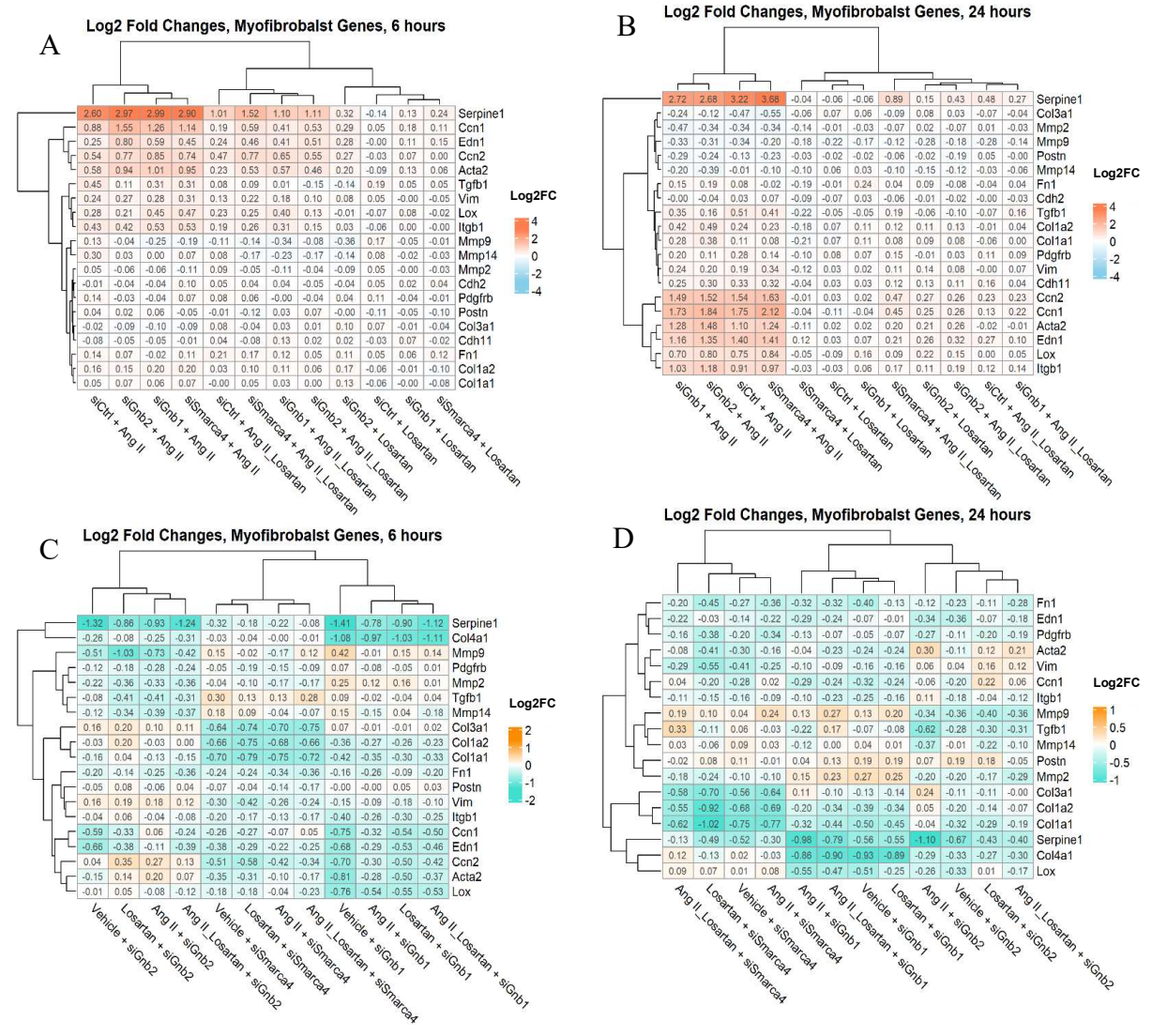


**Figure 30.** Log2FC heat maps depicting changes in canonical myofibroblast genes, collected from various literature reviews of myofibroblast activation between treatment and between siRNA conditions[1, 6, 17, 26, 27, 29, 30, 48, 129-132]. A-B) Log2FC of genes induced by Ang II within each siRNA group. C-D) Log2FC of genes induced by an siRNA within each treatment group. A, C) are at the 6-hour time point and B, D) are at the 24-hour time point.

The gene expression results reported thus far indicate a complex transcriptional regulation of pro-fibrotic (and in some cases, anti-fibrotic) signalling in our RNCF model. We have shown that this model reliably responds to Ang II stimulation and losartan antagonism. Knocking down G $\beta$ 1, G $\beta$ 2 or Smarca4 subunits have varying effects on the Ang II response. GO-term analysis suggests that depleting G $\beta$ 1 or G $\beta$ 2 subunits enhances short-term fibrotic gene expression. However, it is clear that G $\beta$ 1, G $\beta$ 2, and Smarca4 regulate fibrotic gene expression in a complex way with multiple potential mechanisms contributing control of the fibrotic response by G $\beta$  $\gamma$ .

#### **DISCUSSION**

## 4.1 Comparing proliferation and migration phenotypes in the myofibroblast model

Among the aspects of the fibrotic response that we reported on in *Results: Section 2*, fibroblast proliferation and migration are commonly studied phenotypic outputs. Activated fibroblasts are both proliferative and migratory at various stages along their activation processes. We contrasted migration and proliferation by comparing a scratch wound healing assay to simple monitored growth assays.

The scratch assays proved to be a difficult model in which to assess fibrotic migration. In the absence of FBS, the migration rate of the fibroblasts nearly stopped, which is the expected starting point after serum starvation. In most cases, the addition of Ang II accelerated the migration, but usually not more than a fraction of a percent per hour. In many experiments though, the migration rate was so slow in the Ang II condition that the scratches would not close within 24 hours. What became clear is that migration is not the ideal output for our model, because when we started optimizing collagen secretion assays, we noticed a much clearer effect of the losartan and Ang II treatments than with the migration assays.

As discussed in the *Introduction*, fibroblasts exist across a very diverse spectrum of activation states[26, 130]. Myofibroblasts are typically characterized as expressing comparatively large quantities of the cytoskeletal protein,  $\alpha$ -SMA[130]. While we do not have a comparison to a fully quiescent control, our immunofluorescent experiment quantifying  $\alpha$ -SMA protein expression showed a highly developed network of  $\alpha$ -SMA, indicative of a very activated myofibroblast[132]. However, the function of  $\alpha$ -SMA is to close wounds via tissue contraction and it is antithetical to this goal if these myofibroblasts are migrating while doing so. Myofibroblasts express *de novo* 

cadherin-2 to transmit mechanical forces to other myofibroblasts and myocytes, and cadherin-11 to communicate with immune cells[1, 130]. It has been reported that  $\alpha$ -SMA production is negatively correlated with migratory ability[131, 133]. Furthermore, Ara-C treatment reduced the already slow gap closure rate, providing a direct pharmacological intervention that confirmed the principally proliferative myofibroblast phenotype (**Fig. S4**).

Activated fibroblasts, or "proto-myofibroblasts"[130] still divide under pro-fibrotic signalling, while being non-migratory[29, 130]. In this proposed myofibroblast model, we observed a trend towards increased proliferation with the G $\beta$ 1 siRNA. This was the first phenotypic outcome that our lab has seen that indicates the transcriptional effects of G $\beta\gamma$  subunits that we reported on previously[118] may influence fibrotic events downstream of transcription. It is reported that G $\beta\gamma$  dimers affect proliferation but in many complex ways involving multiple different  $\beta$  and  $\gamma$  isoforms[134]. Perhaps a yet undetermined mechanism underlies control of proliferation in others' work, and ours as well.

#### 4.2 Understanding the collagen response to Ang II stimulation in our myofibroblast model

We showed that our RNCFs had a varied and complex response to Ang II induction of collagen secretion. Many reviews of myofibroblasts and activated fibroblasts will report that these cells increase collagen secretion and transcription in response to their agonists, including Ang II[1, 26, 130, 135]. So, we were unsure why our model failed to produce an appreciable collagen secretion signal by immunoblotting after 6 hours of Ang II treatment, and why it was inefficiently blocked by losartan after 24 hours. Furthermore, our qPCR quantification of Col1A1 mRNA showed no effect from Ang II (and losartan by extension). We speculate that the signalling hierarchy of myofibroblasts and activated fibroblasts accounts for this. In the fibroblast literature, the prevailing model is that Ang II activates a feedforward signalling cascade that initiates TGF-

β1 production, leading to the initiation of auto-and paracrine TGF-β signalling[48, 49]. Major evidence supporting this includes reports where Ang II could not induce collagen secretion in a TGF-β1 receptor knockout mouse line [48, 49]. Furthermore, once collagen secretion is initiated, it is usually done so rapidly, and mRNA transcription follows suit rapidly [136]. It is entirely possible that at 6 hours of Ang II treatment, our RNCFs have not produced enough de novo TGFβ1 to activate collagen secretion, but by 24 hours of Ang II, they have. It also stands to reason that blocking the AT1R blocks the Ang II-driven production of de novo TGF-β1, but as is observed in our data reported here, it is not a 100% blockade. TGF-β1 is highly potent and perhaps the small amounts of TGF-β1 that are still produced are enough to activate enough SMAD signalling to stimulate collagen production and secretion. We observed this in the Results section that identifies the morphological differences of Ang II-treated RNCFs compared to TGF-\(\beta\)1 RNCFs, where the TGF-β1 fibroblasts appear much more strikingly "dendritic" which is indicative of increased focal adhesions which hallmark advanced myofibroblast states[1, 26]. Studying Gβγ signalling in our model with antagonized TGF-\beta1 receptors would answer how this proposed non-canonical role of G proteins is modulated by TGF-β1.

### 4.3 Exploring targetted gene expression analysis by qPCR

To complement the phenotypic assays we undertook, Giada Castagnola, for her undergraduate research project, examined the transcriptional changes of some hallmark fibrotic genes: type 1 collagen, Ccn2 (CTGF) and Serpine1. In these experiments, Serpine1 expression was increased with Ang II treatment, but for type 1 collagen, we failed to see an Ang II-induced increase, mirroring the RNA sequencing results. We also began to investigate a few transcription factor subunits, including Egr1, JunB, FosB and c-Fos (Fig. S5), and we observed decreased expression of these transcription factors with Ang II treatment in the control siRNA conditions but

interestingly observed an increase in their expression when  $G\beta1$  was knocked down and the cells were treated with Ang II. Future work further profiling how specific transcription factors change in these siRNA perturbations will be beneficial to understanding the mechanisms of this interaction.

## 4.4 Exploring the gene expression changes via RNA sequencing

The RNA sequencing experiment illustrated a transcriptionally rewired landscape as a result of G $\beta$ 1, G $\beta$ 2, and Smarca4 knockdown.

## 4.4.1 Investigation of knocking down Gβ subunits on other G protein expression

As mentioned in the *Results* section,  $G\beta\gamma$  subunits exist in obligate dimers in the cell. Since there are 5  $G\beta$  subunits and 12  $G\gamma$  subunits and there are 16  $G\alpha$  subunits encoded in mammals, there is overlap in  $\alpha$ - $\beta\gamma$  pairings[137]. Therefore, it stands to reason that altering the  $G\beta1$  or  $G\beta2$  abundance in the cell affects the  $G\alpha$  subunits to which they bind. The below table summarizes the changes we observed in G protein subunits.

Table 5

	6 hours		24 hours	
	Upregulated G proteins	Downregulated G proteins	Upregulated G proteins	Downregulated G proteins
Gβ1 siRNA		$G\alpha_{i3}$ , $G\gamma_{12}$		$G\alpha_{o}$ , $G\gamma_{12}$ , $G\gamma_{3}$
Gβ2 siRNA		$G\alpha_{i3},G\gamma_{12},G\gamma_{7}$	Gγ <sub>7</sub>	$\begin{array}{c} G\alpha_{i3},G\alpha_{o},G\alpha_{12}\\ ,G\alpha_{i1},G\gamma_{12},G\gamma_{3} \end{array}$
Smarca4 siRNA		Gγ <sub>3</sub>		$G\alpha_{o}$ , $G\gamma_{3}$

Table 5. Summary table of changing G protein expression in differential gene expression results

This is consistent with reports in HeLa cells that showed that knocking down G $\beta$ 1 reduced the protein abundance of G $\alpha$ s and G $\alpha$ i3 and knocking down G $\beta$ 2 reduced levels of G $\alpha$ s, G $\alpha$ i3, and

Gα<sub>i1</sub> [137]. We observed similar changes for Gα<sub>i3</sub> in our knockdowns but not the other reported changes. It is understood that Gβγ subunits stabilize the Gα subunits at the protein level when bound as a heterotrimer [138]. Perhaps this disconnect between the mRNA production of a target and the protein levels of that target explains why we do not see all the changes that were reported in the literature. It is also possible that species differences between rats and humans account for this discordance since it was also reported that in human cell lines, Gβ4 subunit knockdown changes the abundances of Gα subunits[137], but Gβ1 and Gβ2 are the predominantly expressed subunits in rats [139]. Interestingly, it was observed that Gβ4 subunits could compensate for the loss of Gβ1 and Gβ2 subunits in HeLa cells [137]. In Khan *et al*, 2015, we also demonstrated that knocking out Gβ1 increased the transcript abundance of Gβ4 subunits in HEK 293 cells[65]. In the RNCF RNA sequencing work presented in this thesis, we observed no such compensation in the Gβ subunits in our sequencing data, however, given the lack of Gβ4 in rats, it is possible that this compensatory mechanism is G protein specific.

Changes in G $\gamma$  subunits were also observed. Interestingly, we saw a switch in the pattern of G $\gamma$ 7, being downregulated in the G $\beta$ 2 siRNA condition at 6 hours but upregulated at 24 hours. In human tissues that G $\gamma$ 7 is predominantly expressed in the brain[140], so to see it changing expression patterns in response to our perturbations in the heart is unexpected. More investigation is needed to determine if perhaps the loss of other G $\gamma$  subunits could cause compensation mechanisms by G $\gamma$ 7. One such other G $\gamma$  subunit that is highly abundant in many tissues is G $\gamma$ 12 [140]. In both G $\beta$  siRNA conditions, we see a reduction in G $\gamma$ 12 transcripts at 6 and 24 hours. This could suggest that G $\beta$ 1 $\gamma$ 12 subunits are an important  $\beta\gamma$  pairing in our RNCFs. It has been reported that G $\gamma$ 12 localizes to F-actin stress fibres in the cytoskeleton of Swiss 3T3 cells[141], potentially implicating stress fibre associated G $\beta\gamma$  in fibroblast activation. Since we are interested in

understanding how cell-surface  $G\beta\gamma$  has transcriptional effects in the nucleus, investigating mechanisms like translocation along stress fibres could be an interesting path to explore.

Our lab has investigated how G $\beta$  subunits regulate the production and stability of other G proteins in HEK 293 cell lines. We investigated the effects of G $\beta$ 1 KO and KCTD (Potassium Channel Tetramerization Domain) KO on G protein transcription [142]. We observed that knocking out G $\beta$ 1 increased the transcript abundance of many other G proteins spanning the  $\alpha$ ,  $\beta$ , and  $\gamma$  families [142]. In contrast to the HEK 293 work, reducing the G $\beta$ 1 and G $\beta$ 2 pools in our RNCF model did not appreciably change the abundance of other G proteins. Another likely explanation is the difference in how the G proteins were depleted. In stable KO cell lines, the cell likely evolves mechanisms to compensate for the G $\beta$ 1 loss, whereas our transient siRNA KD depletes G $\beta$ 5 subunits in a rapid fashion, not allowing the cells to find compensatory mechanisms to counteract the perturbations. This illustrates the benefits of using a transient knockdown system.

Additionally, *Khan et al*, 2015 observed that G $\beta$ 1 proteins were present on the promoter of G $\beta$ 4, implicating G $\beta$ 1 as a direct transcriptional modulator [65]. This is consistent with the observed presence of G $\beta$ 1 at the TSS of fibrotic genes discussed in the work discussed in the *Introduction* from *Khan et al*, 2023[118]. Both publications suggest that G $\beta$ 1 is acting directly on chromatin to modulate transcription, by suppressing fibrotic gene expression in fibroblasts and by supporting G $\beta$ 4 transcription in HEK 293 cells. Comparing our RNA sequencing work to this previous literature, we observe more instances of this modulatory behaviour. We observe that G $\beta$ 5 subunits *oppose changes* to fibrotic gene expression: at basal levels, they support/maintain baseline fibrotic gene expression, and under stimulation conditions, they oppose increases in fibrotic gene expression. Taken together with the work presented by others in the lab, future work can begin to

explain mechanistically how  $G\beta$  subunits have differential effects on G protein subunit transcription and other biological processes within more specialized cell models.

# 4.4.2 Exploring the transcriptomic potentiation of Ang II induction from siRNA knockdown of $G\beta1$ , $G\beta2$ , and Smarca4

We observed that, at 6 hours of Ang II treatment, only the G $\beta$ 1, G $\beta$ 2, and Smarca4 knockdowns increased the enrichment of activated myofibroblast GO terms, not the control siRNA samples. At 24 hours, all conditions had upregulated myofibroblast characteristic-GO terms. In the G $\beta$ 1 siRNA treated samples, Ang II treatment induced pathways such as "Muscle systems processes", "regulation of ERK1 and ERK2 cascade", and "actin cytoskeleton". As discussed in the *Introduction*, activated cardiac fibroblasts develop some attributes of smooth muscle cells as they differentiate into myofibroblasts, particularly genes like Acta2 ( $\alpha$ -SMA), Tagln (transgelin), Par1 (thrombin receptor), Ccn2 (CTGF), and Myh1 (myosin heavy chain 1) [1, 17]. The combination of these genes in the GO term for muscle system processes is such that in G $\beta$ 1, G $\beta$ 2, and Smarca4 knockdown samples, the pathway was statistically enriched. The absence of genes like Smtn (smoothelin) rules out the possibility that these are simply smooth muscle cells since myofibroblasts do not express all smooth muscle genes, just a subset[1, 17].

Among the upregulated GO terms in the knockdown conditions compared to the control conditions, ERK1/2 signalling pathways were enriched. ERK1/2, as discussed in the *Introduction* is a downstream effector of the AT1R activation as a convergence of signalling from both β-arrestin and Gαq signalling pathways[143, 144]. In neonatal cardiac fibroblasts, it has been reported that ERK1/2 activation occurs as a result of transactivation of EGFR in combination with Ca<sup>2+</sup> and PLC signalling, but in adult fibroblasts, it is independent of EGFR transactivation [145, 146]. If we have increased ERK signalling in certain knockdowns compared to others, it could imply

increased activity of the AT1R in these knockdowns, contributing to more advanced fibrotic transcription versus the control siRNA conditions at 6 hours.

The actin cytoskeleton GO cellular compartment term is a hallmark of fibrotic activation. As discussed, the *de novo* expression of α-SMA is a defining feature of fibroblast-myofibroblast transition and fibrotic activation [28, 29, 131]. Certain important genes from this GO term that are upregulated in our knockdown samples: Flt1 (VEGF receptor), Acta2 (α-SMA), Lmod1 (Leiomodin 1), Myo10 (myosin 10), Actn1 (α-actinin-1), and Tpm4 (Tropomyosin 4). Cardiac myofibroblasts isolated from infarct zones have been shown to express VEGF and its receptor Flt1, implicating this signalling pathway in fibroblast activation[147]. Lmod1 is an important smooth muscle protein that is required for smooth muscle contraction, an important myofibroblast function[148]. α-actinin-1 is a smooth muscle protein associated with focal adhesions, a very important myofibroblast function to contract wound areas [149]. Finally, tropomyosin is a component of smooth muscle thin filaments that are involved in smooth muscle contraction [150], and the upregulation of this factor is consistent with the smooth muscle characteristics of myofibroblasts, once again. Taken together, the 6-hour GO enrichment terms are similar among the siRNA-treated samples, and more indicative of activated myofibroblasts than the control siRNA-treated RNCFs.

The GO term enrichments at 24 hours of Ang II stimulation were similar to the 6-hour terms, however there were many more GO terms enriched. A central thread among the terms, however, were processes related to ECM, collagen processes, smooth muscle processes, and cytoskeletal/actin binding, among others (**Supplemental Table 2**). At this time point, the control siRNA-treated samples show the same myofibroblast-associated GO terms as the knockdown samples. However, uniquely, we observed that Gβ2 knockdown led to the upregulation of sterol

and cholesterol metabolism terms. This could indicate that loss of Gβ2 sensitizes myofibroblasts to activation via cholesterol, as it is reported that the LOX-1 receptor (a gene upregulated in our knockdown conditions) is responsible for mediating myofibroblast activation from oxidized LDL cholesterol [151]. A notable GO term that was decreased that contributes to fibrosis is the "regulation of apoptotic processes", which was downregulated only after 24 hours of Ang II in the Smarca4 siRNA treated samples. Myofibroblasts that are heavily activated are usually resistant to apoptosis [129]. For this term to be further downregulated, this could imply that Smarca4 is involved in myofibroblast survival. Myofibroblast apoptosis is associated with fibrosis resolution and scar maturation [152], so it is possible that Smarca4 and mSWI/SNF can affect transcription associated with this resolution.

# 4.4.3 Exploring the transcriptomic repression of basal fibrotic gene expression from siRNA knockdown of G $\beta$ 1, G $\beta$ 2, and Smarca4

When knocking down such important signalling molecules as G proteins and chromatin remodelling subunits, it is important to assess if the knockdowns are affecting the cells drastically independent of agonists or antagonists. We discovered that indeed these siRNAs induced statistically significant gene expression decreases at 6 and 24 hours of vehicle treatment (DMEM). At 6 hours, G $\beta$ 1-treated samples showed downregulated GO terms related to the extracellular matrix, actin fibre formation, and actin fibre contraction. Based on the discussion above, this would imply that we see a basal downregulation of common myofibroblast activation processes; that is, less fibroblast activation. G $\beta$ 2 siRNA treatment downregulated terms associated with ERK1/2 cascades after 6 hours. Again, from above, this indicates less fibrotic activity.

Contrastingly, Smarca4 siRNA did not show changes in fibrotic GO terms, instead showing changes in retinoic acid and vitamin A-related processes. The role of vitamin A and its derivatives

is complex in the heart. They play an important role in the development of resident cardiac fibroblasts during embryonic development and also have been reported to contribute to the epicardial response to injury in the heart (such as after an MI) [42]. On one hand, the retinoic acid receptor was found to be upregulated in a mouse model of cardiac remodelling after myocardial ischemia-reperfusion injury [153] and gene expression downstream of this receptor was elevated in coronary heart disease [154]. On the other hand, retinoic acid signalling was found to be cardioprotective and suppressed myocyte hypertrophy [155]. It is clear that retinoic acid is at play in the heart in other cell types as they respond to injury, and in fibroblasts during development, so perhaps Smarca4 is involved in re-activating transcriptional processes involved in fetal heart development. We did not see other indications of this in our work, but additional investigation could clarify if Smarca4 has this potential role.

The G proteins and Smarca4 reverse roles at 24 hours because we see little downregulation of GO terms in the G $\beta$ 1 or G $\beta$ 2 siRNA treated samples after 24 hours. But looking at Smarca4 siRNA-treated samples, we see a significant downregulation in the actin, cardiac muscle contraction, and extracellular matrix regulation processes in the 24-hour samples. This may suggest that Smarca4 is required for the maintenance of pro-myofibroblast gene expression, and in the absence of an agonist, could contribute to the sustained activation of myofibroblasts, preventing de-activation and regression to quiescence. Fibroblast de-activation is an active area of research [31] [156] and a potential future avenue for follow-up studies to the work presented in this thesis.

### 4.5 Temporal control of fibrotic gene expression

The above discussion of GO terms at 6 hours of Ang II describes processes which are all upregulated by each siRNA condition but not in the negative control siRNA samples. At 24 hours, all siRNA groups, including the negative control, show many of the same fibrotic response GO terms enriched by Ang II treatment. There seems to be a temporal factor involved in how these siRNA regulate fibrotic transcription processes. Interestingly, aspects of our RNA seq data imply that knocking down G $\beta$ 1 and G $\beta$ 2 increases fibrotic processes in our fibroblasts. This is consistent with what was shown in the previous work from *Khan et al* in 2023 where G $\beta$ 1 had a negative modulatory role in regulating RNA polymerase II activity in RNCFs at short time points but did not at longer time points [118]. In the RNA seq data in this thesis, we also see this temporal effect by Smarca4, but the effect of Smarca4 on altered basal transcription is inconsistent with a direct association with this G protein phenomenon. What is also notable is that previous work did not show a role for G $\beta$ 2 in this RNAPII interaction, only G $\beta$ 1. Given both G proteins seem to potentiate the Ang II transcriptional response in our data shown in this thesis, it stands to reason that more work is needed to understand how G proteins regulate the cardiac fibrotic response.

#### LIMITATIONS

As outlined in the *Discussion*, there are a few limitations to the interpretations of these findings. As noted in *Results Section 2*, a portion of the findings was to characterize the fibrotic phenotypes that our RNCF model displayed. This was important information to have proceeding into the RNA sequencing work because it would 1) serve as validations of consistency between experiments and 2) enable a translation of transcriptomic findings to phenotypic outcomes. The rhetorical phrase "RNA doesn't equal protein" is always a caveat to transcriptomic results like these, and therefore having a framework of cellular fibrotic outcomes upon which we can project the transcriptomic findings was helpful. That being said, we presented results that were at times inconsistent between the RNA seq and the qPCR/protein-based assays. This illustrates a limitation of interpreting transcription data in a silo, and it is possible that changes in fibroblast biology are also conferred via translation or post-translational control; factors that cannot necessarily be examined in RNA sequencing analysis.

Our model is a limitation in itself. We demonstrated that this is likely a very activated myofibroblast phenotype. We grow the RNCFs on plastic, which is a very activating substrate. Therefore, the changes we see may be different in a less-activated model. It is important to corroborate these findings with further work in other models that circumvent the hyperactivation phenotype we observe.

We discussed the limitation of the siRNA knockdown being lower for Smarca4 than the other genes. This could limit the biological effect of the changes we see in the Smaraca4 conditions. However, we still observed unique changes in these conditions, indicating that at this knockdown level, statistically significant transcriptional changes are still occurring. The leads identified can be further validated moving forward.

Finally, this work was done in a rodent model, not human cells, therefore differences may exist that limit the direct application of these findings to human clinical cases. As outlined in the *Introduction* and *Discussion*, many studies are done in rodent models, particularly rat neonates for cardiovascular interventions, but as always in medical research, findings must be translated into more relevant human models to verify effects are not species-specific.

## CONCLUSIONS AND FUTURE PERSPECTIVES

The research goals of this thesis were to investigate how  $G\beta\gamma$  influences fibrotic gene expression programs and probe if the mSWI/SNF complex could be a mechanism through which  $G\beta\gamma$  exerts this control. We set out 3 aims: 1) To develop a reliable and efficient primary-cell culture system wherein  $G\beta1$ ,  $G\beta2$ , and Smarca4 subunits are knocked down using siRNA. 2) To characterize the effect that these siRNA knockdowns have on basal and Ang II-induced fibrotic outcomes and myofibroblast phenotypes. 3) To investigate the transcriptomic changes in basal and Ang II-induced RNCFs under  $G\beta1$ ,  $G\beta2$ , and Smarca4 knockdown conditions. The work in this thesis achieved these aims via extensive model development, analysis of phenotypic outcomes like fibroblast growth, migration, collagen secretion, fibrotic marker expression, and thorough exploratory analysis of the broad transcriptional changes that occur with siRNA silencing of  $G\beta$  subunits and Smarca4.

We identified the strengths and limitations of our siRNA knockdown model and characterized its myofibroblast characteristics. We showed that migration, collagen production, and collagen secretion were not relevant phenotypic outcomes for the fibroblast activation state of our model. Instead, proliferation and selective expression of fibrotic genes, like Serpine1, were more reliable outputs to establish changes in the fibrotic response of our RNCFs.

We also identified very interesting changes in up- and down-regulated biological pathways and cellular component makeup in our RNA sequencing data. We showed specific changes in basal gene expression caused by the siRNA knockdowns, as well as changes in how each knockdown condition responded to 6-hour or 24-hour Ang II stimulation. Some of our data suggests that changes in GO terms that we observed indicate that loss of G $\beta$ 1, G $\beta$ 2, and Smarca4 subunits confer a potentiation of the Ang II response to our RNCFs. We also observed that our siRNA knockdowns

reduced basal fibrotic gene expression GO pathways at both 6 and 24 hours. Taken together, our transcriptomic work may suggest the following model:

 $G\beta1$ ,  $G\beta2$ , and Smarca4 oppose changes in gene expression, but only transiently. At baseline levels, these subunits maintain activated myofibroblast expression profiles. Upon short-term fibrotic activation with Ang II, these proteins repress increases in fibrotic transcription but do not repress chronic pro-fibrotic stimulation.

Future directions for this work include experiments that further profile the transcriptional effects of GB subunits and Smarca4, demonstrate a mechanism for this interaction in cardiac fibroblasts, and recapitulate these findings in a model that is more relevant to human cardiac fibrosis. Following up on the RNA sequencing results, it would be illuminating to further investigate the differentially expressed genes between siRNA and between treatment conditions to see if changes are also associated with specific transcription factor binding profiles (through processes like KEGG-pathway analysis or Ingenuity Pathway Analysis). This can inform more transcriptomic analyses like CUT&RUN-seq. Particularly, CUT&RUN investigating where Gβ1, Gβ2, and Smarca4 are located will allow us to confirm whether the changes in GO terms presented in this thesis can be linked to a direct occupancy of G proteins and mSWI/SNF subunits to the same genomic loci, or if they affect fibrotic transcription in separate ways that combine to the observed outcomes. This can help us craft a mechanism for this control. Other experiments such as Co-IP followed by LC-MS of nuclear lysates can identify the interactome of Gβ subunits in the nucleus and provide more direct evidence of a potential protein complex. Finally, transitioning this work out of rats and into models such as human induced pluripotent stem cell (hIPSC)-derived cardiac fibroblast can improve the translatability of these results to improve interpretation and applicability to human disease.

Cardiac fibrosis is paradoxical. It is at the same time critically necessary for survival, and pathologically lethal to whom it afflicts. Its control is well understood through a canonical signalling lens, but non-canonical modulators complicate and precise these processes. My thesis contributes to this growing body of evidence supporting the importance of non-canonical fibrotic modulators. Irrespective of its paradoxical nature, cardiac fibrosis significantly impacts global disease burden and quality of life. A better understanding of how the fibrotic response is regulated can allow future therapeutic targets to be identified that may one day prevent and reverse cardiac fibrosis.

## REFERENCES

- 1. Davis, J. and J.D. Molkentin, *Myofibroblasts: trust your heart and let fate decide*. J Mol Cell Cardiol, 2014. **70**: p. 9-18.
- 2. Global, regional, and national incidence, prevalence, and years lived with disability for 354 diseases and injuries for 195 countries and territories, 1990-2017: a systematic analysis for the Global Burden of Disease Study 2017. Lancet, 2018. **392**(10159): p. 1789-1858.
- 3. Wang, J., C. Gareri, and H.A. Rockman, *G-Protein–Coupled Receptors in Heart Disease*. Circulation Research, 2018. **123**(6): p. 716-735.
- 4. Heart and Stroke Foundation of Canada. *Heart failure*. 2024 [cited 2024 June 20]; Available from: <a href="https://www.heartandstroke.ca/heart-disease/conditions/heart-failure">https://www.heartandstroke.ca/heart-disease/conditions/heart-failure</a>.
- 5. Schwinger, R.H.G., *Pathophysiology of heart failure*. Cardiovasc Diagn Ther, 2021. **11**(1): p. 263-276.
- 6. Segura, A.M., O.H. Frazier, and L.M. Buja, *Fibrosis and heart failure*. Heart Failure Reviews, 2014. **19**(2): p. 173-185.
- 7. Brilla, C.G. and K.T. Weber, *Reactive and reparative myocardial fibrosis in arterial hypertension in the rat.* Cardiovasc Res, 1992. **26**(7): p. 671-7.
- 8. Triposkiadis, F., et al., *The sympathetic nervous system in heart failure physiology,* pathophysiology, and clinical implications. J Am Coll Cardiol, 2009. **54**(19): p. 1747-62.
- 9. O'Riordan, E., et al., *Chronic NOS inhibition actuates endothelial-mesenchymal transformation*. Am J Physiol Heart Circ Physiol, 2007. **292**(1): p. H285-94.
- Feldman, A.M. and D. McNamara, *Myocarditis*. N Engl J Med, 2000. 343(19): p. 1388-98.

- 11. Mandawat, A., et al., *Progression of Myocardial Fibrosis in Nonischemic DCM and Association With Mortality and Heart Failure Outcomes*. JACC: Cardiovascular Imaging, 2021. **14**(7): p. 1338-1350.
- 12. Frustaci, A., et al., *Myocardial cell death in human diabetes*. Circ Res, 2000. **87**(12): p. 1123-32.
- 13. Ponikowski, P., et al., 2016 ESC Guidelines for the diagnosis and treatment of acute and chronic heart failure: The Task Force for the diagnosis and treatment of acute and chronic heart failure of the European Society of Cardiology (ESC)Developed with the special contribution of the Heart Failure Association (HFA) of the ESC. Eur Heart J, 2016. 37(27): p. 2129-2200.
- 14. Simmonds, S.J., et al., Cellular and Molecular Differences between HFpEF and HFrEF:

  A Step Ahead in an Improved Pathological Understanding. Cells, 2020. 9(1).
- 15. Forte, E., M.B. Furtado, and N. Rosenthal, *The interstitium in cardiac repair: role of the immune-stromal cell interplay.* Nat Rev Cardiol, 2018. **15**(10): p. 601-616.
- 16. Dai, Z., et al., Coronary perivascular fibrosis is associated with impairment of coronary blood flow in patients with non-ischemic heart failure. J Cardiol, 2012. **60**(5): p. 416-21.
- 17. Hinz, B., et al., *The Myofibroblast: One Function, Multiple Origins*. The American Journal of Pathology, 2007. **170**(6): p. 1807-1816.
- 18. Kuppe, C., et al., *Decoding myofibroblast origins in human kidney fibrosis*. Nature, 2021. **589**(7841): p. 281-286.
- 19. Weil, B. and S. Neelamegham, Selectins and Immune Cells in Acute Myocardial

  Infarction and Post-infarction Ventricular Remodeling: Pathophysiology and Novel

  Treatments. Frontiers in Immunology, 2019. 10: p. 300.

- 20. Chalise, U., M. Becirovic-Agic, and M.L. Lindsey, *The cardiac wound healing response to myocardial infarction*. WIREs Mech Dis, 2023. **15**(1): p. e1584.
- 21. Daseke, M.J., 2nd, et al., Cardiac fibroblast activation during myocardial infarction wound healing: Fibroblast polarization after MI. Matrix Biol, 2020. **91-92**: p. 109-116.
- 22. Turner, N.A., et al., *Interleukin-1alpha stimulates proinflammatory cytokine expression in human cardiac myofibroblasts*. Am J Physiol Heart Circ Physiol, 2009. **297**(3): p. H1117-27.
- 23. Huang, S. and N.G. Frangogiannis, *Anti-inflammatory therapies in myocardial infarction:* failures, hopes and challenges. Br J Pharmacol, 2018. **175**(9): p. 1377-1400.
- 24. Mouton, A.J., et al., Fibroblast polarization over the myocardial infarction time continuum shifts roles from inflammation to angiogenesis. Basic Res Cardiol, 2019.
   114(2): p. 6.
- 25. Squires, C.E., et al., *Altered fibroblast function following myocardial infarction*. J Mol Cell Cardiol, 2005. **39**(4): p. 699-707.
- 26. Gibb, A.A., M.P. Lazaropoulos, and J.W. Elrod, *Myofibroblasts and Fibrosis*. Circulation Research, 2020. **127**(3): p. 427-447.
- 27. Hillsley, A., et al., A strategy to quantify myofibroblast activation on a continuous spectrum. Sci Rep, 2022. **12**(1): p. 12239.
- 28. Davis, J. and J.D. Molkentin, *Myofibroblasts: Trust your heart and let fate decide*.

  Journal of Molecular and Cellular Cardiology, 2014. **70**: p. 9-18.
- 29. Baum, J. and H.S. Duffy, *Fibroblasts and myofibroblasts: what are we talking about?* J Cardiovasc Pharmacol, 2011. **57**(4): p. 376-9.

- 30. Weber, K.T., et al., *Myofibroblast-mediated mechanisms of pathological remodelling of the heart.* Nature Reviews Cardiology, 2013. **10**(1): p. 15-26.
- 31. Fortier, S.M., et al., Myofibroblast dedifferentiation proceeds via distinct transcriptomic and phenotypic transitions. JCI Insight, 2021. **6**(6).
- 32. Sun, Y., et al., *Infarct scar as living tissue*. Basic Research in Cardiology, 2002. **97**(5): p. 343-347.
- 33. Pierce, K.L., R.T. Premont, and R.J. Lefkowitz, *Seven-transmembrane receptors*. Nature Reviews Molecular Cell Biology, 2002. **3**(9): p. 639-650.
- 34. Salazar, N.C., J. Chen, and H.A. Rockman, *Cardiac GPCRs: GPCR signaling in healthy and failing hearts*. Biochimica et Biophysica Acta (BBA) Biomembranes, 2007.

  1768(4): p. 1006-1018.
- 35. Delaunay, M., et al., *The Role of Cyclic AMP Signaling in Cardiac Fibrosis*. Cells, 2019. **9**(1).
- 36. Aránguiz-Urroz, P., et al., *Beta(2)-adrenergic receptor regulates cardiac fibroblast* autophagy and collagen degradation. Biochim Biophys Acta, 2011. **1812**(1): p. 23-31.
- 37. Villarreal, F., et al., Regulation of cardiac fibroblast collagen synthesis by adenosine: roles for Epac and PI3K. Am J Physiol Cell Physiol, 2009. **296**(5): p. C1178-84.
- 38. Phosri, S., et al., Stimulation of Adenosine A(2B) Receptor Inhibits Endothelin-1-Induced Cardiac Fibroblast Proliferation and α-Smooth Muscle Actin Synthesis Through the cAMP/Epac/PI3K/Akt-Signaling Pathway. Front Pharmacol, 2017. 8: p. 428.
- 39. Phosri, S., et al., Epac is required for exogenous and endogenous stimulation of adenosine A(2B) receptor for inhibition of angiotensin II-induced collagen synthesis and myofibroblast differentiation. Purinergic Signal, 2018. **14**(2): p. 141-156.

- 40. Daaka, Y., L.M. Luttrell, and R.J. Lefkowitz, *Switching of the coupling of the beta2-adrenergic receptor to different G proteins by protein kinase A.* Nature, 1997. **390**(6655): p. 88-91.
- Tanner, M.A., et al., β2-Adrenergic Receptors Increase Cardiac Fibroblast Proliferation
   Through the Gαs/ERK1/2-Dependent Secretion of Interleukin-6. Int J Mol Sci, 2020.

   21(22).
- 42. Wang, S., et al., *Modulation of retinoid signaling: therapeutic opportunities in organ fibrosis and repair.* Pharmacol Ther, 2020. **205**: p. 107415.
- 43. Turner, N.A. and N.M. Blythe, *Cardiac Fibroblast p38 MAPK: A Critical Regulator of Myocardial Remodeling*. J Cardiovasc Dev Dis, 2019. **6**(3).
- 44. Gutkind, J.S. and S. Offermanns, *A New Gq-Initiated MAPK Signaling Pathway in the Heart.* Developmental Cell, 2009. **16**(2): p. 163-164.
- 45. Heineke, J. and J.D. Molkentin, *Regulation of cardiac hypertrophy by intracellular signalling pathways*. Nature Reviews Molecular Cell Biology, 2006. **7**(8): p. 589-600.
- 46. Park, S., et al., *Cardiac fibrosis: potential therapeutic targets*. Translational Research, 2019. **209**: p. 121-137.
- 47. Atlas, S.A., *The Renin-Angiotensin Aldosterone System: Pathophysiological Role and Pharmacologic Inhibition.* Journal of Managed Care Pharmacy, 2007. **13**(8 Supp B): p. 9-20.
- 48. Leask, A., *Potential Therapeutic Targets for Cardiac Fibrosis*. Circulation Research, 2010. **106**(11): p. 1675-1680.
- 49. Schultz, J.E.J., et al., *TGF-β1 mediates the hypertrophic cardiomyocyte growth induced* by angiotensin II. The Journal of clinical investigation, 2002. **109**(6): p. 787-796.

- Wang, J., et al., Mechanoactivation of the angiotensin II type 1 receptor induces β-arrestin-biased signaling through Ga(i) coupling. J Cell Biochem, 2018. **119**(4): p. 3586-3597.
- 51. Sumners, C., et al., *Anti-fibrotic mechanisms of angiotensin AT(2) -receptor stimulation*.

  Acta Physiol (Oxf), 2019. **227**(1): p. e13280.
- 52. Karnik, S.S., et al., *International Union of Basic and Clinical Pharmacology. XCIX. Angiotensin Receptors: Interpreters of Pathophysiological Angiotensinergic Stimuli.*Pharmacological Reviews, 2015. **67**(4): p. 754-819.
- 53. Sumners, C., et al., *Anti-fibrotic mechanisms of angiotensin AT2-receptor stimulation*.

  Acta Physiologica, 2019. **227**(1): p. e13280.
- 54. Khan, S.M., et al., *The Expanding Roles of G*<*em*>βγ</*em*> Subunits in G Protein—

  Coupled Receptor Signaling and Drug Action. Pharmacological Reviews, 2013. **65**(2): p. 545-577.
- 55. Logothetis, D.E., et al., *The βγ subunits of GTP-binding proteins activate the muscarinic K+ channel in heart.* Nature, 1987. **325**(6102): p. 321-326.
- 56. Currie, K.P.M., *G protein inhibition of CaV2 calcium channels*. Channels, 2010. **4**(6): p. 497-509.
- 57. Wang, T., et al., Selective interaction of the C2 domains of phospholipase Cβ<sub>1</sub> and -&#x3b2;<sub>2</sub> with activated

  G&#x3b1;<sub>q</sub> subunits: An alternative function for C2-signaling modules.

  Proceedings of the National Academy of Sciences, 1999. **96**(14): p. 7843-7846.
- 58. Ushio-Fukai, M., et al., Temporal Dispersion of Activation of Phospholipase C-β1 and -γ

  Isoforms by Angiotensin II in Vascular Smooth Muscle Cells: ROLE OF αq/11, α12, AND

- βγ G PROTEIN SUBUNITS\*. Journal of Biological Chemistry, 1998. **273**(31): p. 19772-19777.
- 59. Fruman, D.A., R.E. Meyers, and L.C. Cantley, *PHOSPHOINOSITIDE KINASES*. Annual Review of Biochemistry, 1998. **67**(Volume 67, 1998): p. 481-507.
- 60. Khan, S.M., J.Y. Sung, and T.E. Hébert, *Gβγ subunits—Different spaces, different faces*.

  Pharmacological Research, 2016. **111**: p. 434-441.
- Yost, E.A., et al., Inhibition of G-Protein βγ Signaling Enhances T Cell Receptor-Stimulated Interleukin 2 Transcription in CD4+ T Helper Cells. PLOS ONE, 2015.
   10(1): p. e0116575.
- 62. Zaballos, M.A., B. Garcia, and P. Santisteban, Gβγ Dimers Released in Response to Thyrotropin Activate Phosphoinositide 3-Kinase and Regulate Gene Expression in Thyroid Cells. Molecular Endocrinology, 2008. 22(5): p. 1183-1199.
- 63. Park, J.G., et al., *Transcriptional regulation by the γ5 subunit of a heterotrimeric G* protein during adipogenesis. The EMBO Journal, 1999. **18**(14): p. 4004-4012-4012.
- 64. Robitaille, M., et al., *Gβγ is a negative regulator of AP-1 mediated transcription*. Cellular Signalling, 2010. **22**(8): p. 1254-1266.
- Khan, S.M., et al., Gβ4γ1 as a modulator of M3 muscarinic receptor signalling and novel roles of Gβ1 subunits in the modulation of cellular signalling. Cellular Signalling, 2015.
  27(8): p. 1597-1608.
- Yuen, J.W.F., et al., Activation of STAT3 by specific Gα subunits and multiple Gβγ dimers.
   The International Journal of Biochemistry & Cell Biology, 2010. 42(6): p. 1052-1059.
- 67. Crawford, S.E., et al., *Thrombospondin-1 is a major activator of TGF-beta1 in vivo*. Cell, 1998. **93**(7): p. 1159-70.

- 68. Leask, A., *TGFβ*, cardiac fibroblasts, and the fibrotic response. Cardiovascular Research, 2007. **74**(2): p. 207-212.
- 69. Staessen, J.A., Y. Li, and T. Richart, *Oral renin inhibitors*. The Lancet, 2006. **368**(9545): p. 1449-1456.
- 70. Ellmers, L.J., et al., (Pro)renin Receptor Blockade Ameliorates Cardiac Injury and Remodeling and Improves Function After Myocardial Infarction. Journal of Cardiac Failure, 2016. **22**(1): p. 64-72.
- 71. Fang, Q.Q., et al., Angiotensin-converting enzyme inhibitor reduces scar formation by inhibiting both canonical and noncanonical TGF-β1 pathways. Sci Rep, 2018. **8**(1): p. 3332.
- 72. Wu, L., et al., Effect of angiotensin II type 1 receptor blockade on cardiac remodeling in angiotensin II type 2 receptor null mice. Arteriosclerosis, thrombosis, and vascular biology, 2002. **22**(1): p. 49-54.
- 73. Brilla, C.G., J.S. Janicki, and K.T. Weber, *Cardioreparative effects of lisinopril in rats* with genetic hypertension and left ventricular hypertrophy. Circulation, 1991. **83**(5): p. 1771-1779.
- 74. Brooks, W.W., et al., Effect of Angiotensin-Converting Enzyme Inhibition on Myocardial Fibrosis and Function in Hypertrophied and Failing Myocardium From the Spontaneously Hypertensive Rat. Circulation, 1997. **96**(11): p. 4002-4010.
- 75. Brilla, C.G. and K.T. Weber, *Reactive and reparative myocardial fibrosis in arterial hypertension in the rat.* Cardiovascular Research, 1992. **26**(7): p. 671-677.

- 76. Moiseeva, O.M., et al., Effect of pravastatin on phenotypical transformation of fibroblasts and hypertrophy of cardiomyocytes in culture. Bulletin of Experimental Biology and Medicine, 2007. **143**(1): p. 54-57.
- 77. Rodrigues-Díez, R., et al., *Pharmacological modulation of epithelial mesenchymal transition caused by angiotensin II. Role of ROCK and MAPK pathways.* Pharm Res, 2008. **25**(10): p. 2447-61.
- 78. He, Y.-P., et al., *Involvement of ERK and AKT signaling in the growth effect of arginine vasopressin on adult rat cardiac fibroblast and the modulation by simvastatin*. Molecular and cellular biochemistry, 2008. **317**: p. 33-41.
- 79. Porter, K.E., et al., Simvastatin reduces human atrial myofibroblast proliferation independently of cholesterol lowering via inhibition of RhoA. Cardiovascular research, 2004. **61**(4): p. 745-755.
- 80. Turner, N.A., et al., Simvastatin inhibits TNFα-induced invasion of human cardiac myofibroblasts via both MMP-9-dependent and-independent mechanisms. Journal of molecular and cellular cardiology, 2007. **43**(2): p. 168-176.
- 81. Porter, K.E. and N.A. Turner, *Statins and myocardial remodelling: cell and molecular pathways*. Expert Reviews in Molecular Medicine, 2011. **13**: p. e22.
- 82. Chen, J. and J.L. Mehta, Angiotensin II-mediated oxidative stress and procollagen-1 expression in cardiac fibroblasts: blockade by pravastatin and pioglitazone. American Journal of Physiology-Heart and Circulatory Physiology, 2006. **291**(4): p. H1738-H1745.
- 83. Shyu, K.G., et al., Mechanism of the inhibitory effect of atorvastatin on endoglin expression induced by transforming growth factor-β1 in cultured cardiac fibroblasts. European journal of heart failure, 2010. **12**(3): p. 219-226.

- 84. Edgley, A.J., H. Krum, and D.J. Kelly, *Targeting Fibrosis for the Treatment of Heart Failure: A Role for Transforming Growth Factor-β*. Cardiovascular Therapeutics, 2012. **30**(1): p. e30-e40.
- 85. Iyer, S., G. Gurujeyalakshmi, and S. Giri, Effects of pirfenidone on procollagen gene expression at the transcriptional level in bleomycin hamster model of lung fibrosis.

  Journal of Pharmacology and Experimental Therapeutics, 1999. **289**(1): p. 211-218.
- Wang, Y., et al., *Pirfenidone attenuates cardiac fibrosis in a mouse model of TAC-induced left ventricular remodeling by suppressing NLRP3 inflammasome formation*. Cardiology, 2013. **126**(1): p. 1-11.
- 87. Nguyen, D.T., et al., *Pirfenidone mitigates left ventricular fibrosis and dysfunction after myocardial infarction and reduces arrhythmias*. Heart rhythm, 2010. **7**(10): p. 1438-1445.
- 88. Mirkovic, S., et al., *Attenuation of cardiac fibrosis by pirfenidone and amiloride in DOCA-salt hypertensive rats*. British journal of pharmacology, 2002. **135**(4): p. 961-968.
- 89. Lewis, G.A., et al., *Pirfenidone in heart failure with preserved ejection fraction: a randomized phase 2 trial.* Nat Med, 2021. **27**(8): p. 1477-1482.
- 90. Clapier, C.R. and B.R. Cairns, *The biology of chromatin remodeling complexes*. Annu Rev Biochem, 2009. **78**: p. 273-304.
- 91. Clark, S.C., et al., *Differential nucleosome spacing in neurons and glia*. Neurosci Lett, 2020. **714**: p. 134559.
- 92. Varga, J., et al., *The BAF chromatin remodeling complexes: structure, function, and synthetic lethalities.* Biochemical Society Transactions, 2021. **49**(4): p. 1489-1503.

- 93. Mashtalir, N., et al., *Modular Organization and Assembly of SWI/SNF Family Chromatin Remodeling Complexes*. Cell, 2018. **175**(5): p. 1272-1288.e20.
- 94. Wang, W., et al., *Diversity and specialization of mammalian SWI/SNF complexes*. Genes & development, 1996. **10**(17): p. 2117-2130.
- 95. Jin, B., Y. Li, and K.D. Robertson, *DNA methylation: superior or subordinate in the epigenetic hierarchy?* Genes Cancer, 2011. **2**(6): p. 607-17.
- 96. Zhao, Y. and B.A. Garcia, Comprehensive Catalog of Currently Documented Histone Modifications. Cold Spring Harb Perspect Biol, 2015. 7(9): p. a025064.
- 97. Fahed, A.C., et al., *Genetics of congenital heart disease: the glass half empty.* Circulation research, 2013. **112**(4): p. 707-720.
- 98. Bruneau, B.G., *Chromatin remodeling in heart development*. Current Opinion in Genetics & Development, 2010. **20**(5): p. 505-511.
- 99. Cirillo, L.A., et al., *Opening of compacted chromatin by early developmental*transcription factors HNF3 (FoxA) and GATA-4. Molecular cell, 2002. **9**(2): p. 279-289.
- 100. Takeuchi, J.K. and B.G. Bruneau, *Directed transdifferentiation of mouse mesoderm to heart tissue by defined factors*. Nature, 2009. **459**(7247): p. 708-711.
- 101. Parker, T.G., S.E. Packer, and M.D. Schneider, Peptide growth factors can provoke
  "fetal" contractile protein gene expression in rat cardiac myocytes. J Clin Invest, 1990.
  85(2): p. 507-14.
- 102. Hang, C.T., et al., Chromatin regulation by Brg1 underlies heart muscle development and disease. Nature, 2010. **466**(7302): p. 62-67.

- 103. Liu, L., et al., Deciphering the role of SMARCA4 in cardiac disorders: Insights from single-cell studies on dilated cardiomyopathy and coronary heart disease. Cellular Signalling, 2024. 119: p. 111150.
- 104. Willis, M.S., et al., *BRG1* and *BRM* function antagonistically with c-MYC in adult cardiomyocytes to regulate conduction and contractility. J Mol Cell Cardiol, 2017. **105**: p. 99-109.
- 105. Wang, S., et al., BRG1 expression is increased in thoracic aortic aneurysms and regulates proliferation and apoptosis of vascular smooth muscle cells through the long non-coding RNA HIF1A-AS1 in vitro. European Journal of Cardio-Thoracic Surgery, 2015. 47(3): p. 439-446.
- 106. Fang, F., et al., *Proinflammatory stimuli engage Brahma related gene 1 and Brahma in endothelial injury.* Circulation research, 2013. **113**(8): p. 986-996.
- 107. Huang, W.B., W.Y. Liu, and G.L. Xie, *Role of Brahma-related gene 1 (Brg1) in heart disease*. Chin Med J (Engl), 2021. **134**(9): p. 1061-1063.
- 108. Zhang, X., et al., *Brg1 deficiency in vascular endothelial cells blocks neutrophil* recruitment and ameliorates cardiac ischemia-reperfusion injury in mice. Int J Cardiol, 2018. **269**: p. 250-258.
- 109. Li, Z., et al., BRG1 regulates NOX gene transcription in endothelial cells and contributes to cardiac ischemia-reperfusion injury. Biochimica et Biophysica Acta (BBA) Molecular Basis of Disease, 2018. **1864**(10): p. 3477-3486.
- 110. Enríquez, P., et al., Binding specificity and function of the SWI/SNF subunit SMARCA4 bromodomain interaction with acetylated histone H3K14. J Biol Chem, 2021. **297**(4): p. 101145.

- 111. Duong, T.E. and J.S. Hagood, *Epigenetic Regulation of Myofibroblast Phenotypes in Fibrosis*. Curr Pathobiol Rep, 2018. **6**(1): p. 79-96.
- 112. Ghosh, A.K., et al., p300 is elevated in systemic sclerosis and its expression is positively regulated by TGF-β: epigenetic feed-forward amplification of fibrosis. J Invest Dermatol, 2013. **133**(5): p. 1302-10.
- 113. Glenisson, W., V. Castronovo, and D. Waltregny, *Histone deacetylase 4 is required for TGFβ1-induced myofibroblastic differentiation*. Biochimica et Biophysica Acta (BBA)
  Molecular Cell Research, 2007. **1773**(10): p. 1572-1582.
- 114. Jiang, Y., et al., Histone H3K9 demethylase JMJD1A modulates hepatic stellate cells activation and liver fibrosis by epigenetically regulating peroxisome proliferatoractivated receptor γ. Faseb j, 2015. **29**(5): p. 1830-41.
- 115. Zhang, Y., et al., *Chromatin connectivity maps reveal dynamic promoter—enhancer long-range associations*. Nature, 2013. **504**(7479): p. 306-310.
- 116. Anand, P., et al., *BET bromodomains mediate transcriptional pause release in heart failure*. Cell, 2013. **154**(3): p. 569-82.
- 117. Tang, X., et al., BET bromodomain proteins mediate downstream signaling events following growth factor stimulation in human lung fibroblasts and are involved in bleomycin-induced pulmonary fibrosis. Molecular pharmacology, 2013. **83**(1): p. 283-293.
- 118. Khan, S.M., et al., *Gβγ subunits colocalize with RNA polymerase II and regulate transcription in cardiac fibroblasts.* J Biol Chem, 2023. **299**(4): p. 103064.
- 119. Suarez-Arnedo, A., et al., An image J plugin for the high throughput image analysis of in vitro scratch wound healing assays. PLoS One, 2020. **15**(7): p. e0232565.

- 120. Schneider, C.A., W.S. Rasband, and K.W. Eliceiri, *NIH Image to ImageJ: 25 years of image analysis*. Nature Methods, 2012. **9**(7): p. 671-675.
- 121. Livak, K.J. and T.D. Schmittgen, *Analysis of relative gene expression data using real-time quantitative PCR and the 2(-Delta Delta C(T)) Method*. Methods, 2001. **25**(4): p. 402-8.
- 122. Chen, S., *Ultrafast one-pass FASTQ data preprocessing, quality control, and deduplication using fastp.* iMeta, 2023. **2**(2): p. e107.
- 123. Love, M.I., W. Huber, and S. Anders, *Moderated estimation of fold change and dispersion for RNA-seq data with DESeq2*. Genome Biology, 2014. **15**(12): p. 550.
- 124. Elbashir, S.M., et al., *Duplexes of 21-nucleotide RNAs mediate RNA interference in cultured mammalian cells.* Nature, 2001. **411**(6836): p. 494-498.
- 125. Miller, I., et al., *Ki67 is a Graded Rather than a Binary Marker of Proliferation versus Quiescence*. Cell Rep, 2018. **24**(5): p. 1105-1112.e5.
- 126. Randall, D.W., et al., *Batch effect exerts a bigger influence on the rat urinary*metabolome and gut microbiota than uraemia: a cautionary tale. Microbiome, 2019.

  7(1): p. 127.
- 127. Jiménez, J.A. and M.J. Zylka, Controlling litter effects to enhance rigor and reproducibility with rodent models of neurodevelopmental disorders. Journal of Neurodevelopmental Disorders, 2021. **13**(1): p. 2.
- 128. Lazic, S.E. and L. Essioux, *Improving basic and translational science by accounting for litter-to-litter variation in animal models*. BMC Neuroscience, 2013. **14**(1): p. 37.
- 129. Hinz, B. and D. Lagares, Evasion of apoptosis by myofibroblasts: a hallmark of fibrotic diseases. Nat Rev Rheumatol, 2020. **16**(1): p. 11-31.

- 130. Pakshir, P., et al., *The myofibroblast at a glance*. Journal of Cell Science, 2020. **133**(13).
- 131. Santiago, J.-J., et al., Cardiac fibroblast to myofibroblast differentiation in vivo and in vitro: Expression of focal adhesion components in neonatal and adult rat ventricular myofibroblasts. Developmental Dynamics, 2010. **239**(6): p. 1573-1584.
- 132. Shinde, A.V., C. Humeres, and N.G. Frangogiannis, *The role of α-smooth muscle actin in fibroblast-mediated matrix contraction and remodeling*. Biochimica et Biophysica Acta (BBA) Molecular Basis of Disease, 2017. **1863**(1): p. 298-309.
- 133. Rønnov-Jessen, L. and O.W. Petersen, *A function for filamentous alpha-smooth muscle actin: retardation of motility in fibroblasts*. Journal of Cell Biology, 1996. **134**(1): p. 67-80.
- 134. Schwindinger, W.F. and J.D. Robishaw, *Heterotrimeric G-protein betagamma-dimers in growth and differentiation*. Oncogene, 2001. **20**(13): p. 1653-60.
- 135. Hinz, B., et al., *Mechanical Tension Controls Granulation Tissue Contractile Activity and Myofibroblast Differentiation*. The American Journal of Pathology, 2001. **159**(3): p. 1009-1020.
- 136. Bienkowski, R.S., S.F. Curran, and R.A. Berg, *Kinetics of intracellular degradation of newly synthesized collagen*. Biochemistry, 1986. **25**(9): p. 2455-9.
- 137. Krumins, A.M. and A.G. Gilman, Targeted Knockdown of G Protein Subunits Selectively Prevents Receptor-mediated Modulation of Effectors and Reveals Complex Changes in Non-targeted Signaling Proteins \*. Journal of Biological Chemistry, 2006. **281**(15): p. 10250-10262.
- 138. Gilman, A.G., *G proteins: transducers of receptor-generated signals*. Annu Rev Biochem, 1987. **56**: p. 615-49.

- 139. Shu, J., et al., An RNA-sequencing study identifies candidate genes for angiotensin II-induced cardiac remodeling. Molecular Medicine Reports, 2018. **17**(1): p. 1954-1962.
- 140. Kankanamge, D., et al., *G protein gamma subunit, a hidden master regulator of GPCR signaling*. Journal of Biological Chemistry, 2022. **298**(12): p. 102618.
- 141. Ueda, H., et al., Association of the γ12 subunit of G proteins with actin filaments. Journal of Cell Science, 1997. **110**(13): p. 1503-1511.
- 142. Rizk, R., et al., KCTD Proteins Have Redundant Functions in Controlling Cellular Growth. Int J Mol Sci, 2024. **25**(9).
- 143. Defea, K., Beta-arrestins and heterotrimeric G-proteins: collaborators and competitors in signal transduction. Br J Pharmacol, 2008. **153 Suppl 1**(Suppl 1): p. S298-309.
- 144. Eishingdrelo, H. and S. Kongsamut, *Minireview: Targeting GPCR Activated ERK Pathways for Drug Discovery.* Curr Chem Genom Transl Med, 2013. 7: p. 9-15.
- 145. Booz, G.W., et al., *Involvement of protein kianse C and Ca2+ in angiotensin II-induced mitogenesis of cardiac fibroblasts*. American Journal of Physiology-Cell Physiology, 1994. **267**(5): p. C1308-C1318.
- 146. Olson, E.R., et al., Angiotensin II-Induced Extracellular Signal-Regulated Kinase 1/2

  Activation Is Mediated by Protein Kinase Cδ and Intracellular Calcium in Adult Rat

  Cardiac Fibroblasts. Hypertension, 2008. 51(3): p. 704-711.
- 147. Chintalgattu, V., D.M. Nair, and L.C. Katwa, *Cardiac myofibroblasts: a novel source of vascular endothelial growth factor (VEGF) and its receptors Flt-1 and KDR*. J Mol Cell Cardiol, 2003. **35**(3): p. 277-86.

- 148. Halim, D., et al., Loss of LMOD1 impairs smooth muscle cytocontractility and causes megacystis microcolon intestinal hypoperistalsis syndrome in humans and mice. Proc Natl Acad Sci U S A, 2017. **114**(13): p. E2739-e2747.
- 149. Ciobanasu, C., B. Faivre, and C. Le Clainche, *Integrating actin dynamics*, mechanotransduction and integrin activation: The multiple functions of actin binding proteins in focal adhesions. European Journal of Cell Biology, 2013. **92**(10): p. 339-348.
- 150. Marston, S. and M. El-Mezgueldi, *Role of Tropomyosin in the Regulation of Contraction in Smooth Muscle*, in *Tropomyosin*, P. Gunning, Editor. 2008, Springer New York: New York, NY. p. 110-123.
- 151. Villa, M., et al., *Pro-fibrotic effect of oxidized LDL in cardiac myofibroblasts*.

  Biochemical and Biophysical Research Communications, 2020. **524**(3): p. 696-701.
- 152. Desmoulière, A., et al., Apoptosis mediates the decrease in cellularity during the transition between granulation tissue and scar. Am J Pathol, 1995. **146**(1): p. 56-66.
- 153. Bilbija, D., et al., Retinoic acid signalling is activated in the postischemic heart and may influence remodelling. PLoS One, 2012. **7**(9): p. e44740.
- 154. Bilbija, D., et al., Expression of retinoic acid target genes in coronary artery disease. Int J Mol Med, 2014. **33**(3): p. 677-86.
- 155. Zhou, M.D., et al., *Retinoid-dependent pathways suppress myocardial cell hypertrophy*.

  Proc Natl Acad Sci U S A, 1995. **92**(16): p. 7391-5.
- 156. Suzuki, K., et al., Transcriptomic changes involved in the dedifferentiation of myofibroblasts derived from the lung of a patient with idiopathic pulmonary fibrosis. Mol Med Rep, 2020. **22**(2): p. 1518-1526.